Università
Ca'Foscari
Venezia

Scuola Dottorale di Ateneo
Graduate School

Dottorato di ricerca
in Scienze Ambientali
Ciclo XXVI
Anno di discussione 2013

Reconstruction of Holocene climate dynamics in the Dolomites from a peat bog core: the first multi-proxy study

SETTORE SCIENTIFICO DISCIPLINARE DI AFFERENZA: **CHIM/01**
Tesi di Dottorato di LUISA POTO, matricola 955851

Coordinatore del Dottorato

Prof. Gabriele Capodaglio

Tutore del Dottorando

Prof. Carlo Barbante

Co-tutore del Dottorando

Dott. Jacopo Gabrieli

PhD Thesis

Luisa Poto

September 2013

Reconstruction of Holocene climate dynamics in the Dolomites from a peat bog core: the first multi-proxy study

Luisa Poto

A Thesis submitted for the degree of Doctor of Phylosophy

School of Environmental Science

September 2013

Acknowledgements

This thesis is the end of a long journey that I have not travelled alone. At the end of it, it's a pleasant task to express my thanks to all those who contributed in many ways to the success of this study and made it an unforgettable experience. Well, the list of the people I need to thank will not fit to a single Acknowledgement section. Many other thanks are hidden in my thoughts and in my heart. I hope that this work makes all of you proud of me.

Completing my PhD degree is probably the most challenging activity of the first 29 years of my life, and the best and worst moments of my doctoral journey have been shared with many people. It has been a great privilege to spend several years in the Department of Environmental Science, Informatics and Statistics, and its members will always remain dear to me.

First and foremost I want to thank my supervisor Carlo Barbante. It has been an honour to be your PhD student. I appreciate all your contributions of time, ideas, and funding to make my PhD experience productive and stimulating.

Jacopo, I cannot thank you enough. When others doubted, you remained a fan, with your tremendous help no matter the task or circumstance around you. Your joy and the enthusiasm for research was contagious and motivational for me. I can see the good shape of my thesis thanks to your help and suggestions, because a journey is easier when you travel together and interdependence is more valuable than independence.

Andrea and Piero, for all the time together in our "loculo": thank you most of all because when I became too serious, your humour and friendly sarcasm allowed me to laugh and lightened my perspective. Thank you for your friendship and your invaluable help and support.

Giulio: I truly admire your distinguished helping nature. You have oriented and supported me with promptness and care, and have always been patient and encouraging in times of new ideas and difficulties; you have listened alaways to my ideas, and discussions with you frequently led to key insights. Thank you for your constant moral support.

Michela: thank you! You have personally endured my long-lasting hours on the computer. Thank you for your encouragement, support and, most of all, your humor. You kept things light and me smiling.

All of the other component of the paleogroup: Clara, Natalie, Patrizia, Torben, Simon, Giuliano, Federico and Daniela. Its a great pleasure to spend time with you, not only during the paleomeeting but especially during the building-group events.

I thank labmates in lab "Cescon", and prof Cescon too. Warren, Clara, Francesca, Elena A., Silvia, Fabio, Rossano, Andrea, Roberta, Marco V., Fabiana, Chiara, Elena B., Marco R., Stefano, Sara : thank you for your friendly assistance and for allowing me to be part of a great professional community.

Bill Shotyk, for your insightful comments in my work, for your support, and for many motivating discussions. Your ability to select and to approach compelling research problems, your high scientific standards, and your hard work set an example. Most of all thank you for give me the possibility to have an awesome experience of life and research in Edmonton.

Robert Peroni, for the best experience I had in my life. Thanks to you and to all the Inuit community for having adopted me as a real daughter. Thank you for giving me a house and a bed, even if you didn't have any of them. Thanks for showing me which is the real and genuine life, the one that "happens when you are completing your dissertation" and "doesn't wait until you are finished".

Lorenza, Ale Bally, Ale Bri, Michelle, Chiara, Alice, Cate, Rache, Saia, Giorgia, Vero, Elena: need I say more? You are my life-long friends. For many and many more reasons, I am eternally grateful to you. Thank you for being persistent and encouraging, for believing in me and for the many precious memories along the way.

Many thanks to the workshop of the University of Venice, in particular to Valter, Enrico, Giuliano, and Roberto for the technical support in making the "best boxes for peat cores never seen before".

Of course, no acknowledgements would be complete without giving thanks to my mom and my brother. Both have instilled many admirable qualities in me and given me a good foundation with which to meet life. They've taught me about hard work and self-respect, about persistence and about how to be independent. Mom, especially, was a great role model of resilience, strength and character, and I am grateful for the "smart genes" she passed on to me. Both have always expressed how proud they are of me and how much they love me. I too am proud of them and love them very much. To them this work is dedicated.

Abstract

Paleoclimate and paleoenvironmental studies in the North-Eastern Italian Alps are hampered by the rarity of well-preserved high-altitude deposits and the lack of high-resolution multi-proxy records with adequate chronological control. Records from peat-bogs have been demonstrated to be among the best tools in paleoenvironmental studies to reconstruct past climate conditions and variations in atmospheric composition.

An ombrotrophic peat bog is a domed peatland hydrologically isolated from the influence of local groundwaters and surface waters, in which the surface layers are supplied only by atmospheric depositions. For this reason, they constitute an authentic records of information about past and present patterns in global climatic change.

Here we present the first complete Late Glacial to Holocene peat bog succession from the Dolomites (Danta di Cadore, Belluno, Italian Alps).

In 2011 a 7.0 m deep peat bog core was drilled at Val di Ciampo (Belluno province, 140 m a.s.l.) and its potential as a paleoclimatic and paleoenvironmental archive has been evaluated. The depth-age scale is based upon independent ^{14}C and ^{210}Pb dates, modelled with "Clam" method, this combined with peat stratigraphy, demonstrates that the peat core covers more than 13,200 years (cal BP), extending back to the end of the last part of the Late Glacial.

We determined bulk density, inorganic matter content, and several parameters of pore water such as pore water pH, conductivity, Ca/Mg ratios, and Ca and Ti trends, to identify changes in trophic conditions through the entire profile. This multi-proxy approach confirms that the uppermost 400 cm of the bog are ombrotrophic, and demonstrates that this core is the longest Eastern Alpine ombrotrophic record yet obtained, covering the last 7,000 years.

Chronological constraints of the course of deglaciation in the Southern Alps are fewer than those available for the northern slope of the Alps. For the Piave basin, the mode and timing of deglaciation are well-defined only for the its mid-part, while no data are available for the upper section. In such a context of very limited data the oldest radiocarbon age (13,110-13,330 years cal BP) represents a very valuable result, providing clear evidence that, during the Bölling-Alleröd interstadial, the upper part of the Piave Glacier was ice free, and confirming that the retreat process of Piave Glacier from the Last Glacial Maximum was very rapid. Pollen assemblages at the transition from the Late Glacial to the Early Holocene were studied at high resolution. In this time frame pollens show that denser forests of Gymnospermeae were present during the Bölling-Alleröd interstadial (at approximately

around 13,200 years cal BP), and were reduced by the climatic cooling of the Younger Dryas (12,600 - 11,500 years cal BP), when a more open type of vegetation spread. Then, with the beginning of the Holocene, forests developed again with the expansion of species such as *Corylus*, a warmth-requiring tree.

The investigation of atmospheric deposition during the Holocene is extremely important because it provides information about the climate-related changes in the atmospheric composition as well as the impact of human activities on the environment. With this aim, the concentration of 44 trace elements have been determined at a resolution of 1 cm on the first meter of the bog.

X-ray Fluorescence Core Scanner (XRF-CS) analysis was here applied for the first time on peat bog sequences. Results were combined with those obtained by Inductively Coupled Plasma Mass Spectrometry (ICP-MS), providing information about geochemical processes occurring in the bog, and about their influence on major and trace elements distribution along the profile. XRF-CS signals were calibrated using ICP-MS results, showing very high correlation and demonstrating that even the XRF-CS technique, when applied to peat samples, provides reliable quantitative results.

Particular attention was directed to elements related to mining activity, that has characterized the history of the Cadore region since the Middle Ages. Pb, Ag, Cd concentrations and Enrichment factors (EFs) were determined in the upper 100 cm of the record. In addition lead isotopes were also measured. Concentration levels and EFs of several trace elements such as Pb, Ag and Cd, fit very well the documented chronology about mining activity in Cadore region, indicating that the Val di Ciampo bog recorded the development and the history of mining exploitation at least at a regional scale. In particular, the Pb, Ag and Cd maximum concentrations are recorded between 1950s and 1980s, time interval that corresponds to the highest activity of the mining sites.

Lead isotopes ratios were measured to identify natural and anthropogenic sources of Pb emissions in the first metre of the bog. The isotopic composition of lead shows an increase of Pb deriving from fuel combustion over the last decades that gradually overlie the impacts of mining activity. In fact the uppermost 28 cm (corresponding to the period between AD 1940 and 2011) are characterized by more radiogenic inputs due to leaded gasoline combustion, with a signature closer to coal and fuel. Specifically, the ^{206}Pb/^{207}Pb decreasing trend, indicator of increasing leaded gasoline combustion, reached the minimum value of 1.153 in the 1990s (that correspond to maximum value of Pb flux, 0.75 g cm^{-2} y^{-1}) and then increases again. In these years, in fact, Italy started to follow EU rules to limit global pollutants in the atmosphere, and finally in 2002 banned leaded-fuels.

Val di Ciampo demonstrates a record not only of global (e.i. leaded gasoline combustion) or local (e.i. mining activity) changes in atmospheric inputs, but also more regional trends. In fact, both ^{206}Pb/^{207}Pb and Pb flux

show a particular event between 1975 and 1980: this behaviour is characteristic of the ILE experiment (Isotopic Lead Experiment), a large scale isotopic tracer experiment that was carried out in the Piedmont region of Northwest Italy to study the metabolic paths of this element into the environment. All the gasoline used was labelled with a well isotopically-defined Pb.

The high-resolution physical, chemical and biological data obtained from the analysis of this peat archive improve our understanding of European Alpine Holocene climate and environmental variability and the relationship between natural fluctuations and anthropogenic impacts.

Contents

List of Figures

List of Tables

Part I

Introduction

Importance

Current scientific evidence confirms that global warming of the climate system is unequivocal: it is evident from the measured increase in air and ocean temperatures and from observations of snow and ice melting on different sites worldwide (IPCC, 2007 - *www.ipcc.ch*). Overall, most of the observed increases in global average temperatures since the mid 20th century are very likely due to the increase in anthropogenic forcing and, in particular, in greenhouse gases emissions and atmospheric concentrations (Solomon et al., 2007).

In this framework, the Alps represent one of the areas most vulnerable to climate change in Europe, as they have undergone an exceptionally high temperature increase of around +2°C between the late 19th and early 20st century, more than twice the average rate of warming in the Northern hemisphere (Auer et al., 2005). This situation is leading to an extensive melting of glaciers, rising of the snowline and to changes in the general availability of water resources (Haeberli, 1995).

Climate in mountain regions is influenced by several different factors. In the specific case of North-Eastern Italian Alps, the chain occupies a key position between central Europe and the Italian peninsula: first, it represents a natural orographic barrier against humidity from the North Atlantic; second, the climate in this region is influenced by cold and dry winds from Eastern Europe; finally, the Italian Alps are densely populated up to high elevations, and this particular aspect makes climate changes on the environment directly correlated with societies. All these factors jointly explain the great importance of reconstructing past climatic conditions in the Alpine area, insofar as they can provide information about past circulation patterns in response to both internal and external forcing and to anthropogenic factors.

The literature offers several attempts of reconstruction of past climate variability in the Alps (Wick, 1996; Tinner et al., 1999; Pini, 2002; Finsinger et al., 2006). However, long, continuous and highly resolved records are not widely available in the North Eastern area. In the North Eastern Italian Alps, we still do not have any climatic records that span the whole Holocene (11,000 years to present), the most recent warm (interglacial) period in the Quaternary, which encompasses the rise of human civilization. The study of this time period provides the unique opportunity to distinguish the extent

and magnitude of recent anthropogenic climate changes from longer-term, natural climate variability (Mann et al., 1999).

Climatic fluctuations directly affect human society, especially in particularly sensitive areas such as mountainous regions. The study of the relationship between past climate changes and first human settlements could help us understand the most efficient adaptation strategies and predict the effects of global warming and human activities on the Alpine geological and ecological system. Unfortunately, our knowledge of the interactions between climate and landscape in the Alpine environment is limited by the lack of highly resolved paleoclimatic records. Moreover, insufficient light has been shed on the interactions between climate forcing at different scales and internal variability, which determine Alpine local climate variations.

In this respect, important observations are still needed to understand how contemporary and past climatic phenomena have affected and still affect the environment and the evolution of the Alpine landscape.

Chapter 1

Holocene Climate Dynamics

1.1 The Holocene, a special time

The term Holocene was introduced in 1869 by Paul Gervais and, in 1885, was accepted for the first time by the International Geological Congress as part of the geological nomenclature indicating the "wholly recent" geological period (Bowen, 1978).

The Holocene is the youngest phase of Earth history, and began when the last glaciations ended. The transition from the end of glacial times to the beginning of the Holocene is one of the most detectable stratigraphic boundaries, characterized by dramatic shifts in surface processes followed by different responses in biotic and abiotic components of the ecosystem. Today, paleoclimatologists date the beginning of the Holocene to 11,500 years cal BP, in conjunction with the end of the Younger Dryas (YD) and the beginning of the Preboreal period in Europe (Bjorck et al., 1998).

During the first half of the Holocene, the ecosystems were in a natural state without significant human alterations. Late, Holocene is characterized by the rise of human civilization, which led to a progressive change in land use with the establishment of the firsts human settlements. Later on, human impact continued to increase with the development of farms, agriculture and finally with industrial activity, inducing dramatic changes on climate with respect to its natural variability.

The Holocene is the only period in Earth's history in which human activities began to modify and reshape the nature of its system through systematic impacts on the composition and concentration of atmospheric trace gases, and through deforestation, soil erosion, urbanization and loss of biodiversity. These impacts started inevitably compromising the environment thousands of years ago, and have been doing so at an accelerating rate in the last few decades, changing the scale of their impacts from local to global.

In 2000, Paul Crutzen, Nobel prize winner for the discovery of the ozone depletion mechanisms, underlined the exceptional impact of humans on the

4

climate and coined the term "Anthropocene" to designate the period since the late 18th century when humans began to impact on atmospherics concentrations of CO_2 and CH_4 (Crutzen and Stoermer, 2000). Later, Ruddiman (Ruddiman, 2003, 2007) proposed that the Anthropocene started much earlier, i.e., when early human civilization started to affect global biogeochemical cycles such as carbon cycle with their agricultural practices. This theory was based on ice core records indicating that methane had started to rise about 5000 years BP (Chappellaz et al., 1990; Etheridge et al., 1996).

The Holocene presents also many examples of decline of past civilizations such as the collapse of the classical Central American Maya, the decline of Norse colonies in Western Greenland and of the Asian and African old-world civilizations during the Little Ice Age (LIA, AD 1400 - 1900) (Hodell et al., 1995; De Putter et al., 1998). LIA is a period of cooling of the Northern hemisphere that occurred after a time of relatively warm climate known as the Medieval Warm Period (MWP, AD 1000 - 1300). The LIA was characterized by temperatures cooler of 1°C relative to late 20th century levels.

Thus, it is widely demonstrated that, as it developed during the Holocene, human society had a strong influence on the environment and on climate, while climatic variability played, in turn, an important role in human cultural evolution.

1.2 Holocene climate variability

The main factors of climate change during the Holocene include different forcing factors which can act simultaneously: lower frequency millennial-scale changes associated with orbital forcing, century-scale changes associated with solar forcing and annual- or decadal-scale variability depending on volcanic forcing.

On a multi-millennial time scale, the main factors that affect Holocene climate changes are related to the modification of the orbital forcing. These factors affect the spatial and seasonal distribution of energy that comes from the Sun (figure 1.1).

The changes to the Earth's orbit affect the amount of insolation (INcoming SOLar radiATION) at the upper atmosphere and can be split into three components: eccentricity, obliquity and precession. The term eccentricity describes how much the orbit of the Earth around the Sun deviates from a circle, with the Sun located at one of the focal points of the resulting ellipse. The dominant periods of eccentricity variation are around 100,000 years and 400,000 years.

The obliquity, or tilt, describes the inclination of the Earth's axis of rotation with respect to the Earth's orbital plane. At present, it is around 23 degrees. This tilt changes quasi-periodically and the main periods are $\sim 41,000$ years with components at $\sim 53,000$ years and $\sim 29,000$ years.
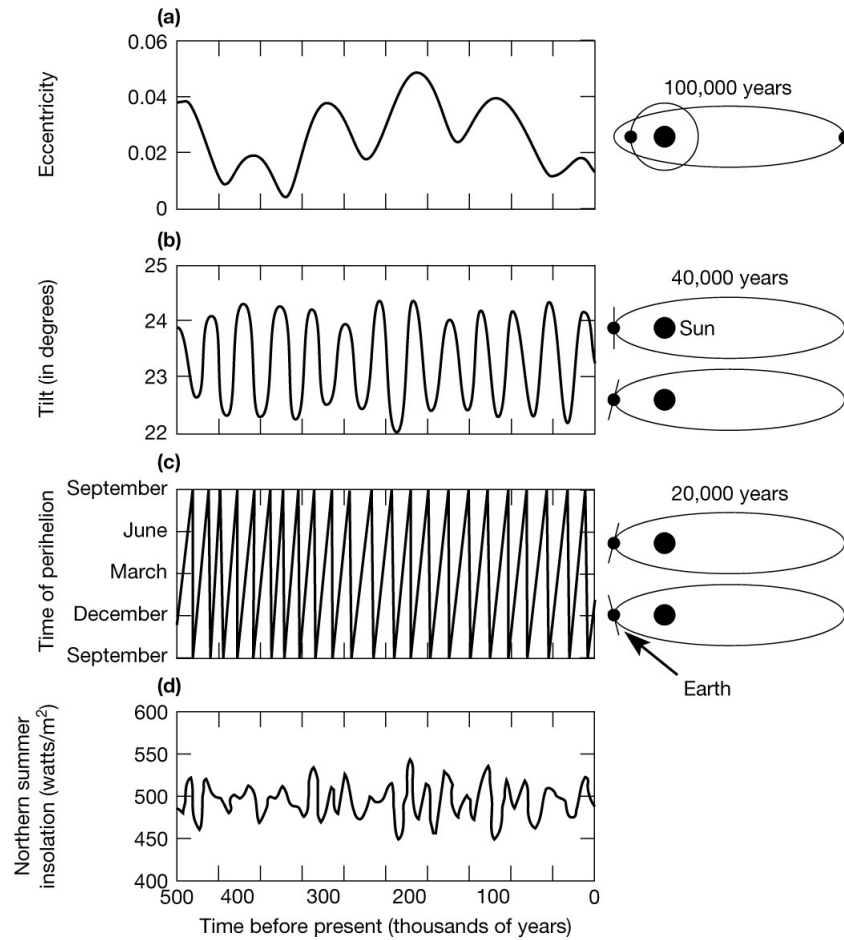
Figure 1.1: Outline of the Holocene climate orbital forcing: (a) eccentricity, (b) tilt, (c) time of perihelion. In panel (d) Northern summer insolation is plotted (from http://www.ic.ucsc.edu).

The obliquity parameter primarily affects the relative amounts of insolation received by high- and low-latitude regions on the Earth's surface.

The precessional parameter describes the relationship between the seasons and the perihelion of the orbit, determining at which point on the orbit the Northern hemisphere winter (Southern hemisphere summer) occurs. This can be pictured as a "wobble" of the Earth's axis of rotation. The main harmonic components of this cycle occur $\sim 21,000$ years.

The first person who linked mathematically the variation of the Earth's orbit with the occurrence of ice ages was the Scottish geologist James Croll (Croll, 1875). His work was later refined by the Serbian mathematician Milutin Milanković Milanković (1969) (figure 1.1). Milanković proposed that ice growth in the Northern hemisphere occurs during times when summer

insolation is reduced. Low summer insolation occurs when Earth's orbital tilt is small and its poles are pointed less directly at the Sun. Low insolation also occurs when the northern summer solstice occurs with Earth farthest from the Sun and when the orbit is highly eccentric, (further increasing the Earth-Sun distance) (Ruddiman, 2008). Milanković theory was the starting point to understand glacial-interglacial cycles explaining that presence of volume responses to 41,000, 21,000 and 100,000 years.

During the Holocene, insolation varies over different time scales, and paleoclimatologists have identified changes in solar activity with temporal resolution lower than those described by Milanković. Through the observation of sunspots, the monitoring of solar activity, and satellite measurements, they have identified the following five most common frequencies: the 11-year Schwabe sunspot, the 22-year Hale double sunspot, the 88-year Gleissberg, the 200-year de Vries and the so-called 1500-year Bond cycles, not to be confused with the homonymic Dansgaard-Oeschger (DO) events occurring during marine isotope stage 3 (MIS3).

Volcanic eruptions can also cause climate changes and lead to short-term cooling effects on overall hemispheric or global mean temperatures (Robock, 2000). These changes derive from the radiative effects of the volcanic aerosol reducing energy received at the surface. This climate forcing factor contributes only to the short-scale variability of the Holocene climate, but if eruptions become more frequent, cumulative effect can result in decadal- or multi-decadal-scale impacts, as reported by Church et al. (2005).

Overall, the climatic variability observed in the Holocene cannot be entirely ascribed to forcing factors: several other feedback mechanisms on the Earth system can play a leading role. The best example of this is the 8,200-year event that resulted from a catastrophic lake drainage at the margin of the Laurentide Ice Sheet.

During the Last Glacial Maximum (25,000 - 18,000 years cal BP, according to calibrated radiocarbon dating), ice sheets were more than 4 Km thick across the Northern Europe and North America, and smaller ice caps existed in the Alps, Andes and East Asia. The subsequent climatic warming and the deglaciation of those areas happened in a series of steps which were synchronous over large parts of the globe, although there may have been some asynchrony between the Northern and Southern hemispheres. Deglaciation took about 9,000 years to be completed in Europe and North America, and it was an unsteady process accompanied by several oscillations in climate. In the circum North Atlantic region, this late Pleistocene thermal oscillation comprised a warming event known as the Bölling-Alleröd interstadial (15,000 - 12,700 years cal BP), which was followed by a cooling event called the Younger Dryas stadial (12,700 - 11,500 years cal BP). Thus, both external and internal forcing and feedback mechanisms have caused the changes during the entire Holocene.

Ice core records from Greenland provide some of our most important

paleoclimatic data for ice age climate in the Northern hemisphere. In particular, the GRIP and GISP2 cores, drilled at the summit of the Greenland ice sheet between 1988 and 1993, provide accurate and well-resolved climate records (figure 1.2).
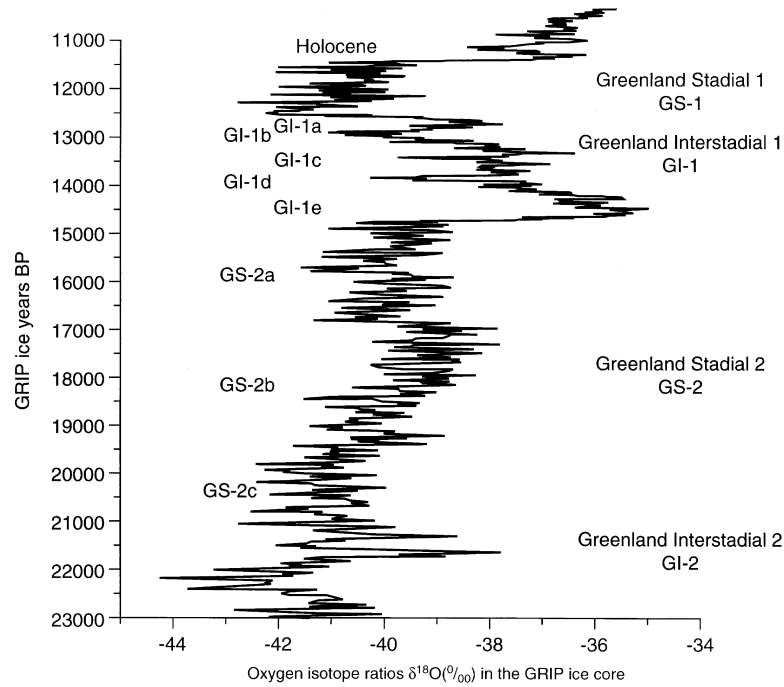
Figure 1.2: The $\delta^{18}O$ record (SMOW) from the GRIP ice core (Dansgaard et al., 1993) between 11,000 and 23,000 GRIP years BP showing the division of the oxygen isotope profile into interstadial (and sub-interstadial) and stadial (and sub-stadial) events. From Walker et al. (1999).

They show that warming steps at the end of the LGM were extremely rapid and point out that the transition to the Holocene involved a temperature rise of 7°C over more than 50 years (Alley et al., 1993). During this transition, many Earth surface systems were impacted: for example, global eustatic sea levels that laid at -40 m around 11,000 years cal BP reached their modern elevations around 6,000 - 5,000 cal BP (Edwards et al., 1993). Meanwhile, soil formation and vegetation cover experienced phases of instability, recording high rates of erosion and sediment flux.

In many mid-latitude Northern Hemisphere regions, a thermal optimum during the Holocene can be identified between 10,000 and 6,000 years cal BP (Foley et al., 1994). However, during this period of long-term climatic trends, there were several interruptions by abrupt cooler events of shorter, centennial duration. Dated around 12,000, 8,200 and 5,200 years cal BP, they are well recorded by the Greenland ice cores as sharp changes in atmospheric methane

concentrations and, in the Tropics, by abrupt lake-level falls (Gasse, 2000).
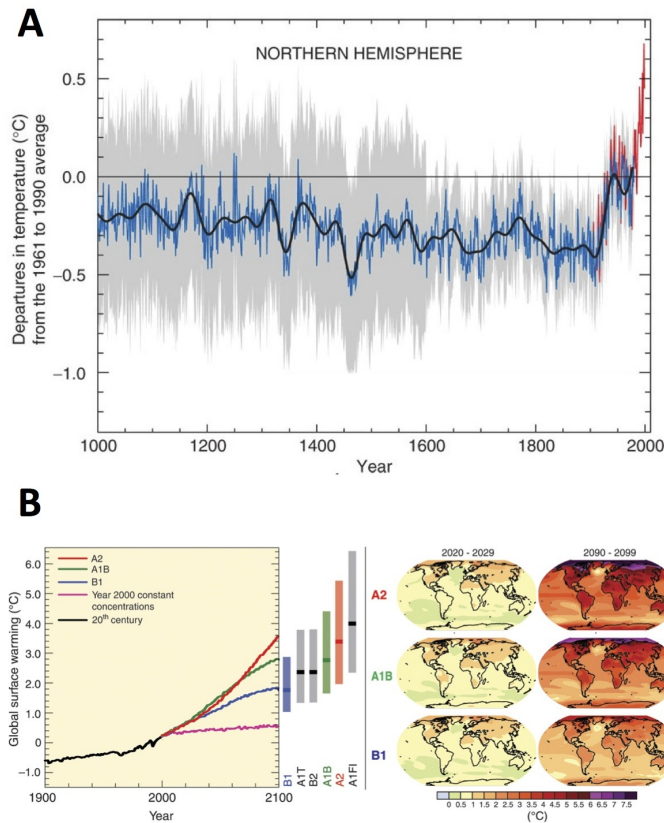
Figure 1.3: Evolution of average temperatures during the last 1000 years (panel A) in the Southern hemisphere (IPCC, 2007). The red line indicates instrumental data, while the blue line indicates the integration between data from different paleoclimate archives such as ice cores, lake sediment cores, peat bogs and tree rings. Panel B shows temperature projections for the next 100 years using different scenarios. Overall, these scenarios are in agreement, indicating a general strong increase of temperatures between +1.9°C and + 3.3°C.

Later Holocene also experienced some significant shifts in climate: the progressive cooling followed the Holocene thermal optimum, and the climatic desiccation of the Northern sub-tropics after 6,000 years cal BP that generated the modern Thar, Arabian and Saharan deserts (Gallagher et al., 2001). Over this long-term climatic trend variations from wet to dry or from cold to warm were recorded in the stratigraphy of peat bogs (Charman et al., 2001) and in the advance and retreat of mountain glaciers. It is still uncertain whether these oscillations represent true, regular cycles of climatic changes.

During the Holocene, the period with the best-resolved and most reliably calibrated climate data is the last millennium. Following the initial work by Mann et al. (1999), scientists generated a number of synthetic curves

describing trend in temperatures. Data for this time frame derive from proxy-climate records (Vivaldo, 2012; Shi et al., 2012; Cunningham et al., 2013), historical observations and - for the last two centuries - from instrumental records (Matyasovszky and Ljungqvist, 2013; Nicholson et al., 2013).

In the Northern hemisphere, these curves present a particular "hockey-stick" shape, indicating that temperatures fell progressively until they reached a minimum in the 17th century, then rose sharply during the last 150 years, reaching today global temperatures which are probably higher than at any time during the last 1,000 years. This suggests that most of the post-1980 warming is of human origin (figure 1.3).

1.3   Holocene records from the Dolomites

The European Alps represent one of the largest and continuous mountainous areas in continental Europe. Following the Alpine Convention, they are shared by eight countries (figure 1.4) and, because of their position, they are very important for the accumulation and supply of water for most of the major European rivers such as the Po, Rhine, Rhone and Danube.

Figure 1.4: Perimeter of the Alps as described by the Alpine Convention. Source: www.alpconv.org

Climatic conditions and deterioration all over the Alps during the Holocene were connected with glacier advances, changes in temperatures and the rate of precipitation. During the last 150 years, the climate of the Alps underwent a significant increase in temperature of $\sim 2°C$, more than twice the average increase that characterized the warming of the Northern hemisphere (EEA, 2009). By the end of the 21st century, temperature trends based on

the Regional Climate Models (RCM), are supposed to increase between + 2.6°C and + 3.9°C. That increase is expected to be more accelerated in the second part of the century (Moreno and Amelung, 2009) (figure 1.5).
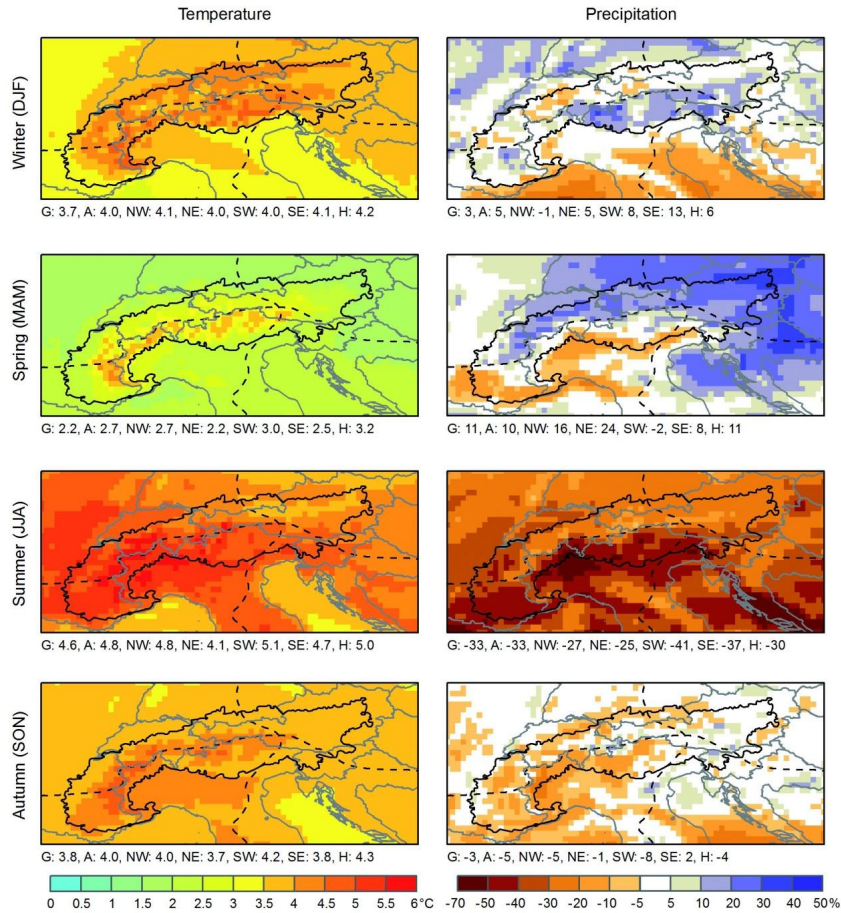
Figure 1.5: Seasonal changes in precipitation and temperature up until the end of the 21st century. Source EEA, 2009

To understand the future climate changes in the Alps region, a regional approach is more than necessary, in the light of the numerous different factors at play in the region. Indeed, regional climate is the result of the interaction of large scale dynamics with orography and physical proprieties that characterized environment at regional and local scale.

Studies of the environmental and climatic evolution of the Italian Alps, from the LGM to the Holocene, are often incomplete: while numerous studies attempt to define and categorize Holocene climate variations in the Western (Wick, 1996; Tinner et al., 1999; Finsinger et al., 2006) and Central Italian Alps (Pini, 2002; Heiss et al., 2005; Orombelli et al., 2005; Valsecchi et al., 2006), only fragmentary data exist for the Eastern Alps (Fairchild et al.,

2001). In particular the latter lack of climate data is due to the scarcity of well-preserved deposits at high altitudes and of high-resolution records with adequate chronological control.

Previous studies examined the late Quaternary history of the Piave River basin, one of the main drainage basins of the Eastern Alps, to describe the geomorphological evolution of this area during the regional deglaciation which characterized the transition from the late Pleistocene to the Holocene (Surian, 1996; Pellegrini et al., 2005; Carton et al., 2009). These studies allowed the reconstruction of a detailed picture of the geomorphological evolution of the middle-lower sector of the Piave basin (e.g., Vallone Bellunese, Quero Canyon) as well as of the alluvial and coastal plains, while questions remain about the modes and times of glacier retreat in the upper sector of the basin (Carton et al., 2009). The main environmental changes during the last glacial-interglacial transition in the South Eastern Alps are described by Avigliano et al. (2000) and Vescovi et al. (2007) using pollen analysis, macrofossils identification and radiocarbon dating of material from the Palughetto area (Cansiglio plateau, Belluno province). However, these studies do not encompass the entire Holocene, and regional reconstructions of vegetation and forest history are still incomplete.

Chapter 2

Reconstructing Holocene climates

The study of past and present global climatic change and of the multiple interactions between geosphere, hydrosphere and biosphere require a holistic approach to better understand these complex and often non-linear relationships.

In paleoclimatic studies, every discipline aims to develop its own method to reconstruct past climate variability choosing different proxies. However, the strongest approach in climatic reconstructions is to combine evidence from differents type of proxy in a "multi-proxy" study. The choice of proxies for such studies is of primary importance. They should provide sensitive climatic indicators and be complementary in their ability to reconstruct climate. Each proxy can provide us with information about one or more climate-related environmental processes. Through a multi-proxy approach, we can therefore obtain information regarding different aspects of the whole environmental, climatic and ecological system.

In environmental reconstructions, the major advantage of the multi-proxy approach resides in the unique opportunity of obtaining independent lines of evidence. Every proxy has its own strengths and weaknesses, but by identifying consistencies, weaknesses, agreements and disagreements among proxies, it is possible to achieve a more reliable paleoclimatic reconstruction. A multi-proxy paleoclimatic reconstruction starts with the collection of the existing climatic data present on the sampling area: instrumental observations of the weather parameters can thereby be correlated with experimental proxy results, in order to produce a detailed record of climate changes. Instrumental data are of primary importance but, even in the best-case scenario, they span for no more than a few decades. Where instrumental observations are lacking, information on the climate can sometimes be obtained from the analysis of historical records. Information from historical documents must be converted into numeric records based on specific indicators (e.g., alti-

tude of grapes cultivations; number of frozen days of rivers). In a second step, these indicators must be related to climatic parameters (e.g., rainfall, temperature, etc.) in order to obtain a final reliable climatic record. Where neither instrumental observations nor historical records are available, we can only rely on indirect measurements (proxy-data) of climate change through a multidisciplinary approach that includes the analysis of the distribution of fossil organic and inorganic compounds.

In an ideal environment, the historical record of atmospheric deposition should be perfectly recorded, and the relationship depth/age continuous and preserved. Moreover, non significant post-depositional physical or chemical transformations which can alter or remobilize the element of interest should be present. According to this definition of ideal environment, tree rings, oceanic corals, lake and marine sediments, ice cores from mountainous glaciers and polar ice caps, and peat cores from ombrotrophic bogs are the most useful matrices for paleoenvironmental and paleoclimatic reconstructions. The analysis of these records makes it possible to interpret past climate changes and to contribute to the understanding of Earth's climate system (e.g., Barber (1981); Chappellaz et al. (1990); Chapman and Shackleton (2000); Fischer et al. (2010); De Vleeschouwer et al. (2012a)).

2.1   Instrumental records

Instrumental records cover a whole range of climatic parameters and can produce long climate series over many years. Among the wide range of different climatic parameters, surface atmospheric temperature plays a key role in the study of climate changes. Over the last 150 years, instrumental records demonstrate that the global atmospheric temperature has risen by about 0.6°C. Air temperature increases can trigger changes in other sectors of the Earth climate system, since climatic parameters are interconnected. One example is the modification of the seasonal snow cover and glacial extent. The dramatic retreat of Alpine glaciers during the last century has been largely documented and considered as a key scientific indicator for global warming and regional climate variation Haeberli (1995). The first attempt to measure the physical proprieties of the atmosphere was done by Galileo Galilei starting from the 17th century. The Florentine Grand duke Ferdinando de' Medici established, within the Accademia del Cimento, the first network of meteorology, consisting in a first stage of only a few meteorological stations in Italy and in Europe (1657 - 1667). This represented a milestone in the history of meteorology, the turning point from documentary to instrumental observations of atmospheric pressure, air temperature and precipitations. The largest available database of instrumental data is in Europe. The earliest continuous monthly meteorological records starts in 1659, with a series of mean air temperature from London (England) by Manley (1974). From the

1780s records of the three main climatic parameters (temperature, pressure and precipitation) are available for many locations in Europe, North America and India. Today, instrumental records have a widely distributed geographical coverage over both land and sea. Observations can be made through surface stations, ships, upper-air station launching radiosondes. These methods, coupled with satellite soundings and images, have produced millions of weather observations each day. The recent transformation of Holocene paleoclimatology from a qualitative to a quantitative science has been made possible by the development of proxy data with modern instrumental climate records. In paleosciences, calibration is needed both to extract paleoclimatic signals and to identify the component of the climate system to which the paleo-signal corresponds.

2.2 Documentary records

The importance of the documentary record is unique, especially for the pre-instrumental period. These documents can provide us with information about anomalous temperatures, storms and extreme events (droughts, floods, etc.). First documentary records containing climatic information date back to the Babylonian civilization, about 4,000 years ago: many activities related to climate variability are recorded, such as those overseeing the supply of water to the city of Larsa (ancient Babylonian city near the Euphrates river) for the period between 1898-1877 BC (Stanley, 1970). As suggested by Ingram et al. (1978) written evidence has a different time span for various regions of the world: for example, in the case of America and Australia, the span is limited to that of European explorers. Written observation of climate are recorded in inscriptions, annals, chronicles, military records, private papers and mercantile accounts. Some of them present a more scientific character, with higher regularity in observations and in content. In the 17th and 18th centuries, some of the diarists gradually introduced instrumental observations into their accounts and this created an useful overlap with the instrumental record before the introduction of formalized meteorological offices.

Also fictional material can offer interesting climate observations such as the novels by Conan Doyle that like so many writers of the time, described the typically yellow colour of the fog in London.

Other documentary information are not written, as maps, often been used to assess changes in hydrological features, coastlines or glaciers (Engeset et al., 2000). Drawing and paintings can also provide evidence of past climate changes. One of the best and most popular example is the retreat of the Franz Josef Glaciers of the Southern Alps of New Zealand (Grove, 1988), whose movements and retreat can even be noticed from its representation on postage stamps (figure 2.1).

There are also valuable images in urban settings: the Venetian painter Canaletto (1697 - 1768) painted accurate pictures of Venice that contains evidences of high water mark in *commune marino* with a thin green line of algae that sign the high water in the canals: this was been used by Camuffo (1993) as evidence of changes in sea level in the Venetian lagoon.

Documentary records represent human experience of climate but the analysis, the interpretation and the verification of the data are to be taken into account because the human observer can be biased and so the climatic characteristics falsified by personal suggestion. The issue of verification and analysis make interpretation of the documentary record extremely ambitious.

Figure 2.1: Franz Josef Glacier retreat, New Zealand: comparison between (left) the glacier tongue recorded in the stamp (2006) and condition pictured in 2011 (right).

2.3   Natural archives of past climate changes

Evidence of climate changes is preserved in natural archives that can be sampled and analyzed through different chemical, physical and biological methods. The goal of paleoclimate studies is to use an archive to reconstruct temporal and spatial patterns of environmental changes linked to regional or global climate. Paleoclimate archives are found in oceans, tree rings, lakes, soils, glaciers, etc. Together, they record the history of Earth's climate changes (figure 2.2).

2.3.1   Ice - core

The turning point in glaciological ice-core community studies was expressed by A.P. Crary in September 1968, during an ISAGE symposium in New Hampshire (Crary, 1968): "So my suggestion for future glaciological studies is simple: Drill, drill and drill some more: know the ice-rock interface as well as the surface is presently known. Study the internal ice so that
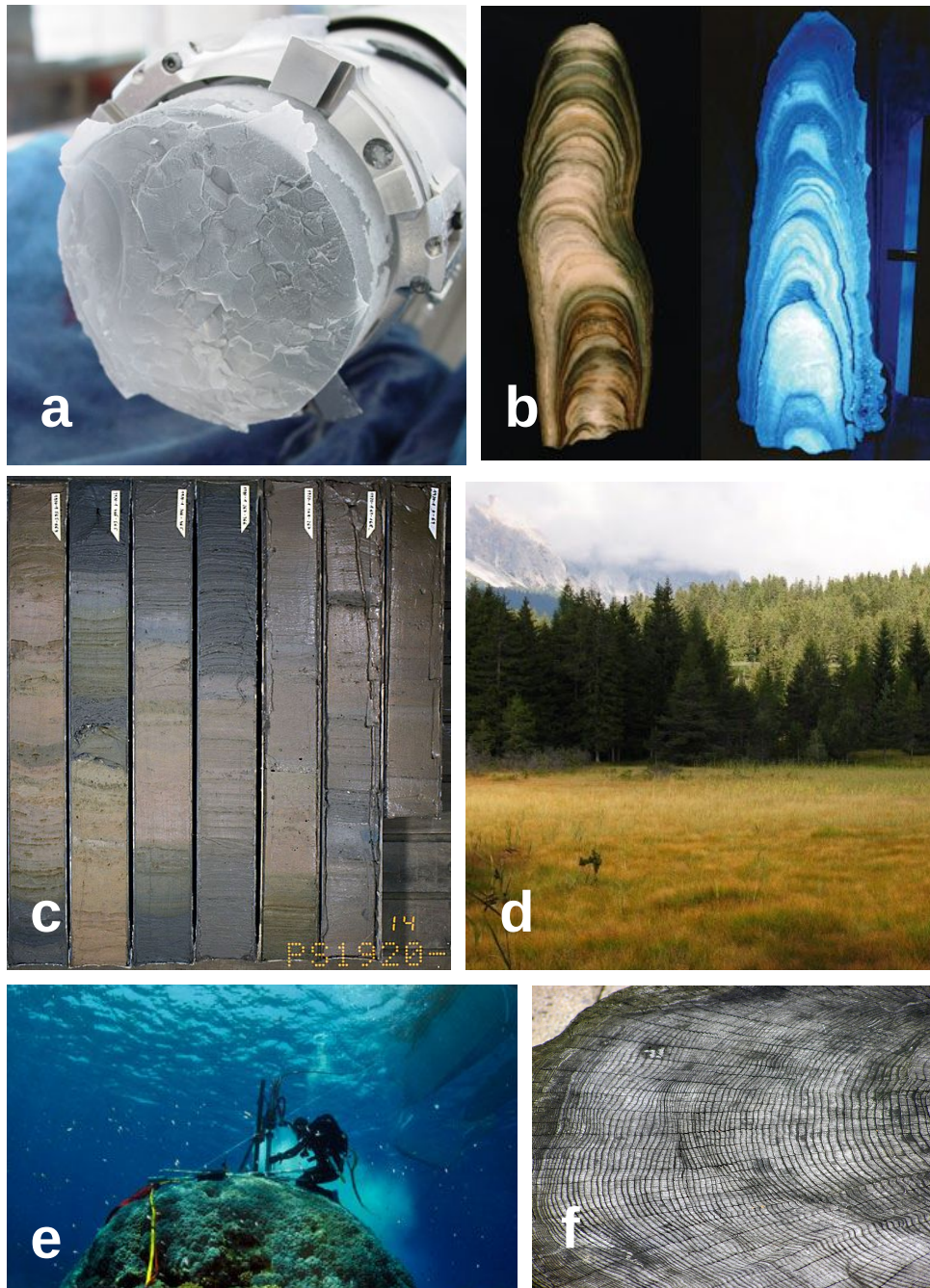
Figure 2.2: Examples of natural archives: (a) EPICA Dome C ice core, (b) two stalagmites, showing the growth "rings" characteristic of speleothems, the one on the right is being illuminated by ultraviolet light, (c) sections of sedimentary cores from Greenland, (d) Danta di Cadore peat bog, (e) researcher coring coral, (f) tree rings.

we can learn and understand the history of accumulated snow and other material that is available to us as far back as the cores take us; drill on the continental divides, on the slopes, on the shelves".

Information about paleo-atmospheres and biogeochemical cycles come from studies of ice cores from Greenland and the Antarctic great ice sheets, but also from Alpine glaciers. Greenland and Antarctic ice cores can provide records that cover the last 130,000 (NEEM) and 800,000 (DomeC) years respectively. The recording of high-resolution water stable isotopes, the proxy of air temperature, as well as the discovery of natural oscillations in greenhouse gases from fossil air trapped in polar ice, are among the most important recent advances in Earth climate sciences. Ice cores provide information about the natural variability in atmospheric trace gases, against which recent changes due to human activity can be compared. In addition to direct measurements of stable isotopes and greenhouse-gas concentrations, ice core records give the possibility to monitor a large suite of chemical compounds (e.g., dust, major ions, trace elements, cosmogenic particles, etc.) which are useful for reconstructing the paleo-atmospheric composition. Thanks to the combination of information coming from these proxies, it is possible to study in detail the factors which influenced climatic variability, such as solar activity, global biogeochemical cycles, volcanic activity, biomass burning, winds and atmospheric circulation changes, and sea-ice dynamics. From the 1960s onwards, there has been a large number of international ice-coring programs, including the Greenland Ice Sheet Project (GISP 1, GISP 2), Greenland Ice Core Project (GRIP), North GRIP (North Greenland Ice Core Project Members 2004), and, in Antarctica, the Vostok ice-core project, the European Project for Ice Coring in Antarctica (EPICA), and the Dome Fuji project. Later, ice coring was extended to mountain glaciers in the mid and low latitudes (outside polar regions). These glaciers are remarkably different from those in polar regions, as they generally cover a much shorter time period, ranging from less than 110 years as observed for an ice core from Col du Dome, France, 1890-1994 (Preunkert et al., 2000), to more than a glacial cycle (100,000 years) for an ice core from the Tibetan Plateau (Thompson et al., 1997). This represents the only example of an ice core from temperate regions which provides a climatic record extending further back than the Holocene period. In fact, from Alpine ice core it is normally impossible to retrieve information regarding climate conditions dating further back than 1,000 - 2,000 years (Sigl et al., 2009).

2.3.2   Laminated sediment records

Laminated sediment paleorecords are normally characterized by a temporal resolution that can span from decadal to inter-annual scale. Laminated sediments are deposited and preserved in lakes and in the oceans, and can be used as paleo-archives, provided that these two main requirements are

respected: (1) variation in input, chemical conditions and biological activity that will result in changing the sediment's composition and (2) environmental conditions that can preserve laminated sediments from bioturbation (Kemp, 1996).

The oceans are a very important source of paleoclimatic information, first and foremost because of their wide distribution (they occupy more than 70% of the Earth's surface). Sediments consist of both biogenic and terrigenous materials. Biogenic components include the remains of planktic and benthic organisms, which allow us to reconstruct past climate and oceanic circulation, in terms, for example, of water temperature, salinity, dissolved oxygen, pH, nutrients and trace elements concentrations (Bradley, 1999). The amount and chemical composition of the terrigenous materials mainly provide information about past moisture and aridity conditions. Moreover, the magnitude and direction of transportation of sediments into the oceans by different phenomena such as fluvial erosion, ice-rafting, and turbidity currents could be recorded. Many projects have contributed to paleoclimate reconstruction from ocean sediment proxies. CLIMAP project (Climate: Long-Range Investigation, Mapping, and Prediction) and the later SPECMAP project (Spectral Mapping Project) strongly increased our understanding of past changes in ocean surface temperatures and provided some important and innovative hypotheses about the orbital forcing and the timing of ice-sheet growth and decay (CLIMAPMembers, 1976, 1984; Hays et al., 1976; Ruddiman and McIntyre, 1981; Imbrie, 1984; Martinson et al., 1987).

Marine sediments also provide valuable insights into Holocene climatic variability, at a very high time resolution, and give information on climate changes. As the other natural archives, they have demonstrated that our present interglacial has not been climatically stable and they suggested that Holocene climate is dominated by millennial-scale variability (O'Brien et al., 1995; Bond et al., 1997; Mayewski et al., 1997; Campbell et al., 1998; Chapman and Shackleton, 2000).

Lakes accumulate sediments from the surrounding environment and, for this reason, cores from lake sediments provide records of environmental and climatic changes. Lacustrine deposits are among the best continental archives for paleoclimate reconstruction because they often offer information about long periods of time and high temporal resolution. As in the case of ocean sediments, the *conditio sine qua non* to have a preserved archive is that the sediments must be varved showing annual or even seasonal variations of climate conditions. Where a continuous record is found, it can span over thousands of years, yielding longer time series than other continental records such as tree rings or speleothems.

Lake sediments are made up of two kinds of components, both used in paleoclimatic reconstructions: autochthonous material, produced by the lake system itself, and allochthonous material, coming from outside the lake

basin. The latter material is transported by streams, rivers, aeolian activity and surface drainage, and can contain fluvial or aeolian clastic sediments, dissolved salts, macrofossils and pollens. Autochthonous material may form by biogenic transformations or inorganic precipitations within the water column. Pollen and macrofossils can be used in vegetation reconstructions, and both terrestrial and aquatic insect parts can be useful to provide other paleoclimatic data (Messager et al., 2013; Hembrow et al., 2013).

Climate studies from paleolimnological records use physical, biological and chemical proxies that are sensitive to climate-driven changes in a lake's energy balance. The ability to understand climate from lake sediment proxies depends on the knowledge of how various direct and indirect climatic forcings interact to influence every proxy (Fritz, 1996). Sediment geochemistry, with grain size variations and magnetic proprieties, biological productivity, changes in diatoms and other communities, inorganic matter deposition within carbonate-rich lakes, can provide information about lake water chemistry, salinity, water balance of the lake, temperatures and composition of meteoric waters entering the drainage basin over time.

2.3.3   Corals

Generally the denomination of "corals" is applied to the members of the order Scleractinia, characterized by a hard calcareous skeleton supporting softer tissues (Wood, 1983). An important subgroup for paleoclimatic studies is the reef-building one, in which the coral polyp lives symbiotically with algae, the hermaptic corals. The unicellular algae produce carbohydrates by photosynthesis and are affected by water depth and water turbidity. Algae fix organic carbon that, diffusing from the algal cell, becomes food for the coral polyps which provide a protective environment for the algae. The principal limiting factor of reef-building corals is the temperature: they must live only in waters at about 20°. If temperature falls down to 18°C, skeletal growth is reduced and lower temperatures may lead to the death of the colony (Bradley, 1999). Paleoclimate studies on corals have focused on environmental records in coral growth rates, trace elements and isotopes, and this brought new insights into paleo-sea surface temperatures (SSTs), ocean circulation and tropical atmospheric circulation system. In the framework of Holocene climate reconstruction, the study of corals plays an important role, providing information on some critical aspects of the climatic system. Corals represent the only direct source of high-resolution data about tropical areas where ocean/atmosphere interactions are fundamental and offer information on important tropical systems such as El Niño Southern Oscillation (ENSO) and monsoons (Linsley et al., 1994; Dunbar et al., 1994; Evans et al., 1999; Tudhope et al., 2001).Coral records can also address paleoenvironmental questions about human impact and anthropogenic modifications of the environment. Century-long records can provide information about nutrient

availability, heavy metals, and other anthropogenic inputs that can show evidence of settlements, land-use changes or processes of industrialization (Fallon et al., 2002). For example, studies about coral growth and calcification allow to understand that the rapid increase of CO_2 levels is reducing the ability of corals to grow their skeleton (Langdon et al., 2000; Tanzil et al., 2009) showing a very strong connection between human activity and reef health, and suggesting new approaches to know how climate and reef environment vary naturally and how humans are impacting these systems.

2.3.4 Speleothems

Unlike dendroclimatology (see next section *Tree rings*) and ice-core paleoclimatology, which began in the early and mid $20th$ century, climatology based on the analysis of speleothems is quite a recent field of study. Speleothems are mineral deposits, mainly calcium carbonate (calcite), precipitated from groundwater in caves. They include stalagmites, stalactites, calcite veins and flowstone. Trace elements can also be present as impurities within the calcite crystals. One of these, uranium, can be used to determine the age of the record, using the uranium-thorium dating method (Frisia, 2012). Water seeping through cracks in a cave's surrounding bedrock may dissolve certain compounds, usually calcite, aragonite, or gypsum. The rate depends on the amount of carbon dioxide held in solution, on temperature, and on other factors. When the solution reaches an air-filled cave, a discharge of carbon dioxide may alter the water's ability to hold these minerals in solution, causing its solutes to precipitate and thus forming speleothems (Atkinson et al., 1987). The deposition of speleothems depends on different geological, hydrological, chemical and climatic factors. Little changes in one of these factors could cause stops on the water percolation, determining cessation of speleothem growth. When this phenomenon is observed over a large geographical area, it is likely due to climatic forcing. (Lauritzen, 1993, 1991; Lauritzen and Gascoyne, 1980; Lauritzen et al., 1990; Brook et al., 1990; Burney et al., 1994; Railsback et al., 1994; Richards et al., 2000; Fischer et al., 2009, 2010; Chu et al., 2012; Rudzka et al., 2012; Wassenburg et al., 2012; Whittaker et al., 2008; Woodhead and Pickering, 2012).

Speleothems may be annually banded or contain compounds which can be radiometrically dated. Thus thickness of depositional layers or isotopic records can be used as climate proxies. Speleothem growth is often linked with glaciation and deglaciation processes. For example, speleothems dated up to 350,000 years before present are found beneath the Columbia Icefield of Alberta, where the geomorphology has been influenced by glacial events (Spotl and Mangini, 2007).

2.3.5   Tree-rings

Dendrochronology is a scientific dating method based on the analysis of patterns of the growth of tree rings. Dendrochronology can date the time at which tree rings were formed to the exact calendar year, allowing to assemble long and continuous chronologies.

The study of the relationships between annual tree growth and climate is called dendroclimatology and started with Andrew E. Douglass's studies published in Ecology in 1920 (Douglass, 1920). The annual growth of a tree is the result of many interrelated biological and chemical processes, and may be affected by different aspects of the microclimate, such as sunshine, precipitation, temperature, wind speed and humidity (Bradley, 1985; Fritts, 1976), and by other non-climatic factors such as competition or soil nutrient characteristics. Dendroclimatology offers paleoclimatic reconstruction for most of the Holocene, with annual resolution.

In particular, the layers of new xylem or wood laid down each year under the bark of a tree (the annual ring) is a natural archive of growth during that year. The environmental conditions influencing that growth may leave an imprint on the properties of the ring. Thus the size, structure, and chemical composition of the ring provide information on those conditions.

There are several sub-fields of dendroclimatology associated with the processing and interpretation of different tree-growth variables. Such variables include tree-ring width (the most commonly exploited information source, e.g., Briffa and Matthews (2002)), densitometric parameters and chemical or isotopic variables (e.g., Epstein et al. (1976)).

Whenever tree growth is directly or indirectly limited by some climate variables, and that limitation can be quantified and dated, dendroclimatology can be used to retrieve information about past environmental conditions. Two types of climatic stress are commonly recognized: moisture stress and temperature stress. Trees growing in semi-arid regions are frequently limited by the availability of water, and dendroclimatic indicators primarily reflect this variable. Trees growing near the latitudinal or altitudinal treeline are mainly under growth limitations imposed by temperature; hence, dendroclimatic indicators in such trees contain strong temperature signals.

Dendroclimatology mainly contributed to the reconstruction of global and hemispheric temperatures during recent centuries and millennia, on various spatial scales. This capacity allows the application of dendroclimatology to a remarkable range of fields of direct relevance to human concerns, in addition to their relevance to the pressing questions of current and impending climate change. These include, for example, hydrology and the management of water resources and the study of the interaction and relationship between climate and ecological systems. Dendroclimatologic studies can be applied both to living or fossil plants which can be dated using the ^{14}C radiocarbon technique.

2.3.6 Peat bogs

Although peatlands have long been identified as effective climatic archives, research on peatlands still receives relatively little attention within the paleoclimatology community (Bradley, 1999). It is noteworthy, however, that the first indices of considerable climatic changes during the Holocene were registered in peat stratigraphical records (e.g.,Blytt (1876); Sernander (1908).

Figure 2.3: The Tollund Man (Silkeborg Museum). The Tollund Man lived during the 4th century BC; he was buried in a peat bog on the Jutland Peninsula in Denmark. Tollund Man is remarkable for the fact that his body, and in particular the face, was so well preserved that he seemed to have died only recently (from *www.mvmnt.it*).

Fens, marshes, and swamps are called minerotrophic wetlands as they receive their nutrition not only from the atmosphere but also from percolating groundwaters. In particular, marshes are fed by flooding surface waters. In contrast to fens, marshes and swamps, ombrotrophic peat bogs are hydrologically isolated from the influence of local groundwaters and surface waters, and mineral and organic matter is supplied exclusively by atmospheric deposition. The mineral matter percentage in these peats is normally less than 2% of the total mass. As a result of their isolation from the surface and underground hydrological system, the chemical composition of bog surface waters is dominated by reactions taking place between rainwater and the organic material (peat). The pore waters, therefore, are oligotrophic, acidic, and generally anoxic. This milieu effectively preserves plant and animal remains for thousands of years, allowing peat bogs to be used as archives of vegetation history, climate and environmental change (figure 2.3).

As described in Chambers et al. (2012), peat bogs records have three main advantages compared to other environmental archives: (i) a widespread distribution around the globe, providing better accessibility, global distribution and ease of sampling (e.g., compared to ice cores); (ii) because peats are almost exclusively constituted by autochthonous organic matter, they can be dated using radiocarbon techniques, leading to high-resolution and low-uncertainty chronologies (e.g., compared to non-varved lake sediments); and (iii) an accurate atmospheric signal, as they are isolated from groundwater (e.g., compared to lake and coastal sediments). Therefore, ombrotrophic mires provide a valuable archive to investigate climate environment relationships and paleo-environmental changes.

Chapter 3

Research Objectives

This dissertation contribute to the understanding of the environmental changes in the Dolomites, North Eastern Italian Alps, by end of the Late Glacial period placing historical records of climate changes into a longer term context of centennial to millennial scale variability. Specifically this study, through the analysis of a selected natural archive, addresses several Holocene paleoclimate benchmarks which characterized Dolomite region after the melting of the ice sheets.

The following primary sets of questions are addressed by analyzing the Holocene peat accumulation in Danta di Cadore bogs, Belluno province, for *(a)* changes in physical and chemical characteristics, and *(b)* changes in biological indicators. The results of this dissertation will contribute to our understanding of climate changes in the North Eastern Italian Alps, representing the first multi-proxy study carried out in this region. In particular, the objectives of this study could be summarized in the following questions:

- *Does Danta di Cadore peat bog represent an ideal natural archive to reconstruct past climate changes in the Dolomites?*

- *When does the Piave Glacier disappear during the Early Holocene and which is the timing that characterizes the retreating of the glacier?*

- *What is the history subsequent to the Piave glacier retreat? And in particular can we divide the amplitude of Holocene climate natural variability from changes related to anthropogenic impacts?*

- *Is our natural archive a record of climate changes on a regional scale and global scale? Can we compare data from this archive with data from other natural archives located in the Southern and Northern Alps?*

- *Did this archive record the human activity that characterized the recent history at a regional scale? Can we use this data to improve the historical and archaeological knowledge that we already have about Cadore region and more generally about Belluno province?*

In addition to these questions, another important point will be discussed, namely the application of a new analytical approach to determine the geochemistry of the peat. Indeed, the present thesis represents the first attempt to understand if the X-Ray Fluorescence core scanner can be used to describe the inorganic composition of the bog.

Chapter 4

Study area

The Dolomites area has been included into the World Heritage Sites in 2009, and includes sites of invaluable interest from botanical, geological, and historical points of view. Among the area's possible natural archives which could be used to reconstruct climate variations during the Holocene, we decided to use peatlands, and in particular the bogs located in Danta di Cadore.
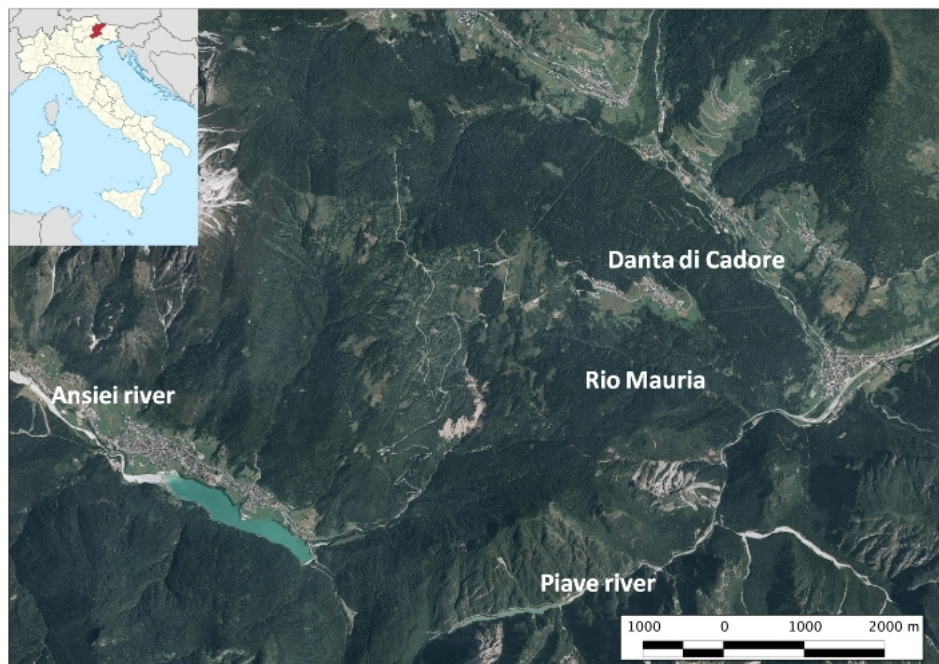
Figure 4.1: Geomorphological setting of Danta di Cadore.

The Danta di Cadore bogs (Belluno province) are located at about 1400 m a.s.l., in the upper sector of the Piave River basin, on the left slope of

the Rio Mauria valley (figure 4.1). This area is a European Community
Interest Site (SIC), identified by code number IT320060 (DIR 92/43/CEE-
2004/78/CE).

During the LGM the Piave basin was affected by widespread glacial cov-
erage (Bruckner, 1909; Castiglioni, 1940, 1967); at 21,000 years cal BP, the
Piave glacier covered the Danta di Cadore area with an estimated ice thick-
ness of 600 m (Bruckner, 1909). The mode and timing of deglaciation in the
mid-Piave basin (Vallone Bellunese) are considered to be well defined (Pel-
legrini et al., 2005). Glaciers retreated rapidly in this section of the Piave
basin, to such an extent that, at 18-19,000 years cal BP, the area was already
ice free. However, the deglaciation process is not well defined in the upper
Piave basin (Danta di Cadore), even though Castiglioni (1967) mapped the
extent of late-glacial stadial moraines.
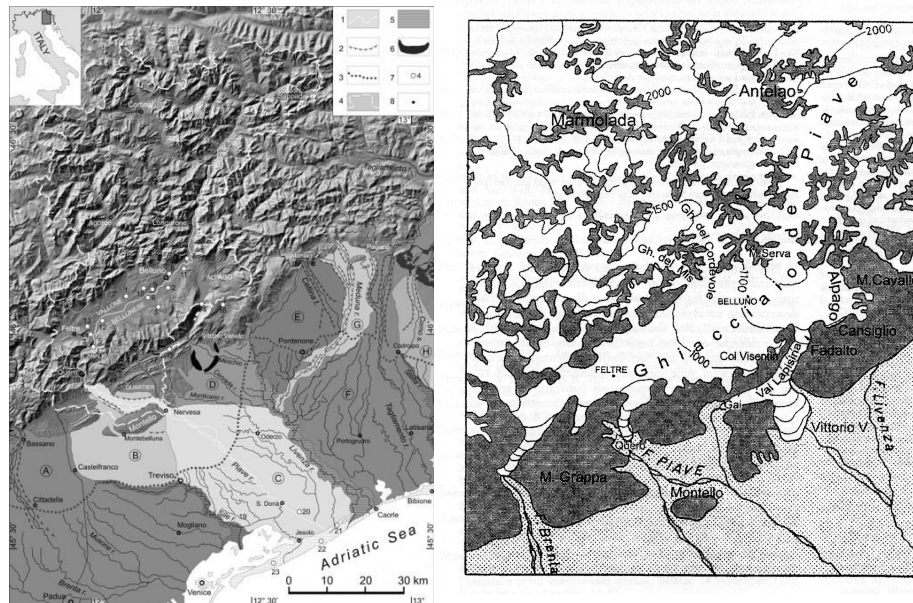
Figure 4.2: On the left the Piave glacier during the Last Glacial Maximum (from
Castiglioni 1940, modified); on the right, the simplified map of the Piave River basin
as outlined by Carton et al. (2009))

Considering the physical setting of the Danta area, it is likely that there
was an absence of local glaciers during the Late Glacial. Thus this area,
which is close to the junction of the Ansiei River valley with the Piave River
valley, was ice free when the Ansiei and Piave glaciers retreated. Such a
retreat could have occurred around 12-13 ky cal BP, according to the gen-
eral framework of glacier expansion/retreat reported by Carton et al. (2009).
Glacial processes created the morphological groundwork for the initial devel-
opment of lakes and subsequent bog development. The Danta peat bogs cur-

rently cover 197 ha. The site includes several peat deposits: Val di Ciampo, Cercená, Palú Longo and Palude della Mauria. Among these sites, Val di Ciampo is particularly unspoiled and represents the best stretch of active raised bog in the area. The presence of these particular ecosystems is the reason why we chose to investigate past environmental conditions through the analysis of a peat bog archive.

Chapter 5

Strategy: peat bog records from the Holocene

5.1 Peatlands: definitions and classification

Peatlands are defined as waterlogged areas in which at least 40 cm of peat has accumulated and where the rate of biomass production is greater than the rate of decomposition (Kuhry and Vitt, 1996). Peat is a blonde to black organic sediment, formed under water-saturated conditions from the partial decomposition of mosses and other bryophytes, sedges, grasses, shrubs, or trees. By definition, the concentration of mineral matter in dry peats is less than 25% by weight. The structure of peat ranges from fibrous to amorphous, and the relative proportion of carbon, hydrogen and oxygen varies according to the botanical composition and degree of decomposition (humification): typical concentrations are in the range 50 - 60 % C, 5 - 6 % H, 0.5 - 2 % N, and 0.1 - 0.5 % S; these elements generally tend to increase with decomposition, while the O content (30 - 40 %) decreases. Thus, these ecosystems continue to represent a sink for carbon, sulphur and nitrogen (Shotyk, 1988), and they are also probable natural sources of greenhouse gases (GHG) such as methane (CH_4) and sulphur dioxide (SO_2) (Sahagian and Melack, 1998).

The acidic, anaerobic waters retard the rate of decomposition of organic materials. For this reason, organic matter (plants and animals) remains preserved in peat profiles for millennia (Glob, 1969; Brothwell, 1986).

In the present study, the chosen classification is the one proposed by the NWWG (1988), which distinguishes between mineral wetlands, if the peat accumulation is less than 40 cm, and organic wetlands (or peatlands), if the peat accumulation is at least 40 cm. In addition, this classification identifies 4 main peatland types: fens, marshes, swamps and bogs.

Fens

Fens are meadow-like peatlands dominated by sedges, grasses, reeds, brown mosses, and shrubs. They are fed by solutions that have percolated through mineral soils.

Marshes

Marshes are wetlands and/or peatlands often associated with bodies of open waters; for this reason, they are subjected to periodic or regular inundations with standing or slowly moving waters. Flood waters can supply detrital mineral material that provides abundant plant nutrients; thus, marshes can be characterized by a luxuriant growth of sedges, grasses, rushes, reeds, and floating aquatic plants in the zones of open water.

Swamps

Swamps are treed peatlands and/or wetlands. Like marshes, they are subjected to periodic or regular inundations. Since most of the water has percolated through the surrounding mineral soils, it may be rich in dissolved solids. The vegetation in swamps is characterized by a cover of deciduous or coniferous trees, shrubs, herbs, and mosses.

Bogs

Bogs are domed peatlands in which the surface layers are hydrologically isolated from the influence of local groundwaters and surface waters. Bogs are supplied only by atmospheric deposition, thus they are characterized by nutrient-poor conditions (Clymo, 1983).

5.2   Peat bog forming system

Peat bogs develop in areas where precipitation exceeds evapo-transpiration and surface runoff, and they can form either by terrestrialization, infilling shallow lakes, or by paludification, water-logging terrestrial soils (Gore, 1983).

The very specialized vegetation at the surface layer, dominated by species of Sphagnum mosses, is due to the excess of water and to the low nutrient supply. Sphagnum (figure 5.1) that grows at the apex whereas deeper parts of the plants die, demands low pH and/or low concentrations of Ca and they contributes to acidifying the environment by releasing H^+ from organic acids in exchange for other cations. This extreme nutrient-poor condition is tolerated by Sphagnum species thanks to their slow growth rate, ability to conserve nutrient resources, long lifespan, and successful vegetative propagation (Backeus, 1985).

Figure 5.1: *Sphagum spp.* from Danta di Cadore peat bog system.

Therefore, the accumulation rate of organic matter is not only controlled by the plant growth rate and the resistance of plant species to decomposition, but also by the water table, which fluctuates in relation to rainfall, run-off, evaporation and the hydraulic conductivity of the peat layers. As a result of the decomposition of organic matter, bog waters are rich in dissolved organic carbon (DOC). Due to the low supply of mineral dust (atmospheric deposition only), the acids produced via the decomposition of organic matter (CO_2 and organic acids) are not neutralized, resulting in acid bog waters (pH 3-4) (Shotyk, 1988; Steinmann and Shotyk, 1997).

Generally, bogs are less decomposed than fen peats. Apart from the common shallow aerobic zone, the slow decomposition of peat bogs comes from the acid conditions and low abundance of nutrients. Mosses die at their base as their tops continue to grow: the dead lower parts sink into the underlying peat layers and are pressed together. Depending on how surface conditions change with time, the structure of the peat bog can vary with depth, presenting layers of a more amorphous character, but also containing woody debris of stalks and root parts. In fens, whose vegetation is dominated by higher plants, the peat accumulation is not confined to the peat surface, as the roots penetrate into old peat and then form a "mixed" peat with new and old organic matter. The decomposition is more intensive than in bogs because of less acidic conditions and more available nutrients (Clymo, 1983; Damman, 1995).

5.3 Physical and chemical proprieties of peat

5.3.1 Degree of decomposition

The physical and chemical properties of peat are strictly connected to botanical composition and to the degree of decomposition. During decomposition, the structure of the peat changes from fresh plant material to amorphous humic matter. In the first stage, the degree of decomposition of the peat matrix is governed by the nature of the environment in which the plant material was initially deposited and by the subsequent position of the water table; in a second stage when the peat is permanently waterlogged, the decomposition is very slow and the degree of decomposition depends mainly on the rate and duration of decomposition in aerobic conditions. In particular, in the acrotelm, the layer of oxygenated peat overlying the water table, a litter mass loss of 80-90% occurs, whereas once the peat is submerged below the water table in the anoxic catotelm, it decomposes at only 0.1% of the rate of the acrotelm (Clymo, 1984; Frolking et al., 2001). Many techniques for determining the degree of decomposition are available. The best-known method is the von Post humification scale (Von Post and Granlund, 1926): it involves taking a sample of raw peat and squeeze it, in order to determine if the water expressed differs in color and turbidity. The result is expressed in degrees of humification on a 10-point scale, in which undecomposed or little decomposed peat, which releases almost clear water, is defined as H1, whereas the completely decomposed peat, with no discernible plant structures, is defined as H10. Although it is a subjective method, its simplicity, reproducibility, speed and ease of use in field has made it very common.
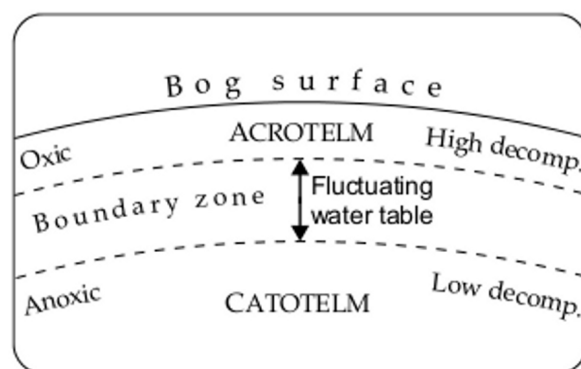
Figure 5.2: Schematic picture showing the position of the acrotelm, where the active decomposition takes place, and the catotelm, with a very low decay rate, in relation to the fluctuating groundwater table near the bog surface. The fluctuations of the groundwater table determine the depth of the acrotelm.

5.3.2 Hydrology

Peatland hydrology influences on different scales the diffusion rates of oxygen and gas, redox status, nutrient availability and cycling, and the composition and diversity of species. The hydrologic state of a wetland can be summarized as the result of the balance between inflows and outflows of water. The water balance equation can be simplified as:

DS = P - E + SI - SO + GI - GO

where DS is water volume stored, P is precipitation minus canopy interception (interception is the part of the precipitation that is caught by the canopy and evaporates back into atmosphere without reaching ground), E is evapo-transpiration, SI and SO are surface water inflow and outflow, respectively, and GI and GO are groundwater inflow and outflow. From the viewpoint of geochemistry and transport, the most important region is the one above the water table, where the pores are still saturated. It is this region, rather than the water table, which marks the limit of saturation. It is almost non-existent for undecomposed, fresh surface peat layers, but is often 20-40 cm thick for more decomposed layers.

If hydrology influences the chemical characteristics of the bog profile, the chemistry of water is affected by local geology, origin (sea, mineral, organic soils, precipitations), biological activity and by the often varying conditions of pH and redox potential (Clymo and Hayward, 1982).

5.3.3 Peat chemistry: dominating processes

The common characteristic of wetland soils is that they are formed under conditions of saturation: during the growing season, saturation last long enough to develop anaerobic conditions. In peat soils, the organic material naturally dominates soil conditions, and the decomposition of the organic components takes place mainly by aerobic microbial activity in the acrotelm, while anaerobic microbial metabolism occurs in the catotelm. In the border zones between acrotelm and catotelm, there are probably other processes of organic matter oxidation, although nitrate, metal oxides and sulphur concentrations are generally low in peat. The most important agents of decay present in peat are fungi (e.g., *Cladosporium, Trichoderma, Geotricum, Fusarium*) and bacteria (e.g., *Bacillus, Pseudomonas, Achromobacter, Desulfovibrio, Clostridium*). Fungal mycelia are abundant in the oxygenated zone and become much rarer in the anaerobic zone (Given and Dickinson, 1975).

The chemical composition can be understood in terms of the processes of death and decomposition of bog plants. Living plants contain mainly proteins, carbohydrates, lipids, and polyphenols such as lignin, along with smaller organic and inorganic compounds. Cellulose, which constitutes a

large fraction of the plants carbohydrate content, forms the cell's walls and shapes the structure of the plants. Other carbohydrates, such as simple sugars, are water-soluble and more transient, consumed by the plant in order to make cellulose or oxidized to provide energy. When a plant dies, its sugars are rapidly released into the environment and consumed by microorganisms. Starches are also quickly digested, while hemicelluloses, pectin and gums are attacked more slowly and tend to survive along with cellulose to form the peat. Nitrogen in plant proteins is lost, largely as ammonium salts going into solution, although some of the amino acids or their derivatives appears in the formation of peat humic compounds. Humic compounds, composed by humic and fulvic acids, are the group with the greatest influence on the properties of the peat. They are characterized by remarkable ion exchange and binding, colloidal affinity and water absorbing capacity (Stevenson, 1994). In addition, as peat humic acids precipitate naturally, they cover the easily degradable organic materials, retarding degradation processes and favoring the conservation of plants and animals remains (Mathur and Farnham, 1985). The heterogeneous group of lipids within plants encompasses fats and oils, which are largely hydrolyzed during decomposition into glycerol, readily consumed in anaerobic conditions, and fatty acids, which remain mostly unaltered in peat, together with other lipids such as waxes and steroids. These substances, extensively extractable by means of organic solvents, are collectively called bitumens (Clymo, 1984).

Woody plants, grasses, reeds and sedges contain varying amounts of lignin, a phenolic material of high molecular weight that works as a cementing substance for the cellulosic cell structure. During plant decomposition, lignin is relatively stable. Mosses and lichens do not possess lignin but have similar chemical substances. In peat analysis, lignin-like elements are often grouped together with humic acids, as these substances are similarly polyphenolic in character. Unlike lignin, humic acids have a high carboxylic acid content and a significant amount of nitrogen. However, a precise identification of all peat constituents is hardly possible.

Since the diffusion of oxygen from the surface down into the soil is very slow, it is often readily consumed by bacterial activity. Bacteria proceed through a sequence of reactions in which the available oxidant determines the dominant process at a particular level. At the same time, these processes will greatly influence the redox potential of the system.

If O_2 is present, aerobic decomposition is the major pathway. When O_2 is depleted, organic matter degradation shifts to denitrification. Once nitrate is fully utilized, metal oxides such as MnO_2 and Fe_2O_3 may serve as oxidants. When the latter are no longer available, the next step could be sulphate reduction. The final step in the oxidation is when the organic matter itself or CO_2 become the electron acceptor (oxidant), and methane is produced as a final product. In bogs and poor fens, due to the small amount of inorganic substances in comparison with the amount of carbon compounds, CO_2-CH_4

transformations dominate the redox potentials in the layers situated below the water table, which does not exclude CH_4 transformations in mineral-soil wetlands.

The pH of wetland soils and water vary widely among wetland types. Organic soils are often acidic, with the exception of rich fens, and mineral soil wetlands often are close to neutral. Some of the dominant elements which get reduced while involved in the oxidation of organic matter also affect the pH, depending on their function as acids or bases in the transformation between oxidized or reduced forms. pH is also influenced directly by the organic compounds, by their decomposition and the following organic acid generation.

5.4 Paleoclimatic reconstructions from peat bogs

Peat formation is widespread across the globe and it is present in any area where production of plant material exceeds its decay. Presently peatlands cover more than 5% of the Earth's total land area, as reported by the International Peat Society (*www.peatsociety.org*). The growth of peat material dependency on moisture and temperature conditions means that rate and nature of peat accumulation is partially determined by climate conditions.

The use of peat, especially from ombrotrophic bogs, as an archive for climatic and environmental change has a long history. The exceptional value of peat for paleoclimate studies was recognized for the first time by Blytt (1876) and Sernander (1908). They developed a scheme known as the *Blytt-Sernander scheme* that established the principal terminology of Holocene climate change. This terminology was used in Europe for more than half a century.

In 1910, the hypothesis of a *regeneration* of peat growth was presented at the Geological Congress in Stockholm (von Post and Sernander, 1910) and this hypothesis, like the one on the autogenic succession of peat (Osvald, 1923), led to a misconception on how ombrotrophic peatlands develop.

From then on, the prevailing view was that peatlands grow thanks to autogenic processes and not under climate control, reducing the potential of peat-based paleoclimatic science (Chambers and Charman, 2004). Successively, Aaby (1976) reported a study on cyclic, sub-Milanković-scale climate changes, basing his interpretation on colorimetric peat humification and data on rizophoda (testate amoebae) from Danish peat cores. Finally, in 1981, Barber (Barber, 1981) rejected the hypothesis that *regeneration* was the primary process of peat accumulation in ombrotrophic bogs. In his study about peat stratigraphy, he shows that peat growth could be stationary for different periods of time, and he concludes that the growth of a peat bog is controlled by climate, while other variables such as hydrology, drainage and the life cycle of plants are all subordinate to climatic conditions. Based

on studies at Bolton Fell Moss, northern England, he proposes that raised mires provide a continuous record of past hydroclimatic change, as they are directly coupled to the atmosphere.

Wetlands do not always act as repositories of climatic and environmental changes, but are influenced by different processes and external forcing. To derive high-quality climatic data from peatlands, the challenge is to select proper sites that represent the most sensitive records connected to climate. In this framework, the hydrological characteristics of a peatland play a key role. We can divide peatlands in two hydro-morphological types. First, ombrotrophic peatlands, fed solely by atmospheric precipitation. Their water balance is a function of climate: it depends on the rate of precipitation and loss in evaporation and, to a lesser extent, on vegetation cover. In this case, peat record can be interpreted as a result of changes in effective precipitation. Second, minerotrophic peatlands depend for their moisture on direct precipitation but also on surface runoff and groundwater. This is the reason why minerotrophic peatlands are less tightly connected to climate changes (Shotyk, 1996). Ombrotrophic peatlands generally overlie minerotrophic peatlands, which developed in the post-glacial period after valley glaciers melted, and which recorded shifts in drainage, climate, hydrology, geomorphology and glacial geology. Over the Holocene, these environments recorded both natural and climatic variability, and the impact of human activities, and their evolution provides a sufficiently lengthy time series to reconstruct past environmental conditions and to assess natural variability in biotic and abiotic systems. Peat cores from ombrotrophic bogs provide valuable records of soil dust, volcanic ash particles (Shotyk et al., 2002a; Weiss et al., 2002; de Jong et al., 2006; Sapkota et al., 2007; Le Roux et al., 2012), marine aerosols (Singh and Kanakidou, 1993), major and trace metals of natural and anthropogenic origin (Pheiffer Madsen, 1981; Shotyk, 1996; Shotyk et al., 1998; Martinez-Cortizas et al., 1999; Weiss et al., 1999; Givelet et al., 2003) and organic pollutants extending back through centuries or millennia (Berset et al., 2001; Dreyer et al., 2005a,b; Zaccone et al., 2009b), and have often been used for paleoclimatic and paleo-vegetational reconstructions (Aaby, 1976; Van Geel, 1978; Tareq et al., 2004; Röpke et al., 2011; Zaccone et al., 2011; Chambers et al., 2012; Langdon et al., 2012).

Even if several studies about peat bogs as archives of atmospheric trace elements depositions have been published, one of the most crucial sometimes unsolved point is the possibility of post-depositional migration of metals. Until now, only Pb and Hg have been shown to be immobile in peat layers (e.g. Pheiffer- Madsen, 1981; Vile et al., 1995; Shotyk et al., 1996; MacKenzie et al., 1997; Benoit et al., 1998; Vile et al., 1999; Weiss et al., 1999; Givelet et al., 2003). Due to the binding capacity of organic matter, one could hypothesize that elements such as Cu would also be immobile along the profile, and that variations in its concentrations could probably reflect atmospheric history. On the other hand, other elements, such as Fe and Zn,

are probably redistributed after deposition, e.g. by plant activity (Livett et al., 1979; Jones, 1987; Livett, 1988; Espi et al., 1997). These considerations must be taken into account when dealing with the profiles of trace and rare earth elements.

5.4.1 Peat chronologies: methods selected for the research purpose

One of the most important factors for the successful use of any paleo-climate proxy is chronological control. Peat, once dried, is more than 50% carbon and is entirely autogenic: as a result, this kind of peat is one of the best Holocene materials for radiocarbon dating. Moreover, it is common to find organic macrofossils preserved in peat which can also be easily dated. The main methods used to establish peat chronologies are based on radiocarbon dating and recent atmospheric fall-out radionuclide.

^{14}C Dating method

There are three main carbon isotopes that occur naturally: ^{12}C, ^{13}C, both stable, and ^{14}C, which is unstable and radioactive: these isotopes are present in the amounts of 98,89%, 1,11% and 0,00000000010% (Piotrowska et al., 2011) respectively, meaning that, in modern material, every atom of ^{14}C exists for every trillion of ^{12}C atoms. The radiocarbon method is based on the rate of decay of ^{14}C. ^{14}C forms in the upper atmosphere through the effect of cosmic ray neutrons upon ^{14}N. Suddenly formed, ^{14}C is oxidized to ^{14}CO$_2$, entering the carbon biogeochemical cycle. Every plant and animal which utilizes carbon in biological food-chains absorb ^{14}C during their life time. As soon as plants and animals die, they stop the metabolic function of carbon uptake and ^{14}C only decays back to ^{14}N, emitting beta particles, and electrons with an average energy of 160 keV.

Arnold (1949) were the first to measure the rate of its decay and they determined that the half-life of ^{14}C beta decay was 5568 ±30 years. The current best value for the half-life is 5720 ±30 years, but the value established in the 1950s is still used and represents the basis for the conventional definition of radiocarbon dating time scale (Piotrowska et al., 2011). After 10 half-lives times, the total amount of radioactive carbon present in a sample become very small: that's why 50-60,000 years cal BP represent the limit of the radiocarbon dating technique.

The radiocarbon age is calculated from the constant concentration of ^{14}C in the biosphere and from the concentration of radiocarbon in the sample at present, setting present at AD 1950: the values of the conventional radiocarbon age of every sample is calculated using the half-life T$_{1/2}$ (Piotrowska et al., 2011). A calibration of the final results is necessary, because radiocarbon ages differ from calendar ages. ^{14}C content of atmospheric CO$_2$
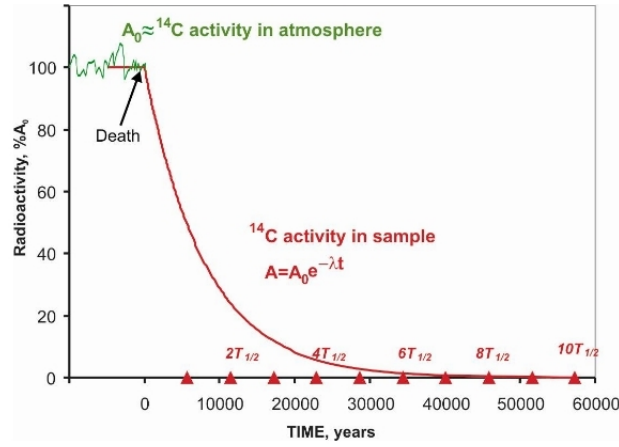
Figure 5.3: Changes of radiocarbon activity in organisms initially assimilating carbon from the atmosphere, then dying at TIME=0 and subsequently being incorporated into a peat sample. The initial radiocarbon activity of the sample would be equal to atmospheric ^{14}C activity (A0), provided that no fractionation occurred during assimilation of CO_2. After death, the ^{14}C content/activity (A) decreases with time according to the law of radioactive decay (λ: decay constant; t: time; $T_{1/2}$: half-life), (Piotrowska et al., 2011).

fluctuates for several reasons: changes in the Earth's magnetic field, in the carbon cycle, changes due to influence of solar wind, cosmic rays, and anthropogenic impacts. The relationship between ^{14}C and calendar age is far from straightforward, and therefore requires a calibration curve (Reimer et al., 2013). The standard ^{14}C calibration often causes single ^{14}C ages to correspond to a range of calendar ages. Moreover the distribution of calibrated dates is usually reduced to 1 or 2 standard deviations calibrated ranges. The calibration of a set of radiocarbon ages is usually performed using dedicated statistical programs such as OxCal, and the currently internationally accepted calibration curves are IntCal09 (northern hemisphere atmospheric; (Reimer et al., 2009)), Marine09 (for marine dates; (Reimer et al., 2009)), and SHCal04 (southern hemisphere atmospheric; (McCormac et al., 2004)).

In order to obtain ages for all the undated depths in a continuous sequence, after calculating and estimating radiocarbon ages, the following step is to build up an age-depth model. The difficulties of age-depth modeling pertain to the irregular distributions of the calibrated ^{14}C dates, which cannot be reduced to single point estimates with symmetric error bars. Moreover, modeling software often uses linear regression or spline functions which generally cannot deal with irregular distributions and do not take into account changes in the accumulation rates or the presence of hiatuses. The model chosen in the present study is the "Clam" age-depth model proposed by Blaauw (2010). This model calculates confidence intervals for the undated levels using a Monte Carlo approach: (i) every calibrated age distribution
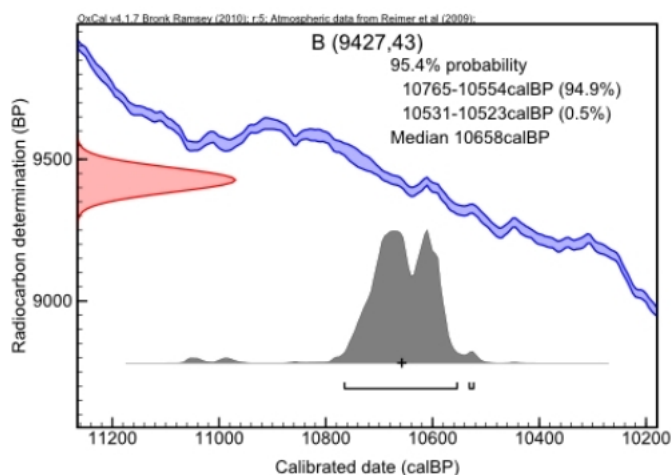
Figure 5.4: Example of calibration of a sample of radiocarbon age. The calibration curve is shown (in blue), and the probability distribution of the sample's calendar age is plotted on the horizontal axis. Probabilities are plotted at an arbitrary scale, and the dark grey areas represent 95.4% ranges of age. (Piotrowska et al., 2011).

is sampled to choose a calendar age with the probability of every year chosen proportional to its calibrated probability; (ii) an age model is built up through these points and (iii) for every undated depth the calendar age is obtained. The sampling process of selecting dates are repeated 1000 times as default. For every depth, its calendar age points are normalized in order to create an estimate of the confidence interval which falls between 1 sd and 2 sd. Finally, in order to find the single best age-depth model among all the iterated age-depth models, "Clam" calculates the weighted mean or the mean point of all sampled calendar ages.

^{210}Pb Dating method

Given the limiting factor of the ^{14}C dating method, namely the extremely low percentage of radioactive ^{14}C in the modern material, a different dating method must be used for peat sequences which cover the last 150 years. Based on the same principle as exponential radioactive decay, the ^{210}Pb dating method can be used to date recent peat chronologies. ^{210}Pb is a natural radionuclide produced by the 238U radioactive chain through the intermediate daughter ^{222}Rn gas, and is supplied to the peat as a combination of supported and unsupported fractions. Determination of these two fractions is essential to date the peat sample. The unsupported ^{210}Pb is the part derived from ^{222}Rn which, diffusing through rocks and soils, reaches the atmosphere and starts to decay: once formed, the ^{210}Pb rapidly binds to atmospheric particles and is deposited on the Earth's surface. In particular, in ombrotrophic peatlands, we assume that the main component of ^{210}Pb

is unsupported (Appleby et al., 1997). ^{210}Pb has a relatively short half-life $T_{1/2}$ of 22.3 years, and the amount of excess ^{210}Pb is detectable only after about seven half-lives (approximately 150 years) (figure 5.5).
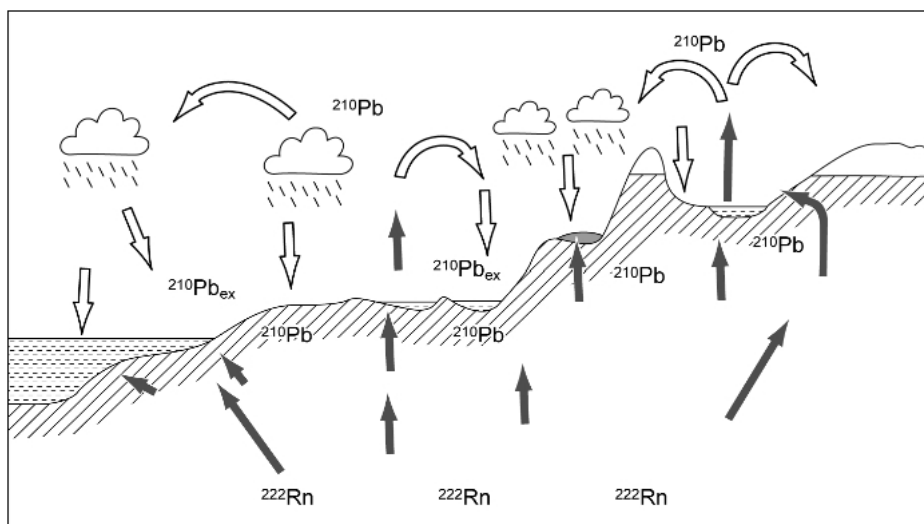
Figure 5.5: ^{210}Pb production and relative atmospheric deposition levels (after Preiss et al., 1996)

In addition to this method, in order to achieve a more accurate final dating, other chronological markers are usually monitored, such as all the radionuclides associated with the development of military weapons and with energy production. These kinds of activity can release in the atmosphere ^{90}Sr, ^{134}Cs, ^{137}Cs, ^{239}Pu, ^{240}Pu, ^{241}Np, ^{241}Pu, ^{241}Am and ^{14}C, and if their signals are detectable in the peat sequence, they could be used within ^{210}Pb data. The best example of the emission in the atmosphere such markers is represented by the catastrophic nuclear reactor explosion at Chernobyl in Ukraine on 26th April 1986, an incident which released 2×10^{18} Bq of ^{137}Cs into the atmosphere. Other older signals can derive from weapon tests which, unlike the "Chernobyl event", push radioactive particles into the high atmosphere, achieving a global distribution (Appleby, 2001).

5.4.2 Proxy data from peatlands for the paleo-environmental and paleo-climatic study

In order to achieve a reliable reconstruction of past climate using ombrotrophic bogs, not all available proxies and techniques have universal applicability, owing to differences in mire-species assemblages, peatland formation, topographic controls, and geochemical characteristics. Peat bogs are an ideal archive for reconstructing Holocene climate dynamics, because they present a high capacity of preservation of several biological proxies and small inorganic particles: this combination of inorganic geochemical proxies with

mineralogical and biological proxies is thought to be the key to a better understanding of the causes and consequences of short-term climatic events in the Holocene.

Among the most widespread proxy data from peat bog sediments, we chose the following ones:

Peat stratigraphy

Visible stratigraphy from peat bogs and mires has been largely used to make interpretations about past climate changes. Along the peat profile, layers that differ in color were considered indicative of different climate conditions: drier, warmer, wetter or cooler. These transitions were used by Scandinavian scientists Blytt and Sernander to describe the postglacial period in Northwestern Europe Blytt (1876); Sernander (1908): they used a transition from a dark, highly decomposed peat to a lighter variety of peat, dated around 850 cal BC, to mark during the Early Holocene the boundary between the dry and warm Sub-Boreal and the cooler and wetter Sub-Atlantic. Several factors play a crucial rule in the differentiation of horizons: the size of the bog itself, the age and dating, the fluctuation of the basal topography, and hydro-morphological conditions. However, even if this technique cannot provide evidence of environmental changes by itself, it could be used in combination with other data (on density, trace elements, pollen, diatoms, chironomids) to retrieve ancillary information.

Peat humification

Peatlands undergoing continuous and active growth accumulate organic mass and sequestrate carbon (C) as excess of vegetation production over decay (Chambers et al., 1997). C is used by vegetation in the photosynthetic process in the form of carbon dioxide which mostly comes from the atmosphere. For their part, peatlands release C during the decay process. Peat humification is considered a paleoclimate proxy that reflects changes in hydrological conditions (Chambers et al., 2012). In particular, peat humification measures the decay in the upper layer of a peat bog, the *acrotelm*. This layer is subjected to the fluctuations of the water table and, in dry condition, it can undergo highly variable rates of decay. Anaerobic decay can continue at a slower rate in the lower horizon, the *catotelm*, releasing methane (CH_4). Peat humification as a proxy of the degree of decomposition can be determined in several ways: by using the von Post scale (Von Post and Granlund, 1926) visually in the field, or by analyzing its fibrosity, and chemical properties with other scales.

Pollen and non pollen palynomorphs

Palynology was introduced in 1916 by von Post (von Post, 1916) and started being applied in the 1940s. It soon became one of the most widely used techniques for the reconstruction of Quaternary paleoecology (Birks and Birks, 2004).

Since the first Holocene paleo-ecological reconstructions, pollen from peatlands has often been the only and sometimes the main proxy used by scientists. Paleopalynology is used to infer information about vegetation history, biostratigraphy, geochronology, climatic changes, and responses to in-situ agricultural practices.
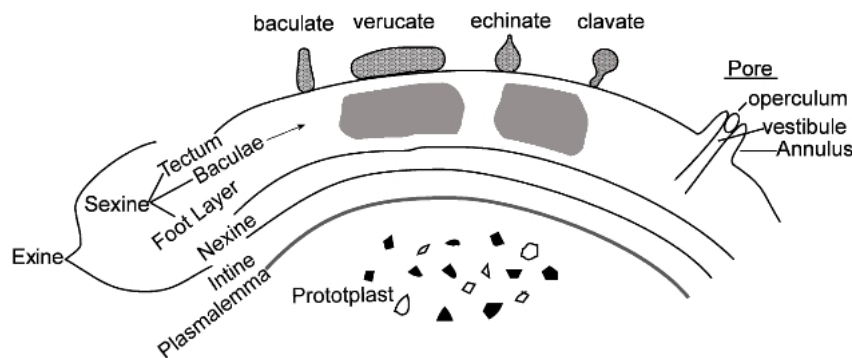
Figure 5.6: Pollen structure.

The theory behind pollen analysis is that pollen grains are released by plants, transported and then deposited upon the Earth's surface. Indeed, pollen, defined as the multi-nucleate gametophyte generation of flowering plants, represents the actual surface vegetation growing over the studied area. Pollen transported through the air (pollen rain) may be deposited over land or water bodies such as peatlands, then sinks to the bottom of the basin and becomes part of the accumulating lacustrine or peat sediment. When pollen is deposited in water, its outer layer (the exine) may remain intact for thousands and even millions of years, because it is made of sporopollenin. Sporopollenin is a substance composed of oxidative copolymers of carotoid and carotenoid esters. It is extremely durable and can be found in anaerobic sediments dating back hundreds of millions of years.

As it becomes part of the fossil record and represents terrestrial vegetation, pollen may be used to interpret the vegetation which existed in the past. Furthermore, since plant taxa growing is climate-related, fossil pollen may be used to interpret past climates. This is useful when attempting to reconstruct the Earth's climate and ecology, as pollen existed before any instrumental records or observations made by humans.

The taxa, or types, of pollen can be determined by pollen morphology or structure. Large databases of images and diagrams are being designed for

the identification of pollen. The presence and amount of pores (holes) and culpi (furrows), as well as their arrangement on the sphere surface, are clues that help us identify pollen taxa.

Stable Isotopes

In studies about climate reconstruction, stable isotopes signatures are extremely valuable proxies. In the particular case of peat bogs, where the only source of water is precipitation, bog plants register isotope ratios as a function of precipitation (Brader et al., 2010). Oxygen isotope ratios are typically measured from cellulose extracted from peat, and it has been demonstrated that they are well correlated with various climatic parameters, in particular with temperature and relative humidity (Chambers et al., 2012). For hydrogen isotopes, measurements are usually performed on leaf-wax biomarkers such as n-alkanes or n-fatty acids: leaf wakes of vascular plants from aquatic environments are widely used to reconstruct the hydrogen isotopic composition of precipitation, and recently started to be applied also to peat samples (Seki et al., 2009). Carbon isotopes in peat can be measured from cellulose, leaf-wax compounds and from non-extracted bulk samples (Chambers et al., 2012). Although paleoclimatic data from these proxies are becoming extremely important, the interpretation of the isotopic composition in peat in terms of environmental changes is complicated by several factors, which include: the varying time resolution due to unevenly spaced dates and growth rates, species-specific differences, partially unknown biochemical pathways in plant tissues, and signal preservation in decomposed peat. Because of these factors, stable isotope records from peat sequences must be used and compared in a wider framework with other proxy-data (Tillman et al., 2010).

Inorganic geochemistry

Mineral dust present in the atmosphere can affect and modify the Earth's climate system in different ways: adsorbing and scattering incoming solar radiations, acting as a nuclei condensation, allowing the formation of clouds, and adsorbing many other chemicals present at the same time in the atmosphere. Thus, the fluxes, mineralogy and chemistry of these particles are extremely important for understanding climate changes connected with changes in atmospheric chemistry and in global bio-geochemical cycles. Over recent decades, various techniques have been developed to optimize the geochemical analysis of the inorganic components of peat samples, enabling the reconstruction of past human activities on the basis of their effects such as atmospheric pollution or environmental changes. These techniques range from non-destructive elemental analyzes, such as X-Ray fluorescence (XRF), to high-resolution inductively coupled plasma mass spectrometry (ICP-MS, HR-ICP-MS). While XRF has the limiting factor of detection limits for some

elements, ICP-MS techniques allow measurements of elements at very low concentrations (down to μg/Kg or ng/Kg). Other techniques have been used for peat geochemistry, such as inductively coupled plasma optical emission spectroscopy (ICP-OES) (Yafa et al., 2004), scanning electron microscopes equipped with an energy dispersive XRF analyzer (SEM-EDX) (Krachler et al., 2002). Scanning XRF is also giving promising results. ICP-MS can also be used to analyze the isotopic composition of peat samples, for example Pb , Sr, Nd and U isotopes.

Part II

Fieldwork and Methods

Chapter 6

Coring, sampling and subsampling

In order to have successful results using peat cores for paleoclimatic studies, is necessary to carefully select an ideal archive that has preserved high quality climatic signals through time.

To reconstruct the history of atmospheric trace element deposition and trends of environmental and vegetational evolution, the first criteria for a good selection are represented by peatland morphology, botanical composition and site hydrology. In particular ombrotrophic peatlands have to be preferred to minerogenic wetlands because they receive nutrition solely from atmospheric deposition in form of wet and dry precipitations and are completely isolated from influences of water runoff or groundwater floating (Shotyk, 1996). A combination of both biological and chemical characteristics has to be studied for identifying ombrotrophic conditions: some of them can be used directly in the field, other successively in the laboratory. Also the bottom mineralogical composition of the basal sediment of the site has to be considered because weathering of minerals from the underlying rocks could be a very important source of ion migration into the minerotrophic section of the peat by diffusion mechanisms (Shotyk and Steinmann, 1994).

6.1 Selection of the site and collection of the peat bog cores

Since peatlands in an alpine province as Belluno are widely distributed, not all these sites are appropriate for the reconstruction of the changing rates of atmospheric deposition. The suitable sampling site was identified on the basis of several previous botanical investigations and geological surveys, carried out with the collaboration of experts in local geology, botany and geomorphology. The in field determination of ecological and geomorphological conditions with the evaluation of the existing data about peatlands
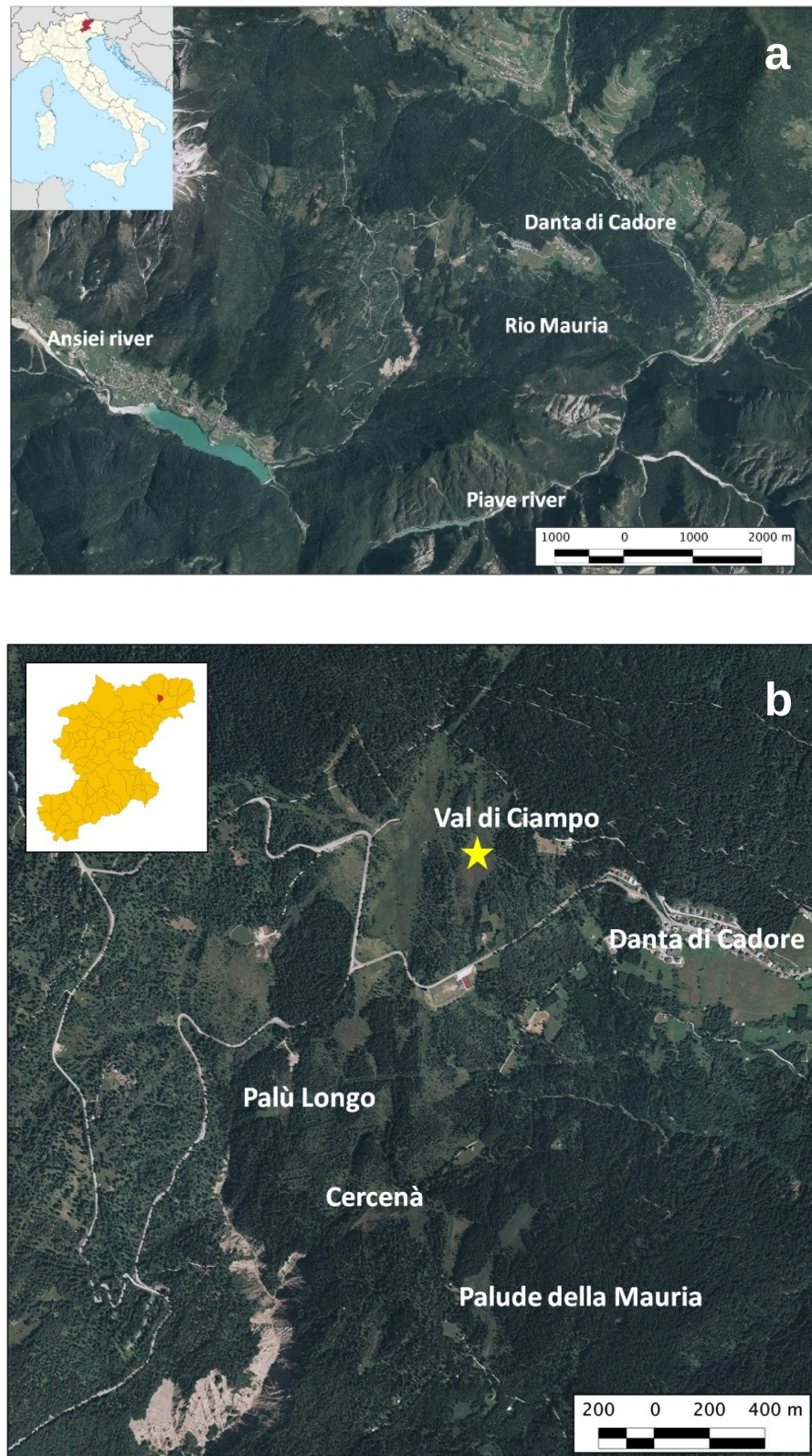
Figure 6.1: Panel (a) Geographical and geomorphological setting of Danta di Cadore. Panel (b) Major peat bogs near Danta di Cadore, the yellow star indicates Val di Ciampo peat bog: the ampling site selected.

and biotopes in Belluno province, lead to a final choice on Danta di Cadore peat bog system. In particular we selected Val di Ciampo bog, one of the best stretch of active raised bog in Belluno province identified by the habitat code 7710* (*http : //www.regione.veneto.it/web/ambienteeterritorio/*).

A visual botanical inspection of modern vegetation growing on the surface of this bog provided the first evidence of ombrotrophy in the uppermost layer of the peat: the presence of *Sphagnum magellanicum, Sphagnum majus, Sphagnum squarrosum, Sphagnum capillifolium, Drosera rotundifolia, Drosera longifolia, Andromeda polifolia* and *Vaccinium microcarpum* indicates oligotrophic and acidic conditions typical of peat deposits hydrologically isolated from the influence of local groundwaters (Shotyk, 1996). The complete vertical peat bog core from Val di Ciampo (46°34'16" N 12°29'58" E) was collected in June 2011.

To provide reliable information about climate, sections from the archive have to be collected as an undisturbed continuous profile, extending back in time as long as possible. The intrinsic low density of the top layers of a bog makes challenging the recovery of a very good quality core. It is very difficult to cut these layers avoiding any form of compression without using the appropriate coring technique, and losing precision during sampling means losing the age-depth relationship. For these reasons bog profile has been collected with the best available technology (figure 6.2). In particular the uppermost layers of the peat were sampled using a 16x16x100 cm modified titanium Wardenaar corer (Wardenaar, 1987). This type of sampler minimizes vertical compression and provides enough peat sample material to conduct a wide range of analysis (Givelet et al., 2004; De Vleeschouwer et al., 2012b; Zaccone et al., 2012). The deepest layers of the bog were instead collected with a Belarus corer (Belokopytov and Beresnevich, 1955), a semi-cylinder 50 cm long and 10 cm wide. We obtained the core from a domed section of the bog, where the total accumulation is more than 6 meters in depth. A total of 7 meters core was finally collected.

6.2 Slicing the core: the subsampling strategy

After the extraction the surface of each core was wrapped in polyethylene cling film. Each core was covered with plastic, labelled and placed in wooden core boxes built specifically to conserve the cores. Boxes lids were attached using screws. In this way, handling of the core in the field is kept to a minimum.

Immediately after collection the entire core was first frozen at -18°C and then cut in cold conditions using a self-modified stainless steel band saw: this way is considered the best to have a high resolution records of atmospheric depositions (Givelet et al., 2004).

Figure 6.2: Val di Ciampo peat bog, as spring (a) and as autumn (b). Wardenaar corer (c-d). Panel (d) shows the high Wardenaar corer capacity of no-compressing during sampling. Belarus corer (e-g). Panel (f) is a picture of a middle core section collected with the Belarus corer, panel (g) shows the final section of the entire core with layers of lacustrine origin.

The core was cut longitudinally in 2 sub-cores. One sub-core was pre-served for continuous X-Ray Fluorescence (XRF) core scanner analysis, while the other was used for physical, chemical and biological measurements. This second sub-core was cut into 1-cm slices and each slice was then divided into 6 squares to obtain several sub-samples. The outside edges were discarded to ensure that only the uncontaminated part of each sample was used for anal-ysis. The sub-samples for each analytical determination were taken from the same position in each slice. The sub-sampling strategy outline is presented in figures 6.3 and 6.4.
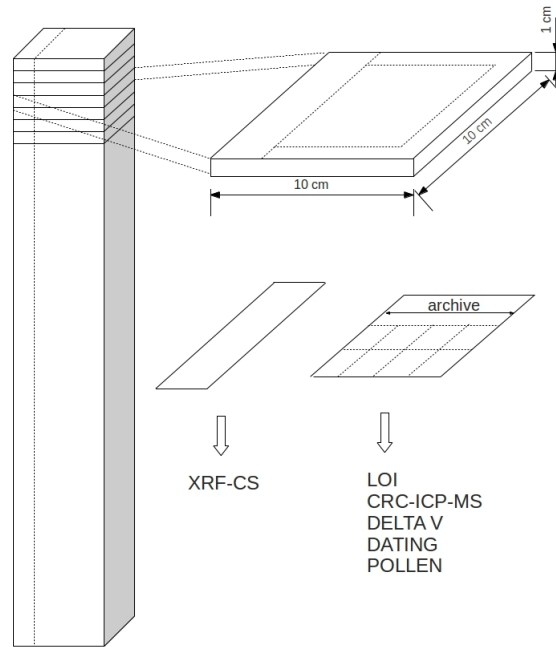
Figure 6.3: Sub-sampling strategy outline.
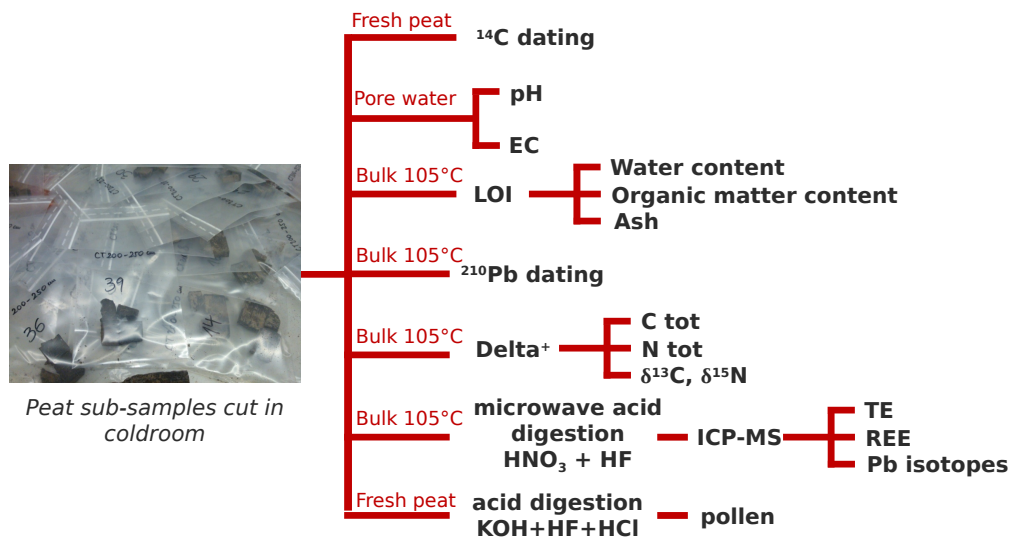
Figure 6.4: Description of the physical, chemical and biological analyses carried on each layer of the bog: the adopted sub-sampling strategy allows the possibility to apply a multi-proxy approach with a wide variety of analyses.

Chapter 7

Dating

High quality data are necessary to build up a reliable and precise age-depth relationship. In order to establish a detailed chronology, multiple dating techniques have been used: Val di Ciampo bog age-depth relationship is based on Accelerator Mass Spectrometry (AMS) ^{14}C, ^{210}Pb and ^{137}Cs measurements.

7.1 Radiocarbon and ^{210}Pb dating

For radiocarbon dating peat, wood macrofossils and shells were carefully selected from the core: in total eight samples were collected at different depths, cleaned with Milli-Q water, dried at 105°C (as described by Piotrowska et al. (2011)).

Successively they were submitted for radiocarbon analysis to the Chrono Centre, Queens University of Belfast ($http : //www.chrono.qub.ac.uk/$).

Figure 7.1: Examples of material submitted to radiocarbon dating. Panel (a) represents *Pisidium* shells from the very bottom layer of the bog, panel (b) shows some wood fragments preserved through the bog.

Radiocarbon dates were then calibrated: this step is of primary importance because past changes in atmospheric ^{14}C concentration could be influenced by fluctuations of radiocarbon content of atmospheric CO_2 for various reasons, as already described in *chapter 5*. Radiocarbon ages were calibrated as calendar years before present (cal BP) with the CALIB 6.0 software (Copyright 1986-2010 Stuiver and Reimer) (Stuiver and Reimer, 1993). The results are presented with 95% confidence intervals and 2 sigma ranges.

In addition to the ^{14}C age dating, the upper 40 cm layers of the bog core were dated using ^{210}Pb and ^{137}Cs measurements. For ^{210}Pb and ^{137}Cs determination, dried peat samples every 1 cm of depth, were analyzed by direct gamma assay in the Liverpool University Environmental Radioactivity Laboratory using Ortec HPGe GWL series well-type coaxial low background intrinsic germanium detectors (Appleby et al., 1986; Appleby, 2001).

7.2 Age-depth model

An accurate age-depth model is necessary to estimate the calendar ages of the undated depths of the core. It can be used with radiocarbon data already calibrated and with data from different type of chronology. Calibrated ^{14}C dates can't be assumed to have a symmetrical errors in a normal distribution, because the results of the calibration show multi-peaked calendar age uncertainties. This asymmetrical distribution prevent the apply of classical interpolation/regression that usually undergoes with normally distributed errors (Blaauw, 2010). To determine the best chronology for all the 7 meters depth sequence, we used the non Bayesian classical age - depth model called "*Clam*" (Blaauw and Christen, 2005; Blaauw et al., 2007; Blaauw, 2010).

Chapter 8

Geochemical analyses

8.1 Physical analysis

During the collection of the core, its sedimentological structure has been observed and described in field. At that point all shifts from mineral rich-layers and organic-rich sediment with all the other particular characteristics of the bog were identified and then re-analyzed in the laboratory.

After visual inspection, first steps of analysis comprehend the determination of ash content, bulk density, water content and pH. Those data help to describe the trophic status of the bog, distinguishing between ombrotrophic peat from minerotrophic peat. Every 1 cm peat components were measured quantitatively by loss-on-ignition (LOI) following the procedure described by Chambers et al. (2011). This procedure allows to evaluate water, organic matter, total inorganic contents and the residual fraction. In particular after recording the peat wet weight, samples were dried at 105°C overnight and the dry mass was weighed using a KERN balance Alt 220-4-NM (1 mg resolution). The ash content was measured after placing dried samples for 5 hours in a muffle furnace at 550°C. To be sure that all organic material was oxidized we tested selected samples at 900°C obtaining the same results: the difference between the two ashing temperatures was less than 0.2% in the final weight.

Pore water pH and conductivity values were used to assess the oligotrophic condition of the bog (typical of ombrotrophic peatland), making wider the framework that describes the total trophic status of the bog. pH and electrical conductivity (EC) were measured on pore water samples using a CRISON multiprobe MM 40+ and EC was corrected for the effect of H^+ content, following Sjórs (1950).

8.2 Chemical Analyses

8.2.1 X-Ray Fluorescence Core Scanner

The X-Ray Fluorescence Core Scanner (XRF) used for the analyses belongs to the third generation Avaatech Core Scanner and its functions, as described below, are summarized following the information given by the Avatech company on its website: $http://www.avaatech.com/services2.htm$.
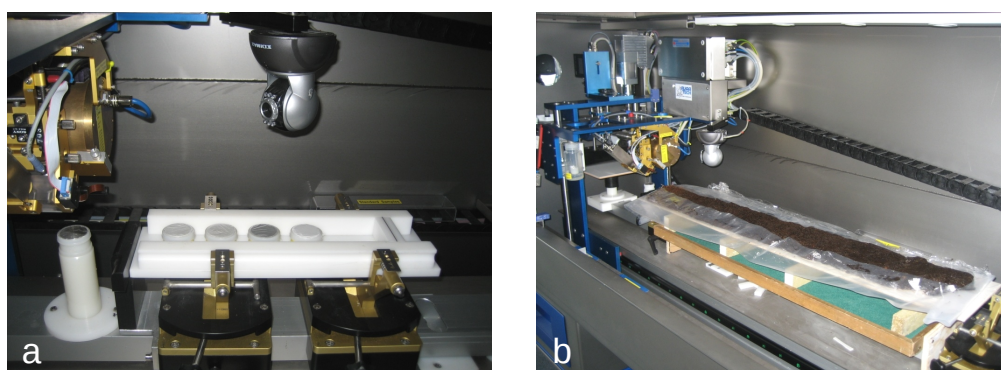
Figure 8.1: X-Ray fluorescence core scanner: panel (a) represent the solid samples used for the calibration step of XRF measurements; panel (b) pictures a peat core ready for the XRF core scanner analysis.

The XRF is equipped with an optical system that provides the excitation of the elements from Mg to U. The radiation comes from an X-ray tube with an Rh-anode. After penetration of the core by incident X-Ray beam, primary fluorescence of the elements in the sample occurs: each element present in the sediments analyzed by XRF core scanner is ionized by the primary X-rays and then emits an element-specific fluorescence radiation that is recorded by the detector. Lighter elements emit weaker fluorescence energy resulting in a smaller critical depth (figure 8.2), and the fluorescence energy increase with the square of the atomic number following the Moseley's law. Thus, the critical depth varies for example from approximately 8μm for Al (atomic number 13), 36μm for Ca (atomic number 20), and 180μm for Fe (atomic number 26) (Tjallingii et al., 2007).

The entire optical system is He-flushed for good light element detection, and the sediment during the analyses are covered with a foil (Ultralene) highly transparent to X-Ray to prevent drying of the sample and the device being soiled.

Other 2 foils are present between the detector and the sediments: the second and the third foil cover the He-flush prism (figure 8.3). The He-flushed prism forms a pseudo vacuum transmission medium between the X-ray source, the sediment, and the detector. The initial element intensities
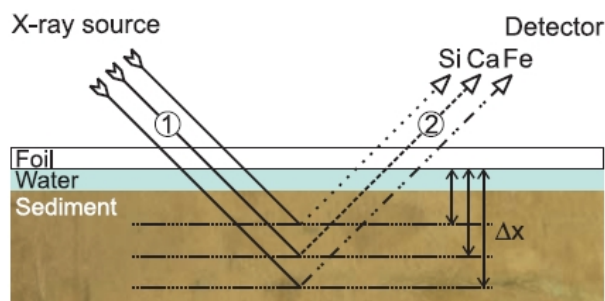
Figure 8.2: XRF beam scheme and critical depth (Delta$_x$). From Tjallingii et al. (2007)
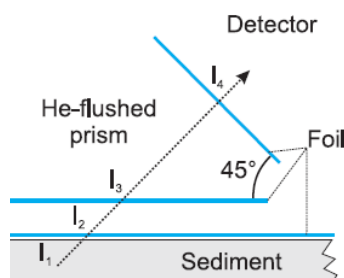
Figure 8.3: Foils placed between sediment and detector. As described by Tjallingii et al. (2007)

(I_1) of the elements were calculated from the transmission of the Ultralene foil and the residual element intensity (I_4) recorded by the detector (figure 8.3) (Tjallingii et al., 2007).

X-Ray fluorescence measurements were carried out using an Avaatech XRF-CS at the Godwin Laboratory for Palaeoclimate Research, Department of Earth Sciences, University of Cambridge (figure 8.1, panel a). Even if this technique gives qualitative data about the presence of selected elements, it can be calibrated using particular standards given by the Avateech company: in this case the calibration is needed to ensure that XRF signal is stable avoiding any possible drift. More details about its calibration are reported in the Part III about Method Validation and quality control.

XRF core scanning measurements were obtained directly at core surface. The split core surface was cleaned and the flat surface without air bubbles or other kind of interruptions was covered with 4 micron thickness Ultralene foil. Selected elements were chosen and detected at 2.5 mm of resolution (2.5 mm downcore window; 12 mm across-core window) with a generator setting of 10kV, 30kV or 50kV: 10kV for the lighter elements Si, S, Ca, Ti, Cr, Mn,

Fe, 30 kV for Cu, Ga, Rb, Sr, Y and 50 Kv for the heaviest element Pb. Sampling time was set at 30 seconds.

Data were evaluated by analysis of the X-ray spectra generated at each energy level by WIN AXIL Batch software. Optimized operating condition for XRF-CS are reported in table 8.1.

Table 8.1: Instrumental settings for the Avateech XRF core scanner.

X-Ray Generation and Detection	
Voltage range	4-50 kV
Anode type	Rhodium
Multi-Channel	2048 chs
Analyzer Resolution	2.5 mm

Peat colour profiles by XRF core scanner

The Avaatech XRF Core Scanner can be equipped with a digital colour Line Scan Camera that records images using Visible and UltraViolet light. With this camera is possible to register the colour of the image using three colour sensors per pixel through the RGB model. In this model sensors capture the intensity of the light in red, green or blue (RGB) spectrum respectively. After that, records are converted in the international standard of space colour that defines L*(lightness) a*(redness) and b* (yellowness), where L* is the luminance and the a* and b* parameters are the two chromatic components (a* from green to red and b* form blue to yellow). A colour Line Scan Camera integrated in the XRF Core Scanner system was used for scanning the colour spectra. Every section of the core was scanned and their images were saved. Profiles of the RGB (red-green-blue) channels and the L*, a* and b* values were produced by averaging pixels perpendicular to the core in a rectangle along the central core axis. Data on colours produced ASCII files. A fixed number of pixels corresponds to a distance on the line scanner, however the scanner itself keeps track of the distance travelled by the camera from its "zero point" at the base of the core, so math is not needed to translate pixels to downcore distance.

8.2.2 CRC-ICP-MS

The inductively coupled plasma-mass spectrometry is a very powerful technique to analyze trace and ultra-trace elements. It is characterized by excellent performance in terms of sensitivity, background signal, elemental coverage, analysis time, detection limits and reliability and has the great

advantage of being linear over at least 6 order of magnitude of concentration (figure 8.4), scanning a wide range of elements at the same time.
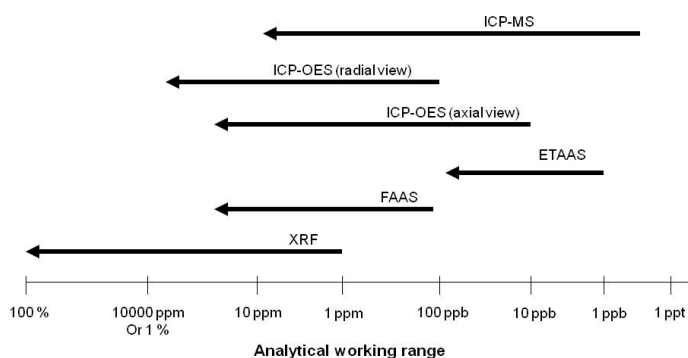
Figure 8.4: Detecion limits range, from Cairns (2008).

The following description of this technique proceeds Taylor (2000) and Cairns (2008). An ICP-MS consists of four main components: a *sample introduction system*, an *interface* to sample the plasma, *ion lens* to separate the ion beam from neutral species and focus it to the mass analyser and a *mass analyser* that separates ions by their mass to charge ratio (m/z) prior to their detection by an electron multiplier (figure 8.5).

The *sample introduction system* has the main purpose to convert the liquid sample into an aerosol: this is achieved using a pneumatic nebuliser in conjunction with a spray chamber. The liquid sample is pumped into the nebuliser using a peristaltic pump and, encountering the nebuliser it is shattered into an aerosol. There are a wide range of nebulisers, concentric, micro-flow, cross-flow and v-groove: among these types, v-groove is generally used analysing samples which contain high levels of solids or particulate matter. This primary aerosol flows into the spray chamber in which the selection of the particles that can enter the plasma takes place: the primary aerosol is directed into the central tube of the spray chamber and there the largest droplets fall by gravity force going out through the drain tube, while the finest droplets, with a mean aerodynamic diameter of 5-10 micron, are transported into the sample injector of the plasma torch. The spray chamber is also cooled at 2°C reducing the solvent vapour that can reach the plasma.

Once the sample has passed through the nebuliser and the spray chamber, it is carried to the torch, where the plasma is generated. A torch consists of three concentric tubes: it is encircled at the top by an induction coil, called the load coil, made from copper and connected to a radio-frequency genera- tor. The radio-frequency generator operates at 27 or 40 Mhz with a power
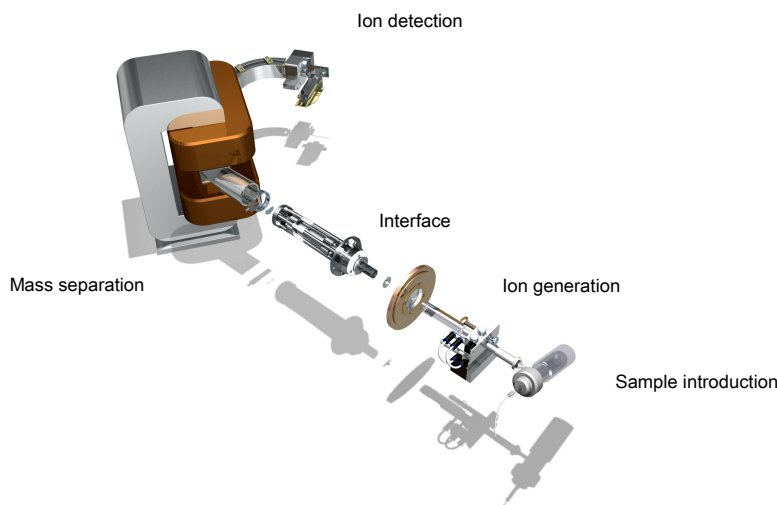
Figure 8.5: Foundamentals of the ICP-MS.

output between 500 to 2000 W. These coils produce a magnetic field that induces a current in the argon gas flow: when Ar gas flows through the torch, a high voltage spark is applied to the gas, which causes some electrons to be stripped from their Ar atoms. These electrons, caught up and accelerated in the magnetic field, collide with other Argon atoms, stripping off still more electrons. This collision-induced ionization of the Ar continues in a chain reaction, breaking down the gas into Ar atoms, Ar ions and electrons, forming what is known as an inductively coupled plasma discharge. The plasma is self sustaining as long as the magnetic field is applied; the annular form of the magnetic field is reflected in the plasma and its characteristics makes the introduction of the aerosol more efficient. The sample aerosol is then introduced into the plasma through the central tube of the torch, called the sample injector. In comparison with other chemical flames, an Argon ICP as a high gas temperature, reaching typically 6000 to 10000 K.

Once inside the plasma the aerosol is desolvated, atomized and then ionized. The ions formed were successively sampled from the *plasma interface*. The interface has two fundamental functions: it has to sample selectively the central channel of the plasma when the sample is present, and then it has to reduce the pressure of the ion source from atmospheric pressure to a pressure typical for mass spectrometers. In fact the mass analyzer region of the instrument requires vacuum for its optimal operation, while the ICP operates at atmospheric pressure. The interface region transfers the ions from the plasma to the mass spectrometer through step-wise pressure reduction. The interface consists of 2 cones, sampling and skimmer. Once the ions leaves

the skimmer cone, they are attracted by two *extraction lenses* to form an ion beam, and they have to be conveyed to the *mass analyzer*. The ion focusing system allow to focus the maximum number of analyte ions from the interface region to the mass spectrometer, and to reject the maximum amount of matrix components, neutral species and photons, which could increase the background signal and cause signal instability.

Prior to be directed to the analyzer quadrupole ions are directed into the collision/reaction cell to overcome the problem of the polyatomic interferences forming when two or more atoms bound together giving the same mass that is equal to the mass of the target ion. By a number of different ion-molecule collision/reaction mechanisms, polyatomic interfering ions are converted to harmless non-interfering species. In Helium mode (collision mode) the interferences are removed based on their physical size: polyatomic interferences are larger than the analytes they interfere with, colliding more frequently with the Helium atoms. Therefore they will loose more energy and will be removed by energy discrimination. In Hydrogen mode (reaction mode) the polyatomic interference reacts with the Hydrogen gas increasing its mass number or will pass the positive charge to the Hydrogen: in each case their mass will be not detected by the mass spectrometer.

The remaining ions finally are directed to the quadrupole where mass analysis occurs through a sequential mass filter, which is able to separate ions based on their mass to charge ratio (m/z).
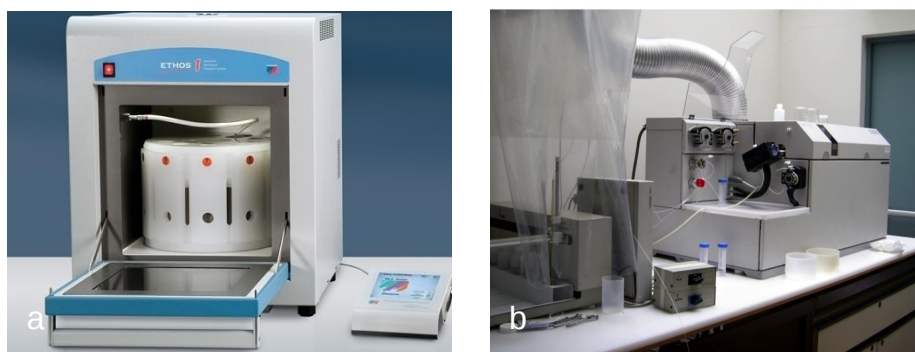
Figure 8.6: Microwave Milestone Ethos1 (panel a) and CRC-ICP-MS (panel b). University Ca' Foscari of Venice.

ICP-MS measurements were performed using an Agilent 7500cx collision/reaction cell inductively coupled plasma mass spectrometer (CRC-ICP-MS) equipped with a CETAC ASX-520 auto-sampler (figure 8.6, panel b). As the sample solutions contained HF, which is corrosive to quartz, an HF resistant V-Groove nebuliser was used and similarly a polyethylene spray chamber. Measurements were carried out using the reaction cell in both helium and in hydrogen mode in order to convert interfering species into

harmless and non-interfering ones. Instrumental ICP-MS parameters are described in table 8.2.

Calibrations of measurements on mineralized peat samples and pore water samples were carried out as defined in the Part III about Method validation and quality control.

Table 8.2: Operating conditions for Agilent 7500cx ICP-MS.

Plasma Conditions	
RF power	1500 W
RF Matching	1.74 V
Carrier gas	1.24 L/min
Make Up gas	0 L/min
S/C temperature	2°C
Ion lenses	
Extract 1	0 V
Extract 2	-155 V
Omega bias-ce	-30 V
Omega lens-ce	-0.6 V
Cell entrance	-30 V
QP focus	-10 V
Cell exit	-30 V
Reaction cell	
H_2 *Gas*	2mL/min V
He Gas	4mL/min V

Pore water chemical analysis

Selected chemical parameters from pore water are necessary to obtain more information about the trophic status that characterizes the bog. In order to extract pore water samples each 1-cm slice over the upper 100 cm was sealed in a polyethylene bag and then squeezed with constant pressure following the protocol defined by Givelet et al. (2004).

Pore water subsamples were immediately analyzed for pH and electrical conductivity (EC) using a CRISON multiprobe MM 40+. The rest of each sample were centrifuged for 10 minutes at 3000 rpm using a Rotina 38, HETTICH. Once centrifuged, they were analyzed at the University of Venice using the AGILENT 7500cx collision/reaction cell inductively coupled plasma mass spectrometer (CRC-ICP-MS) equipped with a CETAC ASX-520 auto-sampler to determine the concentrations of 36 major and trace elements. Before to be analysed with the ICP-MS each sample was acidified with HNO_3, reaching a final concentration of 2%.

Acid-mineralization of peat samples

To analyse a solid sample by ICP-MS it has to be dissolved. The destructive technique of peat samples is usually carried out using a hot acid mixture. Acids normally used are an oxidising acid HNO_3, a complexing agent HCl, or a mixture of HCl and HNO_3 (3:1) known as aqua regia that, forming nitrosile chloride ion in situ, is capable to dissolve most of the noble metals. In the particular case when silicate are to be breakdown, it is necessary to add hydrofluoridric acid (HF): that means that IPC-MS has to be equipped with an HF resistant sample introduction system in place of the quartz nebuliser, spay chamber and torch.

Prior to the dissolving step, one square of each slice of the bog was dried at 105°C overnight and dried peat sample aliquots were homogenized using an agate mortar and pestle. Then approximately 150 mg of homogenized peat were weight into 20 ml Teflon vessel containing different acid mixtures depending on the sample's nature: in peat 9 mL HNO_3 and 1 mL HF, if inorganic sediment 3 mL of HNO_3, 9 mL of HCl and 1 mL of HF.

Samples were dissolved in closed-pressurizzed digestion vessels in a microwave oven Milestone-Ethos1 (figure 8.6, panel a). Each run of digestion was 20 min long, increasing temperature up to 220°C. The heating program consisted of the following steps: room temperature to 220°C in 10 min; holding 220°C for 10 min. For inorganic sediments holding time was extended to 25 minutes. After cooling 2 hours digestion solution were controlled in colourless and homogeneity which indicate absolutely efficient destruction of the organic matter. Then contents of digestion vessels were quantitatively transferred into graduated 50 mL polypropylene tubes and fill to the mark with high-purity MilliQ water.

8.2.3   Delta plus Advantage IRMS

This method describes the determination of $\delta^{15}N$ and $\delta^{13}C$ vs VPDB by flash combustion that is been measured at the Analytical laboratory of the University of Alberta (CA).

9 mg of dried peat samples were weighted with a micro-analytical balance into a silver boat and carefully encapsulated. A complete combustion of peat samples is been achieved by dropping a known mass of sample into a combustion tube containing Chromium (III) Oxide and Silvered Cobaltous/cobaltic Oxide catalysts. An aliquot of purified oxygen is added to the quartz tube, generating a flash combustion reaction which increases the temperature from 1020°C to between 1800 to 2000°C. The carbon and the nitrogen contained in the flash combusted sample is converted to CO_2, N_2 and NO_x. These combustion gases, are carried via a stream of UHP Helium through a reduction furnace filled with reduced copper wires, where NO_x is reduced to N_2. Then, depending on the analysis requested, the gas stream
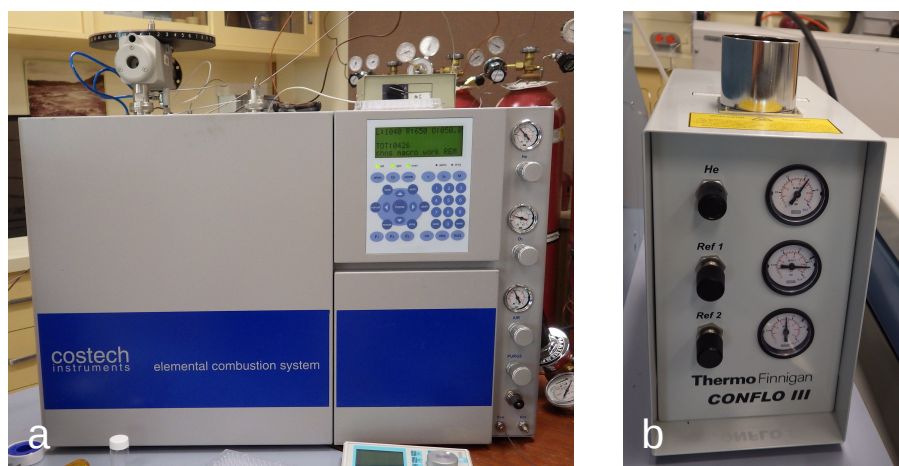
Figure 8.7: Costech 4010 Elemental Analyzer (panel a) and the Thermo Finnigan ConFlo III Interface (panel b) connected with the Thermo Finnigan Delta plus Advantage. University of Alberta (CA).

passes through determined sorbent traps. The resulting CO_2 and N_2 gas is separated on a 2m x 6mm OD stainless stell Porapak QS 80/100 mesh packed chromatographic column and enters the Thermo Finnigan Conflo III. The original sample size is then reduced by an open split interface where a He dilution capillary ensure no atmospheric air enters the sample stream while effectively diluting the sample to a size appropriate for sensitivity of the mass spectrometer. The sample is piked up at atmospheric pressure by a sniffer capillary and introduced into the isotopic ratio mass spectrometer, Thermo Finnigan Delta plus Advantage IRMS, held at vacuum of around 1.0 x 10-6 mBar. The sample travels into the ion source which focuses a positively charged ion beam down the flight tube. The beam is bent by precision magnet where the resultant ions are deflected into three gold-lined Faraday Cup collectors that are tuned for the masses of interest. The collectors detect the change and produce a ratio output. Intensities of mass 46/45/44 for Carbon and mass 28/29/30 for Nitrogen are measured. Internal standards are calibrated against the International Reference scale (^{13}C vs vPDB and ^{15}N vs V air). Raw data are then referenced to PDB or V air through a linear regression calculated from the internal standard results.

Chapter 9

Biological analyses

9.1 Pollen analysis

The study of the fossil pollen grains preserved in peat sediments is possible because they well conserve thanks to *sporopollenin*, a resistant biopolymer present in the outer layer of the pollen wall, the *exine*: *sporopollenin* makes palynomorphs extremely resistant to strong acids, but sensitive to oxidizing agents. These intrinsic characteristics are the basis for the extraction procedures that are needed to remove from samples organic material, silicate and carbonate in order to investigate pollens. Samples for pollen analysis were processed every 1 cm in the final 50 cm of the core. All samples were taken with a volumetric piston sampler (1 cm^3) and then treated according with the standard methods described in Faegri and Iversen (1964):

- A measured volume of peat was placed in a centrifuge tube with water and 2 *Lycopodium* spore tablets. These tablets contain a known amount of spore which are fundamental parameters to calculate the relative pollen concentration after the sample's treatment (Stockmarr, 1971) (figure 9.1, (a)).

- If peat was suspected to have traces or calcareous sediments HCl 10% has been added to the tubes, and after completed the reaction, the tube was centrifugated at 3,000 rpm for 4 minutes and carefully dacanted (figure 9.1, (b - c)).

- KOH 10% was added and the tubes were placed in boiling water for 10 minutes, and the residue after centrifugation was sieved at 250μm to eliminate organic matter (figure 9.1, (d)).

- HF 35% was added to destroy clay or silt content. The tubes were placed in boiling water for 15 minutes and content centrifuged and decanted.

64

- Another step with HCl 10% was needed at that point to remove the colloidal silica.

- Tubes content was treated with glacial acetic acid and then with and acetylation mixture made up with acetic anhydride and concentrated sulphuric acid 9:1 by volume. This mixture was put in boiling water for 3 minutes and is necessary to colour the pollen grains making them more visible under the microscope.

- Finally the remaining content into the tubes was filtered at 10 micron and than conserved under glycerin jelly and mounted on slides fixed with cover slips (figure 9.1, (e and f)).
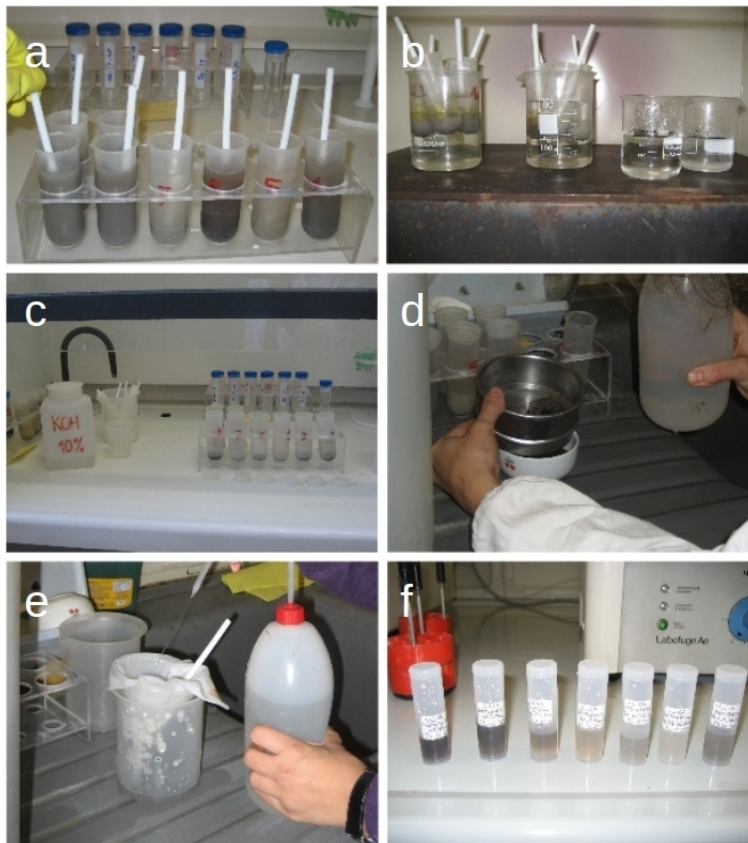
Figure 9.1: Some laboratory steps of pollen analysis procedure.

The identification of pollen grains was performed at x400, x630, x1000 magnification under a Zeiss binocular light microscope at the University Ca' Foscari of Venice. Nomenclature of the pollen species refers to Moore et al. (1991) key. For precise and accurate pollen identification a pollen

reference collection was made from fresh material collected in field. Other microfossils were identified, where possible, following Van Geel et al. (1980). Spelling of plant names is according to Pignatti (1982). In pollen slides also black and opaque micro-charcoal remains longer than 10μm were counted. A minimum of 400 terrestrial pollen grains was counted, and the pollen sum was calculated including all the terrestrial pollen types. Pollen percentages were plotted using C2 software including trees, shrubs and upland herbs, excluding Cyperaceae, aquatics and spores.
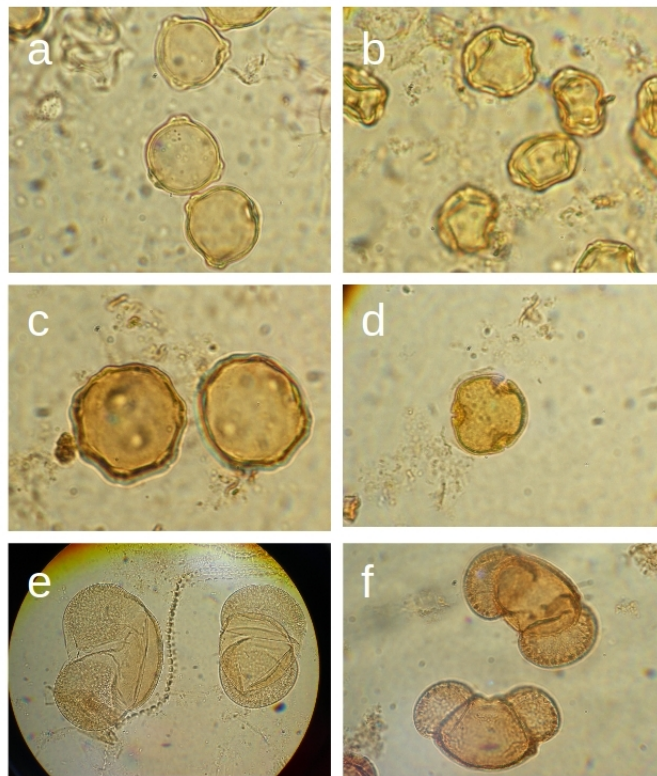
Figure 9.2: Pollen reference: (a) *Betula pendula*, (b) *Alnus viridis*, (c) *Juglans nigra*, (d) *Tilia cordata*, (e) *Picea excelsa*, (f) *Pinus cembra*.

Chapter 10

Data analysis

Statistical treatment of the data has been done with R software. Analytical data sets were examined through the descriptive statistics that provides information about min, max, mean, median, 1st quartile and 3rd quartile values, the most common statistical indexes of position and data distribution. In order to study the linear correlation between variables the coefficient correlation was calculated: it can vary between -1 and +1, the absolute negative correlation and the absolute positive correlation. The validation of the correlation between XRF and ICP-MS methods was confirmed extrapolating the significance of the coefficient using the Student's t-value. Student's t-test results were compared with the tabular critical Student's t-values to confirm or not the initial hypothesis of positive correlation.

Principal component analysis (PCA) was performed to explore data meaning and to divide a multivariate data-set into natural clusters. PCA is a way of identifying patterns in data, and of expressing the data in such a way as to highlight their similarities and differences. Since patterns in data can be hard to find in data of high dimensions, where the luxury of graphical representation is not available, PCA is a powerful tool for analysing data. The other main advantage of PCA is that once these patterns have been found in the data, the data can be compressed by reducing the number of dimensions without much loss of information. Since PCA is mainly concerned with identifying correlations in the data, let us first focus our attention on the meaning of correlation. Correlation measures the simultaneous change in the values of two or more variables. There are numerous models for describing the behavioural nature of a simultaneous change in values, such as linear, exponential, periodic and more. The linear correlation is used in PCA. PCA is carried out by computing the linear correlation coefficients between all variables. PCA has been carried out with R software using the function *princomp*: it determines principal components (PCs) of the data set. This function comprehends the $cor = TRUE$ option that standardizes variables

to zero mean and unit standard deviation. The factors are then extracted: they are the eigenvectors of the correlation matrix. The factors are arranged according to the decreasing order of explanation of the total variance of data. Only the first few factors are usually kept for the interpretation, since they explain nearly all the variance of data. Plotting the eigenvalues against the corresponding PC produces a scree plot that illustrates the rate of change in the magnitude of the eigenvalues for the PC. Then PC loading and scores are determined and their relationship, associated with the PCs are illustrated through a bi-plot display where the initial variables are graphically represented in several two-dimensional plots, using the eigenvectors as new orthogonal reference axes. The coordinates of the initial variables in these new axes are equal to the correlation coefficients between these variable and the corresponding factors.

In order to identify the relative importance of natural versus anthropogenic component of trace elements concentrations, we calculated the *Enrichment Factor* (EF), normalizing element concentrations with a conservative lithogenical element (Sc in this case) assuming that the conservative element has an uniform flux through time. EF is an empiric index that commonly is used for supporting the hypothesis that the presence of some elements derives from anthropogenic sources, and allows to identify and quantify human interferences on the global biogochemical cycle. EF has been calculated as:

$$(\text{TE/Sc})_{sample} / (\text{TE/Sc})_{background}$$

where TE represents the trace element considered each time, and Sc is the lithogenic element used to calculated the number of times a sample is enriched in a particular element (TE) compared to the natural, pre-anthropogenic background value.

Part III

Method validation and quality control

Chapter 11

Physical determination

11.1 Bulk density, water and ash content

Peat components in terms of bulk density, water and ash content, were measured by loss-on-ignition (LOI) as described by equations 11.1. Bulk density was calculated by measuring the dry weight of each sample, subtracting the estimated amount of water (using water content calculated from drying the subsamples in 105°C) from the wet weight of the initial sample. Dry bulk density was then derived by dividing dry weight with volume of the initial samples. Dry samples were burnt at 550°C and ash content was finally calculated by dividing sample weight after burning with the dry weight of the initial sample.

$$Water content(\%) = \frac{Weight_{wet} - Weight_{dry}}{Weight_{wet}} * 100$$

$$Bulk density(gcm^{-3}) = \frac{Weight_{dry}}{Volume_{freshsample}}$$

$$Ash(\%) = \frac{Weight_{550}}{Weight_{105}} * 100$$

Equation 11.1. Peat components determination.

To maximize the accuracy of loss-on-ignition analyses the crucibles were always weighed at room temperature immediately after cooling in a dessicator. Even if the LOI procedure is well established ((Chambers et al., 2012)), we made some replicates to determine the precision of our measurements (n=3). Precision for water content measurements has always better results than bulk density or ash content because water is the major component of peat at this depths. Results are given in table 11.1:

Table 11.1: Reproducibility of LOI measurements

	Sample 37.5 mean dev.std. (%)	**Sample 101.5** mean dev.std. (%)	**Sample 106.5** mean dev.std. (%)
Bulk den.	0.091 ± 0.001 1.40%	0.125 ± 0.003 2.84%	0.115 ± 0.003 2.97%
Water	90.5 ± 0.001 0.001%	86.39 ± 0.003 0.004%	87.22 ± 0.003 0.004%
Ash	7.04 ± 0.34 4.89%	3.77 ± 0.14 3.74%	5.40 ± 0.21 3.91%

Chapter 12

From XRF-CS to ICP-MS discrete analysis

12.1 Combined XRF-CS and ICP-MS technique

The most precise and widely used conventional technique for major and trace element analysis of peat cores is ICP-MS measurements after a pressurized microwave-assisted mixed-acid digestion of peat. ICP-MS provides accurate chemical time series from peat cores but typically has low resolution (1-3 cm) with discontinuous data sets. In this way, abrupt climate events could be underestimated or not detected because of the low accumulation rates characteristic of ombrotrophic peatlands (Chambers et al., 2012).

X-Ray Fluorescence core scanning (XRF-CS) is a computer-controlled core-scanning technique that analyzes the elemental composition of geological samples as intensities expressed as total counts or counts per second, which are proportional to the individual elemental concentrations (Tjallingii et al., 2007). The main advantage of XRF-CS is the rapid and nearly continuous determination of the elements investigated on the surface of split sediment cores, with a potential spatial resolution much higher than all the other conventional destructive methods (which generally resolve records at a resolution > 0.5 cm). Due to these characteristics XRF-CS can be particularly useful when sedimentation rates are high and finely chronologically resolved information is needed (Jansen et al., 1998).

There have been many recent geochemical studies of climate and environmental variations over geological time periods where XRF-CS has been used as part of multi-proxy approaches. Scanning XRF has been used for studying marine and lacustrine sediments (Jansen et al., 1998; Haug et al., 2001), for high resolution time series, stratigraphic correlations and detailed sedimentary and climatic reconstructions on different time scales (Haug et al., 2001; Lamy et al., 2001). Tian et al. (2011) used non-destructive XRF core scanning to present a high resolution K/Al and Ti/Al record from the Ocean

Drilling Project site at 1143 in the South China Sea over the past 5 Ma, while Lauterbach et al. (2011) have studied sediments from lake Mondsee at sub-annual resolution, obtaining geochemical data using a micro-XRF scanner combined with data from stable isotopes, ostracods and pollen to demonstrate environmental responses to late glacial climate fluctuations. Balascio et al. (2011) used a multi-proxy approach, applied to lake sediments, that included XRF-CS, molecular biomarkers, magnetic susceptibility and analyses of diatom assemblages to evaluate salinity and water column changes over the last ca. 8000 years. Vegetation reconstruction using XRF and stable isotopes on lake sediments delineated Holocene climate history. Analyses of pollen and plant microfossils, together with scanning XRF, were used to evaluate changes in the environment related to climate evolution during the last deglaciation period in the Norwegian Arctic (Aarnes et al., 2012). Ice cores from the Antarctic were also analysed using XRF to evaluate the composition of dust trapped in the ice (Marcelli et al., 2012). Giralt et al. (2011) reconstructed climate changes with meteorological, limnological, and XRF-CS data from Lake Sanabria in Spain. Another study of climate changes employing XRF core scanning techniques described a novel approach in which the authors used Rb/Sr ratios from lake sediments in western Norway to evaluate the impact of snow avalanches and flooding over the last 8000 years (Vasskog et al., 2011). All the examples listed above indicate the wide potential for XRF core scanning techniques applied to environmental archives with the aim of producing high resolution data series.

The advantages of XRF core scanning led us to apply this technique to study past and present patterns of global climatic changes recorded by Danta di Cadore peat bog. Thus, high resolution XRF scanning data were combined and calibrated with parallel ICP-MS measurements. To the best of our knowledge, prior to this study there have been no published attempts to combine XRF-CS with more conventional analytical techniques in order to obtain paleoclimatic information form peat bog archives.

12.2 ICP-MS calibration and detection limits

12.2.1 ICP-MS calibration

The external calibration method was used for the quantification of the analytes. A 10 mg L^{-1} mother solution was prepared diluting together two 10 mg L^{-1} multi-elemental standard solutions (CLM-2AN containing Ag, Al, As, Ba, Be, Ca, Cd, Co, Cr, Cs, Cu, Fe, Ga, K, Li, Mg, Mn, Na, Ni, Pb, Rb, Se, Sr, Tl, U, V, Zn; IMS-101 containing Ce, Dy, Er, Eu, Gd, Ho, La, Lu, Nd, Pr, Sm, Sc, Tb, Th, Yb, Y). Calibrations were performed using 5 calibration standards ranging from 0.5 to 100 μg L^{-1} in order to cover, for each element, the concentration ranges present in peat samples.

A second 10 mg L^{-1} mother solution containing the major crustal ele-

ments (Fe, Al, Na, K, Ca, Mg, Ti) was also prepared from single standard solutions (ULTRA Scientific, 1000 mg L^{-1}).For the major crustal elements, calibrations were performed using 3 calibration standards ranging from 400 to 2000 μg L^{-1}. For some elements, the concentration levels in peat samples varied greatly and could cover several orders of magnitude. In these cases, to guarantee the linearity of the calibration curve, calibrations at different concentration levels were performed.

A 10 μg L^{-1} Rh solution (ULTRA Scientific, 1000 mg L^{-1}) was continuously mixed with the sample flow into the ICP-MS nebulizer through an on-line T connection. Considering the peristaltic pump velocity and the tubing internal diameter, the final Rh concentration was about 1.0 μg L^{-1}. The Rh signal was used as internal standard to correct instrumental drift and plasma fluctuation. The intensity of standard solutions were fitted using a linear regression, and the y-axis intercept at zero concentration, which was assumed to represent an average blank of the standards, was subtracted for calibration. For all the elements $R^2 > 0.998$ were obtained.

12.2.2   ICP-MS procedural blanks and detection limits

Concentrations of all elements in ultrapure water were below that of the most diluted standard, for each element in its analytical range. Thus, the use of ultrapure water for the preparation of standards and blank was justified. Procedural blanks were determined from the analysis of acidic blank solutions (supra-pure grade HF and HNO_3, ultra-pure water) obtained during the digestion procedure (section 8.2.2). Since the blank concentrations could vary each time, it was important to check them prior to every analysis. At least one blank was prepared for each digestion batch. The procedural blanks were used for blank subtraction.

For Be, Cu, Y, Sm, Eu, Gd, Tb, Dy, Ho, Er, Tm, Lu, Tl, Th and U the procedural blanks were under the detection limits. For the other elements detectable procedural blanks were recorded but they were many times less than the lowest concentrations determined in peat samples (table 12.1).

Solution detection limits for the ICP-MS technique were calculated as the concentration corresponding to 3 times the standard deviation of the measurement of the 10 acidic blank solutions obtained during the digestion procedure. Peat sample detection limits (DL) were calculated fixing an average peat sample mass of 100 mg and a final digestion volume of 50 mL (table 12.1). For major elements (Ca, Mg, Na, K, Al, Fe, Ti), DL ranged from 0.4 (Ti) to 10.3 (Ca) mg Kg^{-1} of peat while for trace elements from 0.001 (U) to 0.15 mg Kg^{-1} (Cu). For rare earth elements, DL were always below 0.001 mg Kg^{-1} of peat, except for La, Ce, Sm and Gd (0.0015 - 0.0023 mg Kg^{-1}).

Table 12.1: Detection limits ICP-MS peat measurements.

	Blank values (μg/L)	Mean peat concentration (μg/L)	Ratio peat/blank values	Solution DL (mg/L)	Peat DL (mg/Kg)
Li	0.010 ± 0.002	1.9	191	0.006	0.003
Be	< DL	0.19	ND	0.007	0.003
Na	9.1 ± 0.62	330	36	1.9	0.7
Mg	2.3 ± 0.42	1832	799	1.3	0.5
Al	8.5 ± 2.5	6979	819	7.4	3.0
K	43.1 ± 1.9	1256	29	5.7	2.3
Ca	29.3 ± 8.5	7260	247	25.6	10.3
Sc	0.043 ± 0.010	2.0	45	0.030	0.012
Ti	1.1 ± 0.32	399	355	0.9	0.4
V	0.025 ± 0.006	11.8	465	0.017	0.007
Cr	2.5 ± 0.21	41.2	17	0.6	0.3
Mn	0.070 ± 0.0087	19.9	285	0.026	0.010
Fe	141 ± 6.1	3244	23	18.2	7.3
Co	0.007 ± 0.001	2.0	283	0.003	0.001
Ni	0.11 ± 0.020	10.2	91	0.06	0.02
Cu	<DL	14.2	ND	0.39	0.15
Zn	0.39 ± 0.092	20.8	53	0.28	0.11
Ga	0.013 ± 0.002	6.0	460	0.007	0.003
As	0.039 ± 0.009	2.6	67	0.027	0.011
Se	0.10 ± 0.018	0.48	5	0.055	0.022
Rb	0.012 ± 0.004	6.9	558	0.011	0.004
Sr	0.036 ± 0.009	33	923	0.028	0.011
Y	< DL	2.4	ND	0.004	0.001
Ag	0.011 ± 0.003	0.43	38	0.009	0.004
Cd	0.0052 ± 0.001	0.37	70	0.004	0.002
Ba	0.18 ± 0.022	107	594	0.067	0.027
La	0.0057 ± 0.001	4.6	821	0.004	0.002
Ce	0.0061 ± 0.002	8.6	1418	0.005	0.002
Pr	0.0008 ± 0.0002	0.97	1183	0.001	0.001
Nd	0.0051 ± 0.0010	4.1	810	0.003	0.001
Sm	< DL	0.85	ND	0.0057	0.0023
Eu	< DL	0.18	ND	0.0008	0.0003
Gd	< DL	0.91	ND	0.0032	0.0013
Tb	< DL	0.11	ND	0.0010	0.0004
Dy	< DL	0.65	ND	0.0016	0.0006
Ho	< DL	0.11	ND	0.0009	0.0004
Er	< DL	0.35	ND	0.0014	0.0006
Tm	< DL	0.038	ND	0.0005	0.0002
Yb	0.001 ± 0.0003	0.301	290	0.001	0.0001
Lu	< DL	0.037	ND	0.0008	0.0003
Tl	< DL	0.16	ND	0.0009	0.0004
Pb	0.037 ± 0.008	55.4	1482	0.024	0.009
Th	< DL	1.4	ND	0.0057	0.0023
U	< DL	0.65	ND	0.0024	0.0009

Table 12.3: Reproducibility of ICP-MS peat measurements.

	Sample 37.5 mean dev.std. (%)	Sample 101.5 mean dev.std. (%)	Sample 5.5 mean dev.std. (%)
Li	0.091 ± 0.002 2.7%	0.73 ± 0.057 7.8%	0.53 ± 0.028 5.3%
Be	0.033 ± 0.002 6.1%	0.11 ± 0.010 9.1%	0.03 ± 0.001 4.0%
Na	46.8 ± 1.2 2.6%	97 ± 3.4 3.5%	148 ± 8.1 5.5%
Mg	482 ± 23 4.9%	461 ± 14 3.1%	1258 ± 50 4.0%
Al	1225 ± 97 7.9%	4054 ± 34 0.8%	1222 ± 50 4.1%
K	168 ± 12 7.2%	401 ± 34 8.5%	1189 ± 64 5.4%
Ca	2322 ± 107 4.6%	3042 ± 121 4.0%	2383 ± 133 5.6%
Sc	0.21 ± 0.021 9.4%	1.5 ± 0.17 11.4%	0.32 ± 0.012 3.9%
Ti	29.3 ± 3.4 11.5%	204 ± 0.42 0.2%	82 ± 3.6 4.4%
V	2.52 ± 0.28 11.3%	4.85 ± 0.09 1.9%	2.43 ± 0.12 5.0%
Cr	1.78 ± 0.16 9.2%	3.63 ± 0.18 5.0%	2.12 ± 0.30 14.3%
Mn	2.00 ± 0.021 10.4%	3.83 ± 0.31 8.1%	48.6 ± 1.2 2.5%
Fe	717 ± 89 12.4%	1427 ± 18 1.2%	784 ± 47 6.0%
Co	0.56 ± 0.037 6.6%	0.79 ± 0.037 4.7%	0.52 ± 0.033 6.4%
Ni	1.4 ± 0.12 8.5%	2.3 ± 0.09 3.8%	1.3 ± 0.17 12.6%
Cu	3.9 ± 0.67 16.9%	8.3 ± 1.87 22.6%	4.0 ± 0.22 5.4%
Zn	3.4 ± 0.27 8.0%	5.1 ± 0.38 7.6%	29.0 ± 1.41 4.9%
Ga	0.96 ± 0.11 11.0%	3.38 ± 0.13 3.9%	2.21 ± 0.11 4.9%
As	0.64 ± 0.087 13.7%	0.74 ± 0.03 4.0%	0.24 ± 0.015 6.3%
Se	0.10 ± 0.013 12.6%	0.25 ± 0.018 7.0%	0.08 ± 0.015 14.7%
Rb	1.4 ± 0.19 13.7%	2.1 ± 0.21 10.0%	5.7 ± 0.27 4.8%
Sr	8.0 ± 0.52 6.5%	16.6 ± 0.19 1.2%	9.3 ± 0.48 5.2%
Y	0.38 ± 0.019 4.9%	1.5 ± 0.021 1.4%	0.36 ± 0.015 4.3%
Rh	0.063 ± 0.026 4.1%	0.36 ± 0.015 4.1%	0.83 ± 0.035 4.2%
Ag	0.065 ± 0.004 5.9%	0.065 ± 0.013 20.0%	0.035 ± 0.007 18.5%
Cd	0.11 ± 0.013 11.2%	0.072 ± 0.001 1.5%	0.15 ± 0.010 6.5%
Ba	15.5 ± 1.2 7.7%	67 ± 3.7 5.6%	39 ± 1.9 4.9%
La	0.86 ± 0.17 20.1%	3.2 ± 0.09 2.8%	0.59 ± 0.03 5.7%
Ce	1.4 ± 0.13 8.9%	5.7 ± 0.09 1.6%	1.1 ± 0.06 5.2%
Pr	0.14 ± 0.07 5.1%	0.63 ± 0.004 0.6%	0.13 ± 0.006 4.7%
Nd	0.68 ± 0.14 19.9%	2.7 ± 0.01 0.3%	0.56 ± 0.03 5.0%
Sm	0.12 ± 0.013 10.6%	0.54 ± 0.007 1.3%	0.11 ± 0.005 4.9%
Eu	0.017 ± 0.001 2.9%	0.12 ± 0.001 0.8%	0.026 ± 0.001 5.9%
Gd	0.14 ± 0.007 4.9%	0.61 ± 0.001 0.2%	0.14 ± 0.011 8.0%
Tb	0.0068 ± 0.0002 3.6%	0.073 ± 0.001 0.1%	0.013 ± 0.001 5.5%
Dy	0.092 ± 0.002 2.0%	0.44 ± 0.001 0.1%	0.079 ± 0.006 7.6%
Ho	0.006 ± 0.001 8.2%	0.076 ± 0.002 2.8%	0.015 ± 0.001 4.4%
Er	0.038 ± 0.002 5.1%	0.22 ± 0.002 0.9%	0.050 ± 0.002 3.1%
Tm	< DL	0.027 ± 0.001 2.7%	0.006 ± 0.001 0.9%
Yb	0.0033 ± 0.008 21.1%	0.19 ± 0.001 0.5%	0.043 ± 0.003 7.3%
Lu	< DL	0.025 ± 0.002 2.5%	0.006 ± 0.001 6.7%
Pt	< DL	< DL	< DL
Tl	0.037 ± 0.001 2.5%	0.030 ± 0.001 1.2%	0.076 ± 0.006 7.4%
Pb	15.5 ± 1.1 7.2%	33.1 ± 2.7 8.3%	7.1 ± 0.43 6.1%
Th	0.16 ± 0.019 12.0%	1.1 ± 0.011 1.0%	0.14 ± 0.006 4.0%
U	0.058 ± 0.003 4.3%	0.55 ± 0.045 8.2%	0.055 ± 0.001 2.6%

12.2.3 ICP-MS precision, accuracy and reproducibility

The analytical precision and accuracy were systematically evaluated for peat samples using the reference material *CRM NIMT/UOE/FM001*. It derives from ombrotrophic peat and was obtained during a inter-comparison exercise (Yafa et al., 2004), certified for 16 trace elements. CRM samples were analyzed in every digestion batch(every 6 samples). The mean value of precision and recovery for all the tests (n=14) are reported in table 12.5. Our data appeared very accurate agreeing very well the certified values with recoveries ranging between 77% (Na) to 117% (Cd). The precision was normally better than 10% while only for Cd did it exceeded 23%.

For sediment samples precision and accuracy were evaluated using the reference material *MESS-3*, a marine sediment reference material for trace metals and other constituents supplied by National Research Council of Canada. The mean value of precision and recovery for all the tests (n=10) are reported in table 12.6. Our data appeared very accurate agreeing very well with the certified values with recoveries ranging between 95% (Ni) to 102% (Mn). The precision was always better than 10%.

Table 12.5: Accuracy and precision ICP-MS peat measurements (CRM NIMT/UOE/FM001).

	CRM certified concentrations (mg/Kg)	CRM found concentrations (mg/Kg)	Precision (%)
Na	817 ± 307	636 ± 35	5.5
Mg	582 ± 168	677 ± 31	4.6
Al	3792 ± 337	4049 ± 223	5.5
Ca	683 ± 198	712 ± 64	9.0
Ti	357 ± 18	383 ± 1.6	4.2
V	7.8 ± 1.1	7.9 ± 0.44	5.6
Cr	6.36 ± 0.44	6.2 ± 0.48	7.7
Mn	7.52 ± 0.41	7.5 ± 0.45	6.0
Fe	921 ± 84	962 ± 80	8.3
Co	0.88 ± 0.09	0.88 ± 0.05	5.4
Ni	4.10 ± 0.37	4.1 ± 0.23	5.6
Cu	5.28 ± 1.04	4.9 ± 0.44	9.1
Zn	18.6 ± 1.9	18.6 ± 1.00	5.4
As	2.44 ± 0.55	2.40 ± 0.14	6.0
Cd	0.58 ± 0.9	0.68 ± 0.16	23.5
Pb	174 ± 28	185 ± 16	8.8

0.5 mL of a 10 mg L^{-1} certified Pt solution (ULTRA Scientific) was added to the samples before the digestion step to check the recovery. The Pt signal (final concentration about 100 μg L^{-1}) was used as internal stan-

Table 12.6: Accuracy and precision ICP-MS sediment samples measurements (CRM MESS-3).

	CRM certified concentrations (mg/Kg)	CRM found concentrations (mg/Kg)	Precision (%)
Li	73.6 ± 5.2	75.2 ± 2.3	4.5
V	234 ± 10	225 ± 3	5.6
Cr	105 ± 4	101 ± 2.5	6.5
Mn	324 ± 12	335 ± 25	6.7
Ni	46.9 ± 2.2	44.1 ± 3.1	4.0
Cu	33.9 ± 1.6	35.3 ± 0.67	7.2
Zn	159 ± 8	162 ± 6.2	9.1
As	21.2 ± 1.1	23.4 ± 0.85	5.7
Cd	0.24 ± 0.01	0.35 ± 0.05	8.1
Pb	21.1 ± 0.7	20.5 ± 1.5	4.2

dard to correct different recovery ratios. Reproducibility of the method was tested by digesting and analyzing replicate samples (n=3). Replicate analyses (table 12.3) revealed a good agreement for all elements with standard deviations always better than 23%. The results of the reproducibility tests were consistent with the precision obtained with CRM samples, indicating no significant contribution to the total uncertainty due to the matrix variability.

12.3   XRF-CS calibration and detection limits

XRF core scanner calibration is only a tuning procedure which ensures a stable signal eliminating any possible instrumental drifts. Four powdered standards, supplied by the Avateech company, were analyzed every day prior to and after the analysis of peat to monitor signal drifts. The analysis of these four standards showed stable signals. Elements up to Fe were detected at 10kV, for Br to Sr at 30kV and for Ba at 50kV. Detection limits for Avateech XRF core scanner are measured on dry standard reference materials (table 12.8). And are provided by the Avateech company. The standard samples are measured for 30 seconds with an irradiated (analytical) area of 150mm^2. Mg counting time was 100 seconds and Pb counting time 300 seconds (www.avateech.com).

12.4   XRF vs ICP-MS correlation

In this work we applied a novel approach combining high resolution XRF-CS with ICP-MS techniques to study the chemical signature of the Danta di

Cadore peat bog. Table 12.7 reports techniques advantages and drawbacks in terms of detection limits, pre-analytical steps, time required for sample preparation and analysis, and spatial resolution.

The first considerable difference is represented by the detection limits ranges, in fact ICP-MS shows lower detection limits compared to XRF core scanner (table 12.8). Before the ICP-MS analysis, samples have to be dried at 105°C, homogenized, powered and then digested in adequate acidic solutions. Microwave assisted acid digestion in closed pressurized vessel is a well-established method of sample dissolution and has the advantage of involving a reduced amount of sample and reagents, but at the same time has a long-standing drawback: the large amount of time needed for sample preparation procedure, about 30 min per sample (which includes sample processing, heating, homogenizing and digestion times). In contrast, XRF-CS measures the chemical composition of the sediment as element intensities in counts per second (cps) and requires only a few pre-analytical steps (table 12.7). That means that the techniques greatly differ in time required for the analysis: XRF-CS needs 30 seconds per position measurement for each energy range, versus ca. 35 minutes per sample for ICP-MS (sample preparation and analysis). The XRF core scanner in addition gives the possibility to achieve a very high resolution (<1 mm) compared to ICP-MS ($\geq$ 1cm).

Table 12.7: Comparison of pre-analytic steps, time needed to prepare and analyze peat samples and spatial resolution for ICP-MS and XRF Core Scanner.

	XRF Core Scanner	**CRC-ICP-MS**
Detection limits range	ppm	ppt/ppb
Pre-analytic steps	Flattening surface sample covering with Ultralene foil	Processing and Digesting
Sample preparation time	5min/50cm	30min/sample
Sample analysis time	30sec/position	5min/sample
Spatial resolution	0.1mm	$\geq$1cm

As discussed by Westerhold and Roehl (2009), the possible deviations and inconsistencies between the elements profiles obtained with XRF core scanner and ICP-MS techniques, related to the nature of the dataset (ones qualitative, the other quantitative) can be explained by: (i) water content, (ii) particle size distribution and (iii) sampling and digestion quality for ICP-MS analysis. In this perspective we monitored water and ash content at 1 cm of resolution following the LOI method (see section 11.1), and we assessed the quality of our ICP-MS measurements as reported in section 12.3.

Furthermore it has to be taken into account that there are differences in terms of the sampling volumes that are analysed. XRF beam penetrates the core surface varying with density. ICP-MS analysis are performed processing at least 1 cm^3 of wet samples.

Table 12.8: Detection limits (d.l.) for chosen elements for XRF Core Scanner. D.l. for XRF were measured at 10kV and at 30 sec count time. D.l for ICP-MS were calculated as 3 times the standard deviation of all processing blanks.

	XRF (ppm)	ICP-MS (ppb)
Al	2000	7.5
Si	1000	n.a.
S	< 5000	n.a.
K	400	5.7
Ca	200	25.6
Ti	< 1000	0.95
Mn	100	0.03
Fe	45	18.2
Sr	5	0.03
Ba	40	0.07
Pb	10	0.02

Along the first meter of the bog we measured trace elements at 2.5 and 10 mm of resolution by XRF-CS and ICP-MS respectively. In figure 12.1 and 12.2 results from XRF-CS and ICP-MS measurements of two selected elements (Pb and Sr) are reported. Considering the different sampling resolution of these two tecniques, four adjacent XRF-CS measurements were averaged to compare with ICP-MS data.

The XRF and ICP-MS results for both Pb and Sr were always in good agreement and the comparison of the results indicates that there is a strong correlation between the intensities measured with the XRF core scanner and the concentrations determined by ICP-MS.

To calculate the correlation coefficient, XRF counts and ICP-MS concentrations were linearly interpolated using a depth scale of 1 cm. The R squared correlation coefficients, shown in figure 12.1 and 12.2, are 0.89 for Pb and 0.87 for Sr. We extrapolated the significance of the correlation using the Student's t-value tr = r as described by Wilhelms-Dick et al. (2012). Student's t-test on the linear correlation gives positives values for Pb and Sr (10.33 and 9.33), both outside the range between -∞ and t(n-2, 1%), where the latter value is 2.76 (tabular critical Student's t-value), rejecting the null first hypothesis of no positive correlation. Water content was measured in the first meter of the bog to monitor its influence on the correlation between XRF and ICP-MS data: the highest water content (84 and 94% , between 0-60 cm) corresponds to high correlation between XRF and ICP-MS data, demonstrating that this physical parameter doesn't influence the correlation.

Although it has been demonstrated that changes in particle size over depth can influence XRF core scanner measurements, they are unlikely to have influenced our results. In fact ombrotrophic bogs are characterized by

a very low presence of inorganic component (5-15%), and so the presence of dust or particulate have no particular impact on the XRF measurements (see section 18.2). Additional measurements have been carried out on samples (n=10) with higher inorganic composition (ash > 70%) in order to assure that this high correlation remains also with changes in physical composition of the core. Results gave a high degree of significant correlation between XRF-CS and ICP-MS measurements also in the minerotrophic peat and in the inorganic sediments, with R squared values of respectively 0.78 (Pb) and 0.82 (Sr) for minerotrophic peat and 0.79 (Pb) and 0.88 (Sr) for inorganic sediments. Overall, despite the huge difference between sampled volumes there is a significant correlation.

The significant correspondence obtained indicates that XRF core scanning can be used to produce a quantitative high-resolution elemental analyses of peat samples, after a cross-check with ICP-MS. Our results show that several major and trace elements can be detected successfully using the scanning XRF spectrography and that scanning XRF technique is suitable when a high resolution, rapid and non destructive analysis is needed on fresh peat samples. Even though XRF core scanning provides a qualitative estimate of the elemental concentrations, very good correlations between scanning XRF and conventional ICP-MS indicate that quantitative estimation is also possible after constructing the appropriate calibration curves. Additional data are needed to identify which elements do not have the same behaviour of Pb and Sr.
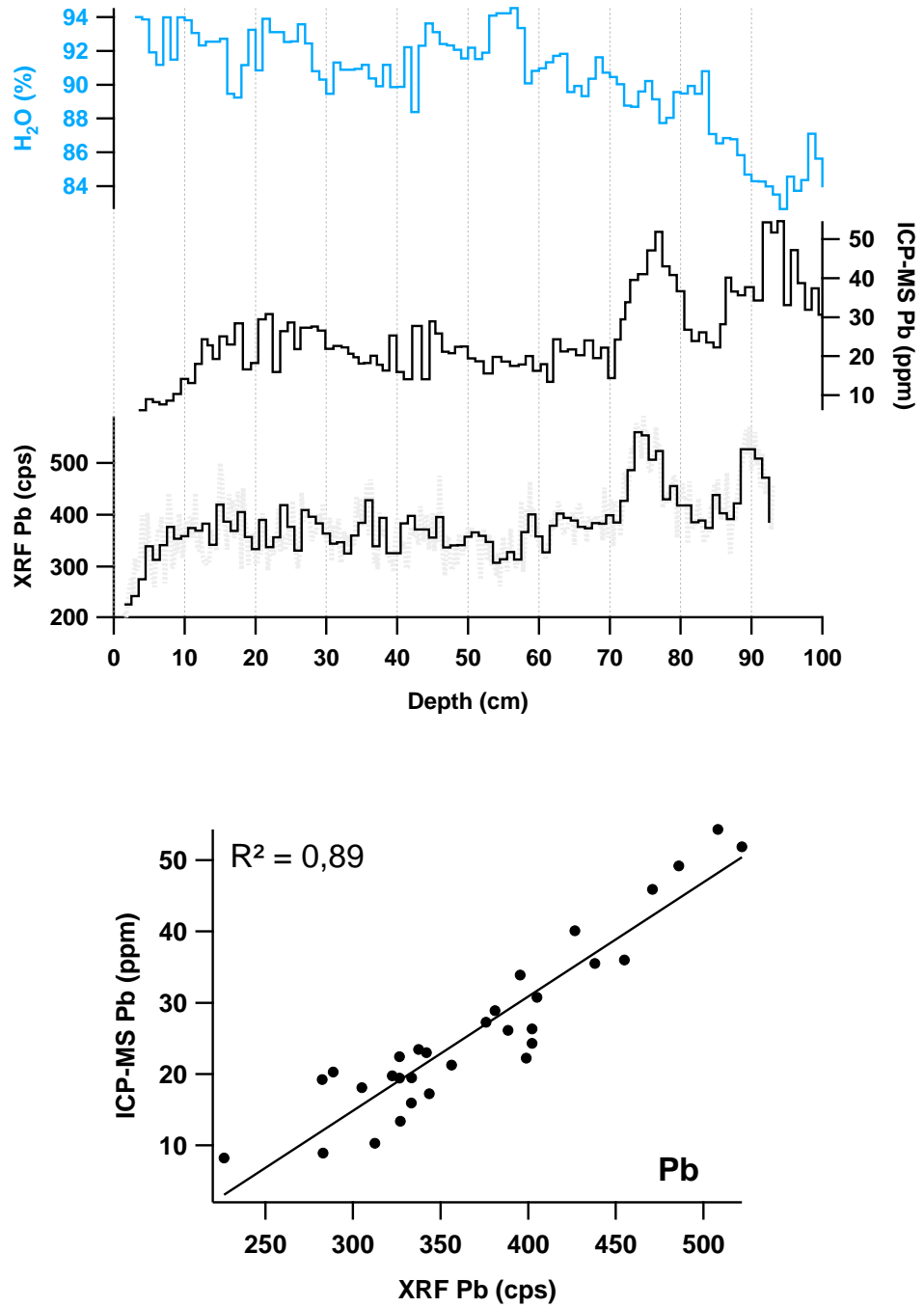
Figure 12.1: First graph represents Pb intensities, concentrations and water content along the first meter of Danta peat bog. Second graph reports the correlation coefficient calculate between XRF-CS and ICP-MS measurements.
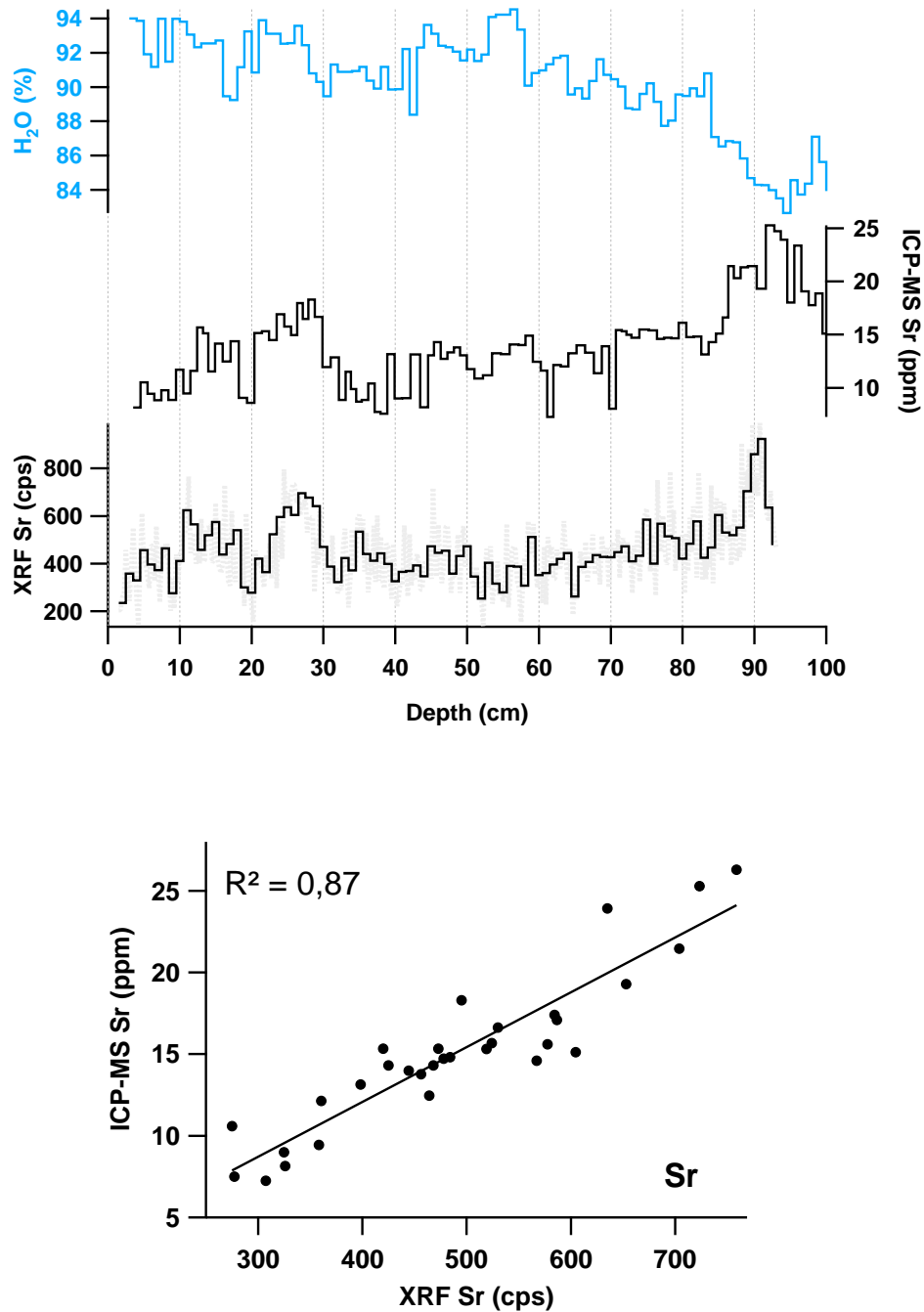
Figure 12.2: First graph represents Sr intensities, concentrations and water content along the first meter of Danta peat bog. Second graph reports the correlation coefficient calculate between XRF-CS and ICP-MS measurements.

Chapter 13

Trace elements analysis of pore water

13.1 Calibration and procedural blanks

The external calibration method was used for the quantification of the analytes. A 10 mg L^{-1} mother solution was prepared diluting together a 1000 mg L^{-1} multi-elemental standard solution (IMS-102 containing Al, As, Ba, Be, Bi, Cd, Ca, Ce, Cr, Co, Cu, Ga, In, Fe, Pb, Li, Mg, Mn, Ni, K, Rb, Se, Ag, Na, Sr, Tl, U, V, Zn). Calibrations were performed using 5 calibration standards ranging from 0.5 to 50 ug L^{-1} in order to cover, for each element, the concentration ranges present in peat samples. A second 10 mg L^{-1} mother solution containing the major crustal elements (Fe, Al, Na, K, Ca, Mg, Ti) was also prepared from a 50 mg L^{-1} multi-elemental standard solution (IMS-102, 1000 mg L^{-1}). For the major crustal elements, calibrations were performed using 5 calibration standards ranging from 50 to 1000 μg L^{-1}. For some elements, the concentration levels in peat samples vary greatly and could cover several orders of magnitude. In these cases, to guarantee the linearity of the calibration curve, calibrations at different concentration levels were performed. The intensity of standard solutions were fitted using a linear regression, and the y-axis intercept at zero concentration, which was assumed to represent an average blank of the standards, was subtracted for calibration. For all the elements R^2 > 0.998 were obtained.

13.2 Procedural blanks and detection limits

Concentrations of all elements in ultrapure water, were below that of the most diluted standard for each element in its analytical range (table 13.1). Thus, the use of ultrapure water for the preparation of standards and blank was justified. Solution detection limits for ICP-MS technique were calculated as the concentration corresponding to 3 times the standard deviation of the

measurement of the 10 acidic blank solutions. For major elements (Ca, Mg, Na, K, Al, Fe, Ti), DL ranged from 0.13 (Mg) to 0.77 (Na) ug L^{-1} while for trace elements from 0.003 (U, Gd, Cs) to 0.11 mg kg^{-1} (Zn).

Table 13.1: Detection limits ICP-MS pore water measurements.

	Blank values (μg/L)	**Mean peat concentration** (μg/L)	**Ratio peat/blank** values	**Solution DL** (μg/L)
Li	0.026 ± 0.0029	0.71	28	0.009
Na	1.45 ± 0.26	855	591	0.772
Mg	0.39 ± 0.044	1493	3833	0.132
Al	1.41 ± 0.19	332	235	0.558
Ca	62 ± 2.7	4780	77.10	8.2
Ti	0.36 ± 0.10	5.1	14.17	0.31
V	0.044 ± 0.0017	1.08	25	0.005
Cr	0.029 ± 0.004	0.40	14	0.013
Mn	0.04 ± 0.003	0.24	7	0.008
Co	0.027 ± 0.0045	0.28	10	0.014
Ni	0.14 ± 0.016	0.74	5	0.049
Cu	0.12 ± 0.023	1.2	10	0.069
Zn	0.46 ± 0.039	3.4	7	0.117
Ga	0.016 ± 0.0011	0.33	21	0.003
As	0.17 ± 0.015	1.4	8	0.044
Rb	0.022 ± 0.0024	9.9	441	0.007
Sr	0.017 ± 0.0039	9.9	5.75	0.012
Cd	0.027 ± 0.0068	0.088	3	0.020
Cs	0.0047 ± 0.0011	0.14	29	0.003
Ba	0.059 ± 0.0048	9.4	158	0.014
Tl	0.0076 ± 0.0017	0.079	10	0.005
Pb	0.025 ± 0.0037	1.35	54	0.011
U	0.027 ± 0.0011	0.027	10	0.003

13.3 Accuracy, precision and reproducibility

The analytical precision and accuracy was evaluated using a rain water certified reference material (TMRAIN-04), provided by Environment Canada, certified for 21 trace elements. The mean value of precision and recovery for all the tests (n=5) are reported in table 13.2. Our data appeared very accurate agreeing very well the certified values with recoveries ranging between 75% (Zn) to 119% (Ni). The precision was normally better than 10% while only for Al it exceeded 14.9%.

Table 13.2: Accuracy and precision ICP-MS pore water measurements.

	CRM certified concentrations (μg/L)	CRM found concentrations (μg/L)	Precision (%)
Li	0.39 ± 0.08	0.33 ± 0.021	6.4
Na	90*	75 ± 6.3	8.5
Mg	170*	173 ± 17	9.8
Al	1.7 ± 0.9	3.0 ± 0.44	14.9
Ca	600*	431 ± 27	6.5
Ti	0.47*	0.61 ± 0.14	5.2
V	0.64 ± 0.12	0.60 ± 0.032	5.4
Cr	0.79 ± 0.17	0.65 ± 0.064	9.8
Mn	6.1 ± 0.78	6.8 ± 0.31	4.5
Co	0.22 ± 0.04	0.23 ± 0.0097	4.2
Ni	0.80 ± 0.17	0.95 ± 0.042	4.4
Cu	6.2 ± 0.10	6.1 ± 0.21	3.4
Zn	11.5 - 12.2 *	8.6 ± 0.57	6.6
As	1.07 ± 0.25	1.21 ± 0.087	7.2
Sr	1.7 ± 0.26	1.6 ± 0.097	6.2
Cd	0.48 ± 0.12	0.38 ± 0.021	5.6
Ba	0.73 ± 0.15	0.86 ± 0.085	9.9
Tl	0.33 ± 0.07	0.37 ± 0.011	3.0
Pb	0.29 ± 0.09	0.27 ± 0.0087	3.2
U	0.25 ± 0.06	0.28 ± 0.0051	1.8

Chapter 14

Pb isotopes profile by ICP-MS

Pb isotopes ^{204}Pb, ^{206}Pb, ^{207}Pb and ^{208}Pb were determined. A sample of SRM 981 Common Lead Isotopic Standard (NIST, Gaithersburg, MD, USA) was dissolved in cold 1:1 (v/v) diluted HNO_3 (65%) which was diluted to a total lead concentration of 10 μg L^{-1}, and used as a mass bias correction solution for isotope ratio analysis every 4 samples. Comparison between standard values analysis and certified values was useful to calibrate the instruments before each run. The final total Pb concentration of peat digests ranges from 5 to 53 μg L^{-1}, thus each solution was diluted in order to obtain a final sample with a lead content < 10 μg L^{-1} to ensure that all ICP-MS measurements were carried out in the pulse counting detection mode.

14.1 Precision and accuracy

Isotope ratio measurements have traditionally carried out with Thermal ionization mass spectrometry (TIMS) and ICP-MS with a multiple collectors (MC). These techniques are characterized by very high precision that permits to measure very small changes in radiogenic isotopes measurements. Although ICP-QMS cannot compete with these techniques in term of precision, the precision of all our measurements, derived from 6 consecutive replicates, gave each ratio calculation RSD <0.4%, which is sufficient to our data to be used.

Measurements of the certified referenced peat material don't include data about lead isotope ratios, thus a clear definition of accuracy is not possible during this analysis. In order to understand if the calculated isotope ratio values are in an acceptable range, in the discussion of results they are compared with other data from measurements of lead isotopes from peat bog samples.

Chapter 15

C and N isotopes profiles by Delta$^+$ IRMS

Validation of this method is based on the following references:

- Official methods of Analysis of AOAC International, (2000). AOAC International, Arlington, VA. Method 972.43, Micro-chemical Determination of Carbon, Hydrogen and Nitrogen, Automated method.

- Method of soil analysis, part 3. Chemical method, soil science society of America Book series 5. Soil science society of America, Inc., Madison, Wisconsin. Dumas Method, Determination of total Nitrogen and total Carbon by Combustion.

- ECS 4010 Elemental Combustion System CHNS-O Operating Manual, Costech Analytical Technologies Inc., Valencia, CA.

- de Groot P.A., Handbook of Stable Isotopic Analytical Techniques, Volume 1, Elsevier, 2004, ISBN:0 444511148

15.1 Stability and linearity

To monitor the stability, measurement of isotopic composition of the working gas is fundamental. This test is known as the "zero enrichment" test and it consists of introducing typically ten pulses of working gas into the instrument and recording the standard deviation of the δ-values, relative to one of these pulses considered as standard. Generally the acceptable standard deviation for CO_2, N_2 and CO must be less than 0.1‰.

Working gas is used also to determine the linearity of the instrument. This measurement is similar to the "zero-enrichment" test, but the intensity of the working gas is increased during the sequence. Linearity for CO_2, N_2 and CO must be less than 0.1‰per volt: intensity of the working gas

must to encompass intensity of the sample that has to be determined, i.e. if samples are measured between 4000mV to 1500mV, linearity measurement has to cover the 3000-16000 mV range.

15.2 Calibration

15.2.1 Primary calibration materials

In IMRS measurements "calibration" refers to the calibration of the δ-scale rather of the m/Z scale. Isotope ratios are reported as δ-values expressed in part per thousand difference from accepted zero points:

- For carbon: VPDB (Vienna Peedee Belemnite). PDB is a calcium carbonate Cretaceous belemnite from the Peedee formation in South Carolina. Now exhausted, it has been replaced by another carbonate (NBS-19) versus the hypothetical VPDB, where V stay for "virtual".

- For nitrogen: atmospheric nitrogen.

15.2.2 Secondary reference materials

In this calibration natural or synthetic material calibrated versus the primary calibration materials are used. Their δ-values differ from the primary calibration materials because they have an uncertainty associated. These δ-values and uncertainties are reviewed and revised over time, and the results are shown on website http://nucleus.iaea.org.

Table 15.1: Secondary reference materials for $\delta^{13}C$ measurements, purchased by NIST.

Description	Nature	$\delta^{13}C\%_0$	SD
NBS22	oil	-30.031	0.043
NBS19	oil	+1.95	0.042
LSVEC	lithium carbonate	-46.6	0.2

15.2.3 Laboratory internal Standards

The internal standards used for the analysis have been verified using primary and the secondary materials. These are used in normalization and quality assurance: a known mass of these standards are analyzed for $\delta^{13}C$ and $\delta^{15}N$ and the results are used to create calibration curves for sample analysis. During the isotopic measurements all these standards were monitored: Wheat flour, Sorghum Flour and Low Organic Soil purchased by Elemental Microanalysis.

Table 15.2: Secondary reference materials for δ^{15}N measurements, purchased by NIST.

Description	Nature	δ^{13}C‰	SD
IAEA-N1	ammonium sulphate	+0.4	0.2
IAEA-N2	ammonium sulphate	+20.3	0.2
IAEA-NO-3	potassium nitrate	+4.7	0.2

15.2.4 External Reference Standards

At every batch of 12 samples, 1.0 mg of "Ke" standard (-22.43 δ^{13}C$_{VPDB}$, +6.8 δ^{15}N$_{AIR}$) was analyzed for δ^{13}C and δ^{15}N and the results are used to create external calibration curves for sample analysis.

15.3 Quality control

15.3.1 Blank determination

Empty silver sample capsules are introduced with the autosampler using the same Elemental Analyzer parameter set for the samples analysis: in fact a signal form blank can result from the atmospheric gases introduced by the autosampler.

Measurements on samples are corrected by this blank determination following the equation:

$$Blank_{corr} = \frac{\delta_{sample} * Area_{sample} - \delta_{blank} * Area_{blank}}{Area_{sample} - Area_{blank}}$$

were:

δ_{sample} is the value of the sample, δ_{blank} is the value of the blank, and Area$_{sample}$ and Area$_{blank}$ is the area of the sample and the blank peak respectively.

15.3.2 Precision and accuracy

Accuracy is based on the average per cent recovery of the standard measured against the theoretical concentration. Precision is given by calculating the relative standard deviation of the data set. Results are given below:

There are several processes that can alter the bulk peat ^{15}N signature, i.e., kinetic fractionation, decomposition, nitrification and denitrification and microbial incorporation of N which can demonstrate part of enrichment in ^{15}N. All these processes are also inter-related with changes in species composition, not from C$_3$ to C$_4$ (avoided by the analyses of ^{13}C), but along sphagnum species, and different species can be together in bulk peat. Although the

Table 15.3: Accuracy and precision

Identifier	Certified	Found	Precision %
Wheat flour amt%N	1.36	1.36 ± 0.003	0.22
Wheat flour amt%C	39.38	39.57 ± 0.27	0.68
Wheat flour δ^{15}N	2.85	2.98 ± 0.02	0.61
Wheat flour δ^{13}C	-27.21	-27.28 ± 0.03	0.11
Sorghum flour amt%N	1.47	1.42 ± 0.020	1.4
Sorghum flour amt%C	41.26	40.43 ± 0.016	0.04
Sorghum flour δ^{15}N	1.58	1.61 ± 0.01	0.62
Low organic soil amt%N	0.13	0.12 ± 0.0007	0.06
Low organic soil amt%C	1.52	1.41 ± 0.011	0.78
Low organic soil δ^{15}N	6.70	6.71 ± 0.02	0.29
Low organic soil δ^{13}C	-27.46	-27.43 ± 0.02	0.07
Low organic soil δ^{15}N	7.60	7.70 ± 0.10	1.29
Low organic soil δ^{13}C	-22.43	-22.55 ± 0.05	0.22

value of bulk peat ^{15}N is considered to be a significant environmental proxy (Zaccone et al., 2011), is not clear if our profile reflects an undisturbed ^{15}N signal, and additional researches are necessary to understand the climatic signal under the ^{15}N record.

Part IV

Results

Chapter 16

In field peat bog stratigraphy

The Val di Ciampo bog was drilled and 12 sections were extracted. Every section of the core was observed permitting a primary in field stratigraphic description.

A compact peat fills nearly the entire core reaching the bottom part of the bog where sediments of different origin are present. In particular the deepest part of the core shows the presence of *gyttija*, a lacustrin organic-rich sediment, between 600 and 680 cm. A mineral-rich layer at depths below 680 cm is identified, consisting mainly of *silt* and *clay* sediments. Above the clayey-silty deposit, at a depth between 600 and 620 cm, a layer in which wood fractions are mixed with organic sediments is identified. The presence of well-preserved wood samples enabled a precise 14C which represents the date in which bog started to accumulate. The rest of the core seems to be mainly composed of poorly decayed *Sphagnum* remains.

The field description of the recovered core sections was summarized as follows:

0 - 400 cm *Sphagnum* peat with other herbaceous plant remains. Low degree of decomposition. High water content.

400 - 600 cm *Sedge-sphagnum* peat, with increasing degree of decomposition, and lower water content.

600 - 680 cm Gyttija, organic-rich sediments, wood detritus, sediment from sapropel lake. Between 600 and 620 cm a layer with wood fractions is present.

680 - 700 cm Clayey-silty sediments with *Pisidium* shell remains.

Chapter 17

Chronology

17.1 ^{14}C Radiocarbon determinations

Samples selected for radiocarbon dating were cleaned, dried and then submitted for the analysis at the Chrono Center, Queens University of Belfast. Radiocarbon dates were calibrated using Calib software 6.0. Samples analyzed for ^{14}C are listed in table 17.1. Apart from the deepest samples, all radiocarbon ages were determined from wood fragments and bulk samples. The deepest one was determined from shells of *Pisidium*.

Results of every single calibration are reported in figure 17.1 and table 17.1. Each plot in figure 17.1 presents how radiocarbon measurements have been calibrated. The left-hand axis of all graphs shows radiocarbon concentration expressed in years "before present" BP and the bottom axis shows calendar years derived using tree ring data. The two blue lines indicates radiocarbon measurements from tree rings, plus or minus one standard deviation and the red curve on the y-axis reflects radiocarbon concentrations in the samples. The grey histogram represents the possible ages for the samples and usually the higher the histogram, the more likely that age is. Thus the final result of the calibration is expressed as a range, in which we can find the calibrated date with a 95% of probability (2 sigma interval). In Figure 17.2 all the radiocarbon determinations (left-hand axis) are plotted against the respectively calibrated dates cal BP, where the blue line indicates the radiocarbon measurements on tree rings with the relative one standard deviation.

The oldest age falls in the 13,100 - 13,300 years cal BP range, revealing that this archive continuously covers the whole Holocene and the last period of the Late Glacial (i.e., about the last 1500 years of the Late Glacial).
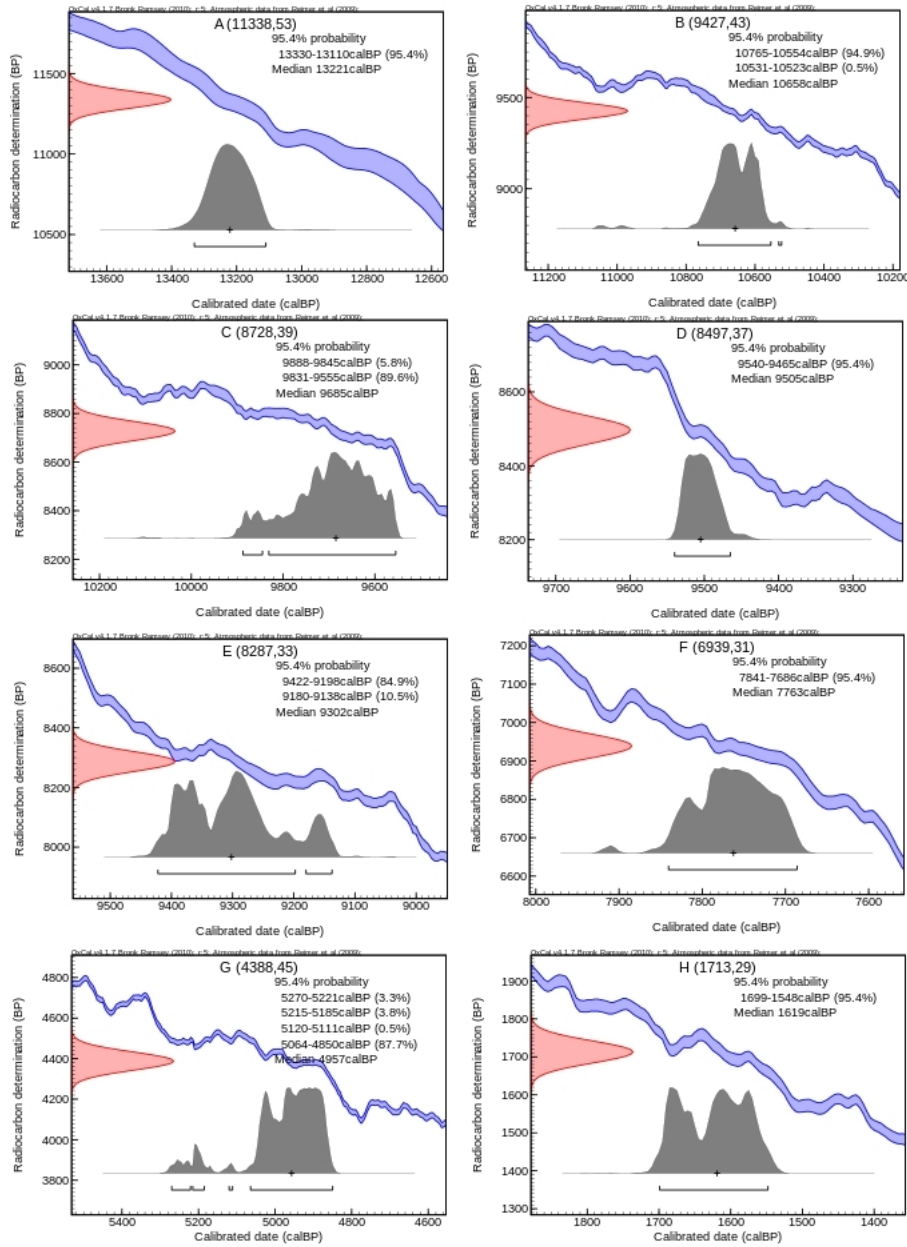
Figure 17.1: Radiocarbon ages calibration. Results obtained using Calib software 6.0 (Copyright 1986-2010 Stuiver and Reimer). For each graph the left-hand axis shows radiocarbon concentration expressed in years "before present" BP and the bottom axis shows calendar years derived using tree ring data. The two blue lines indicates radiocarbon measurements from tree rings, plus or minus one standard deviation and the red curve on the y-axis reflects radiocarbon concentrations in the samples. The grey histogram explains the possible ages for the samples.
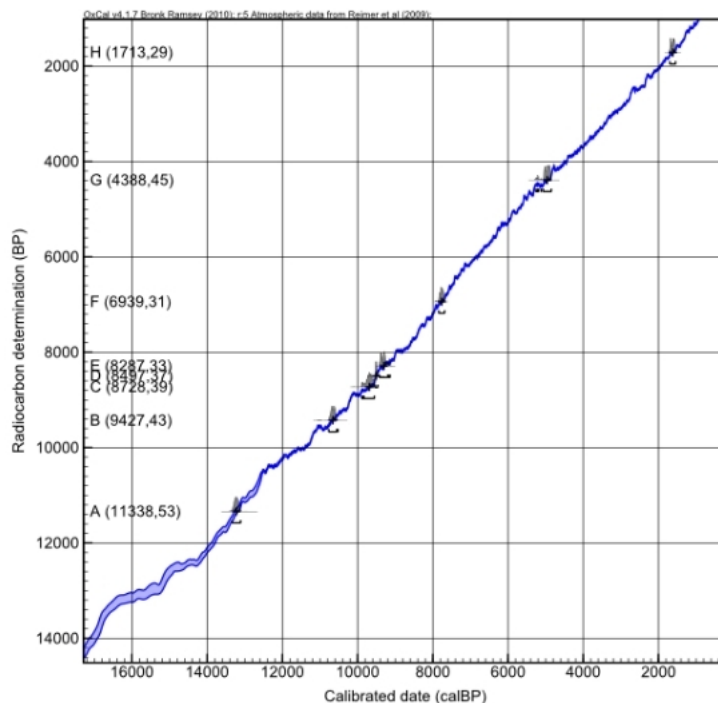
Figure 17.2: Calibration curve by Reimer et al. (2009). The blue area shows radiocarbon measurements on dated tree rings, (average value plus and minus one standard deviation). Radiocarbon data points lie above the calibration curve with the combined ^{14}C uncertainties.

Table 17.1: Radiocarbon dating results and calibration. For each depth the correspondences sample material type, the radiocarbon determination and the calibrated range (cal BP) are reported.

Depth (cm)	Material Type	^{14}C Age	^{14}C age cal BP (range)
109 - 110	Peat	1713 ± 23	1555 - 1695
263 - 264	Wood	4388 ± 45	4850 - 5060
394 - 395	Wood	6939 ± 31	7687 - 7839
558 - 559	Wood	8497 ± 37	9198 - 9421
591 - 593	Wood	8287 ± 33	9466 - 9539
608 - 609	Wood	8728 ± 39	9554 - 9824
657 - 658	Wood	9427 ± 43	10554 - 10764
695 - 696	Shells	11338 ± 53	13110 - 13330

17.2 ^{210}Pb measurements

In ombrotrophic peatlands it is assumed that atmospheric depositions supply all nutrients and inorganic materials. It means that the largest fraction of ^{210}Pb in peat is produced by the decay of gaseous ^{222}Rn in the atmosphere and not supported by local ^{226}Ra activity: for this reason it's called "unsupported" ^{210}Pb(Appleby et al., 1997). Total, unsupported and supported ^{210}Pb and ^{137}Cs activities were measured in the first 36.5 cm of the peat core and their relative activities are reported in table 17.2.

Table 17.2: Total, unsupported and supported ^{210}Pb and ^{137}Cs activities as measured in the first 36.5 cm of the core.

Depth cm	Total ^{210}Pb Bq Kg^{-1}	Unsupported ^{210}Pb Bq Kg^{-1}	Supported ^{210}Pb Bq Kg^{-1}	^{137}Cs Bq Kg^{-1}
1.5	446.0 ± 22.3	446.0 ± 22.3	0.0 ± 0.0	589.1 ± 8.3
4.5	406.8 ± 21.4	406.8 ± 21.4	0.0 ± 0.0	319.3 ± 6.2
6.5	477.5 ± 33.8	476.3 ± 34.5	1.2 ± 7.0	273.4 ± 8.4
8.5	386.4 ± 31.7	383.6 ± 32.4	2.8 ± 6.7	259.8 ± 7.8
10.5	172.3 ± 12.3	169.4 ± 12.7	2.9 ± 2.7	212.0 ± 4.2
12.5	258.8 ± 17.6	247.4 ± 18.4	11.4 ± 5.6	247.7 ± 5.2
14.5	238.6 ± 15.6	228.3 ± 16.2	10.3 ± 4.5	298.0 ± 5.2
16.5	176.3 ± 8.9	172.0 ± 9.3	4.2 ± 2.8	207.4 ± 2.5
18.5	135.9 ± 15.5	133.7 ± 15.8	2.1 ± 3.4	102.9 ± 3.7
20.5	67.5 ± 10.6	67.5 ± 10.6	0.0 ± 0.0	83.7 ± 2.6
22.5	89.3 ± 9.5	89.3 ± 9.5	0.0 ± 0.0	97.9 ± 2.4
24.5	97.3 ± 12.2	97.3 ± 12.2	0.0 ± 0.0	64.9 ± 2.6
26.5	66.1 ± 14.1	66.1 ± 14.1	0.0 ± 0.0	48.5 ± 3.1
28.5	57.8 ± 9.7	57.8 ± 9.7	0.0 ± 0.0	41.1 ± 2.1
30.5	26.9 ± 8.1	26.7 ± 8.4	0.2 ± 2.0	43.5 ± 2.0
32.5	30.7 ± 6.8	30.7 ± 6.8	0.0 ± 0.0	52.8 ± 1.7
34.5	16.5 ± 9.1	16.5 ± 9.1	0.0 ± 0.0	38.7 ± 2.0
36.5	34.5 ± 11.7	26.6 ± 12.4	8.0 ± 4.1	47.3 ± 2.5
38.5	6.7 ± 7.2	6.7 ± 7.2	0.0 ± 0.0	45.1 ± 1.7

Using the CRS dating model (Appleby and Oldfield, 1978; Appleby, 2001) we assessed that thickness subject to ^{210}Pb measurements represents 100 years of deposition (table 17.3 and figure 17.3). Over that time, unsupported ^{210}Pb concentrations exponentially declined with depth, suggesting a relatively uniform net peat accumulation rate, with a mean value of 0.020 ± 0.003 g cm^{-2} y^{-1} (or 0.24 ± 0.03 cm y^{-1}). A few non-monotonic features at 10-11 cm and 20-23 cm may indicate discontinuities in the normal process of peat accumulation in the 1960s and 1990s (figure 17.3). The relatively high ^{137}Cs concentrations ($> 3{,}600$ Bq m^{-2}) suggest that a significant fraction of the ^{137}Cs in the uppermost part of the core derives from the 1986 Chernobyl
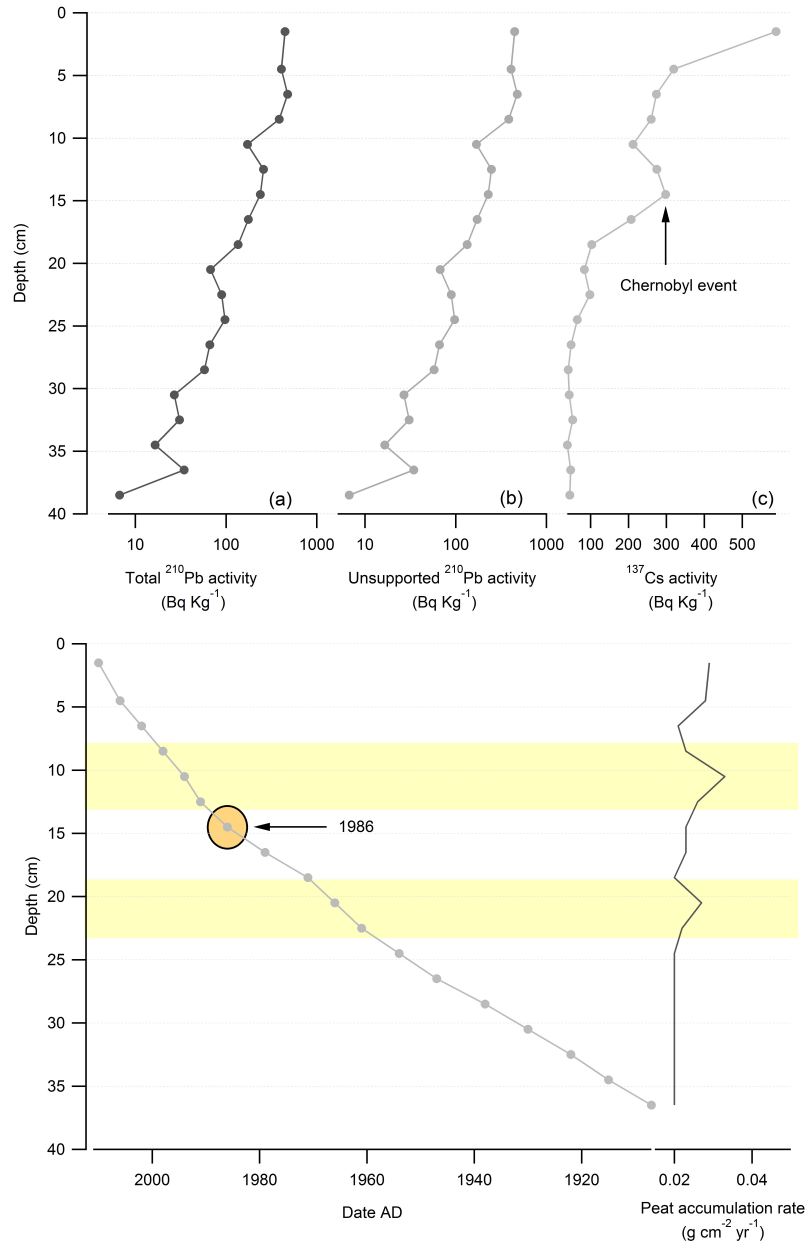
Figure 17.3: The first graph shows radionuclides measured in Danta di Cadore peat core demonstrating total ^{210}Pb (a), unsupported ^{210}Pb (b) and ^{137}Cs (c) concentrations versus depth. The second graph represents radiometric chronology of the core and the probable 1986 depth suggested by the ^{137}Cs stratigraphy. Peat accumulation rates show discontinuities of the process of peat accumulation in the 1960s and 1990s (yellow bars).

accident fallout. The ^{137}Cs activity has the highest values (589 Bq kg^{-1}) in the living plant material in the uppermost 5 cm of the core, but ^{137}Cs is also detectable below this depth, implying a significant mobility of this radionuclide. This vertical migration is consistent with ^{137}Cs trends observed both in other Swiss (Zaccone et al., 2007) and Irish (Mitchell et al., 1992; Gallagher et al., 2001) bog profiles.

^{210}Pb dates calculated using the CRS dating model place 1986 at a depth between 12 and 13 cm, and 1963 at a depth between 18 and 19 cm below the surface (table 17.3). An extrapolation of the chronology in the uppermost sections is consistent with the supposition that the ^{137}Cs peak at 14.5 cm records fallout from the 1986 Chernobyl reactor fire.

Table 17.3: Final chronology as resulted by ^{210}Pb and ^{137}Cs dating methods. For each depth also sedimentation rate has been calculated.

Depth cm	Chronology Date AD	Sedimentation Rate g cm^{-2} y^{-1}
0.0	2011 ± 0	
1.5	2010 ± 1	0.029
4.5	2006 ± 2	0.028
6.5	2002 ± 2	0.021
8.5	1998 ± 3	0.023
10.5	1994 ± 3	0.033
12.5	1991 ± 3	0.033
14.5	1986 ± 4	0.023
16.5	1979 ± 4	0.023
18.5	1971 ± 4	0.020
20.5	1966 ± 4	0.027
22.5	1961 ± 4	0.022
24.5	1954 ± 4	0.020
26.5	1947 ± 5	0.020
28.5	1938 ± 6	0.020
30.5	1930 ± 8	0.020
32.5	1922 ± 10	0.020
34.5	1915 ± 12	0.020
36.5	1907 ± 14	0.020

Chapter 18

Physical stratigraphy

Physical proprieties of peat, such as texture, organic content, pH, colour, water content and ash content are the basis for its classification: in fact they reflect peat-forming and peat-development processes. Results of its assessment by XRF Line scan camera and LOI measurements allow to implement all the information already obtained with the in field bog stratigraphy (figure 18.1) and are listed in this chapter.
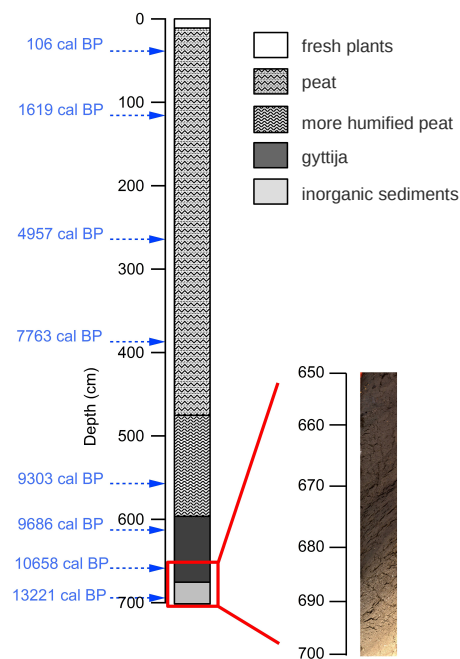
Figure 18.1: Figure represents the summary of the in field peat bog stratigraphy, with the boundary layers between fresh material, peat, gyttija and inorganic sediment, associated with the measured ^{14}C data points.

18.1 Colour and photos of peat sections by XRF core scanner

XRF equipped with line scan color camera allowed to obtain very high resolution images of every section of the core. Pictures were made at 20ms (milliseconds) and are presented in figure 18.2 and 18.3. These images immediately confirm the preliminary description of the bog profile as recorded in the field, and allow a better discrimination from peat and other type of sediments accumulations.

The line scan camera was also used to record the RGB color spectra. Results of colors and luminescence profiles are showed in figure 18.4 where these parameters are plotted against depth. Colors spectra identified several clear changes along the profile. The first peak on the top of the core is related with the presence of living plants and in particular of *Sphagnum magellanicum* as confirmed by the high signal in the R spectrum. This species is in fact characterized by bright red pigments in its structures and leaves. Other two peaks are present under 600 cm of depth: the first, very sharp, is related to the presence of wood remains; the other one follows an increasing trend evident for all the component of the RGB spectrum, corresponding to the transition from organic-rich sediment to a clayey-silty lacustrin deposit.

18.2 Physical proprieties of the peat

A better determination of peat components has been carried out following the loss on ignition (LOI) technique. The results of LOI analyses are presented in figure 18.5. Bulk density and ash content show a similar profile being in a stable range between 0 and approximately 400 cm, and starting to increase under this depth. In particular dry bulk density values vary between 0.03 and 0.11 g/cm^3 (0 and 450 cm), 0.11 and 0.36 g/cm^3 (450 and 600 cm) and reach a maximum value of 0.82 g/cm^3 (600 and 700 cm). The statistical significant correlation observed between water content and dry density (R= - 0.97, p$\leq$ 0.05), indicates that the variation in the water holding capacity of peat is negatively correlated to the bulk density, thus confirming a vertical stratification of the peat organic matter with a zone of elevated density and, consequently, a reduced permeability and hydraulic conductivity. This is consistent with observations previously reported by Boelter (1969) and Zaccone et al. (2009a). The ash content is constantly between 1.8 and 4.7% until a depth of 400 cm below the surface, increases to 4.7 - 9.8% by 450 cm, and then jumps to 90% at a depth of 600 cm in correspondence with the mineral-rich sediments. Maximum ash and bulk density values are reached together down 600 cm of depth. Following the ASTM classification (American Society for Testing Material, 1990) the reported values of ash content and

Figure 18.2: 20ms pictures taken by XRF line scan colour camera. 0 - 400 cm.
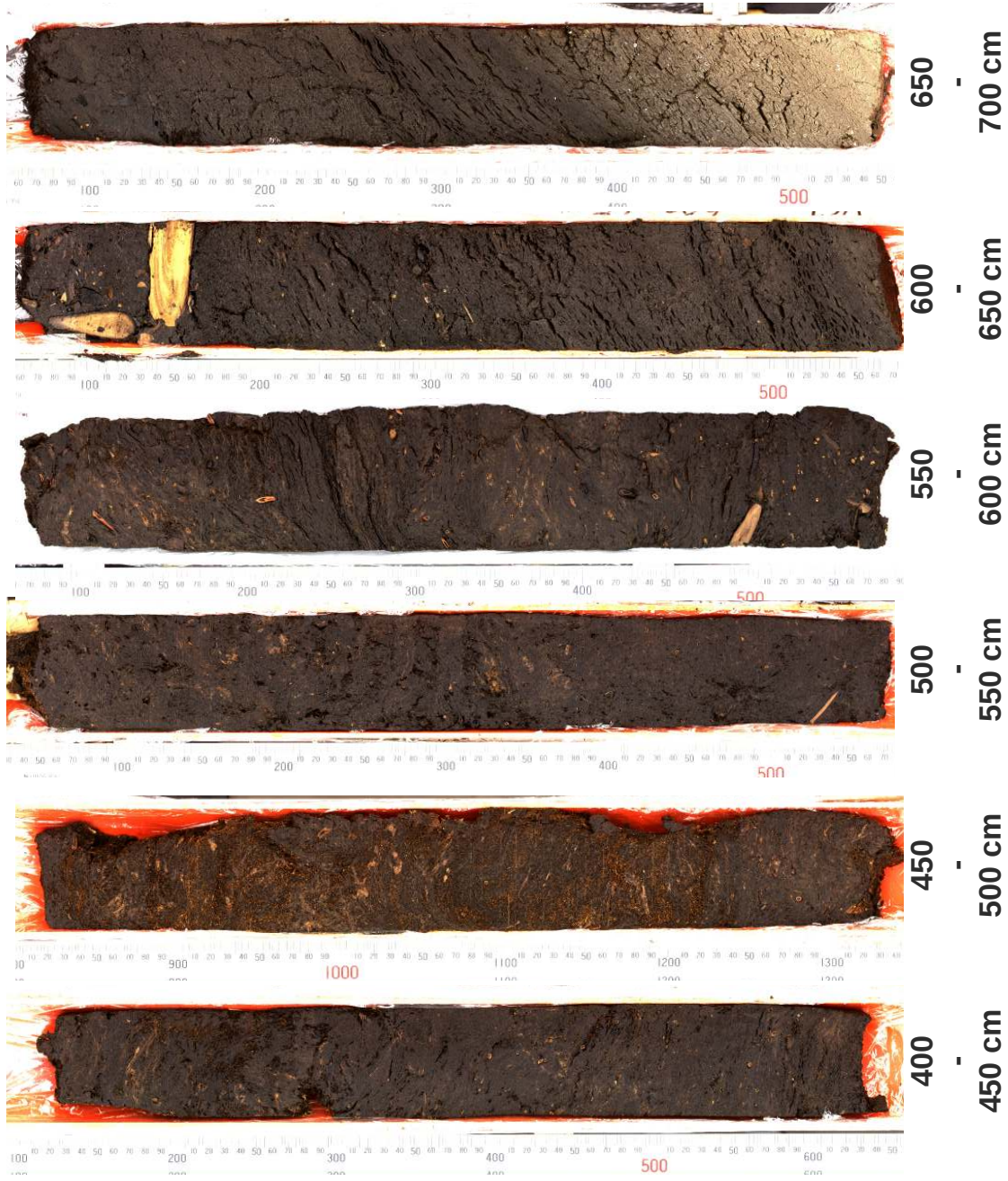
Figure 18.3: 20ms pictures taken by XRF line scan colour camera. 400 - 700 cm.

bulk density until 400 cm of depth correspond to ombrotrophic conditions. These two components explain very well the transition from ombrotrophic to minerotrophic peat better defining the final physical characteristics of the entire core.

Pore water extracted every cm from the first meter of the core was analyzed for pH and electrical conductivity (EC). Results are reported in figure 18.5. pH values appear to be constant with depth with values that indicates acidic conditions (pH between 4.0 - 4.5) and an oligotrophic status typical of habitats dominated by *Sphagum* spp. The fairly constant pH in pore water suggests that dissolution of mineral matter (mainly carbonates) is insufficient to neutralize the acidity generated by the decomposition of organic matter (Shotyk, 1988; Neuzil et al., 1993).

EC was measured and then corrected for the effect of the H^+ content, following Large et al. (2009). Low EC values indicate that water in the peat contains little dissolved inorganic matter and that significant diagenetic mineral precipitation is unlikely (Large et al., 2009). With the exception of the upper 10 cm, EC shows low values between 20 and 65 μS/cm. The increase in the upper part of the bog is very likely due to living *Sphagum spp.* material with its high ion exchange activity (Ferrat et al., 2012).
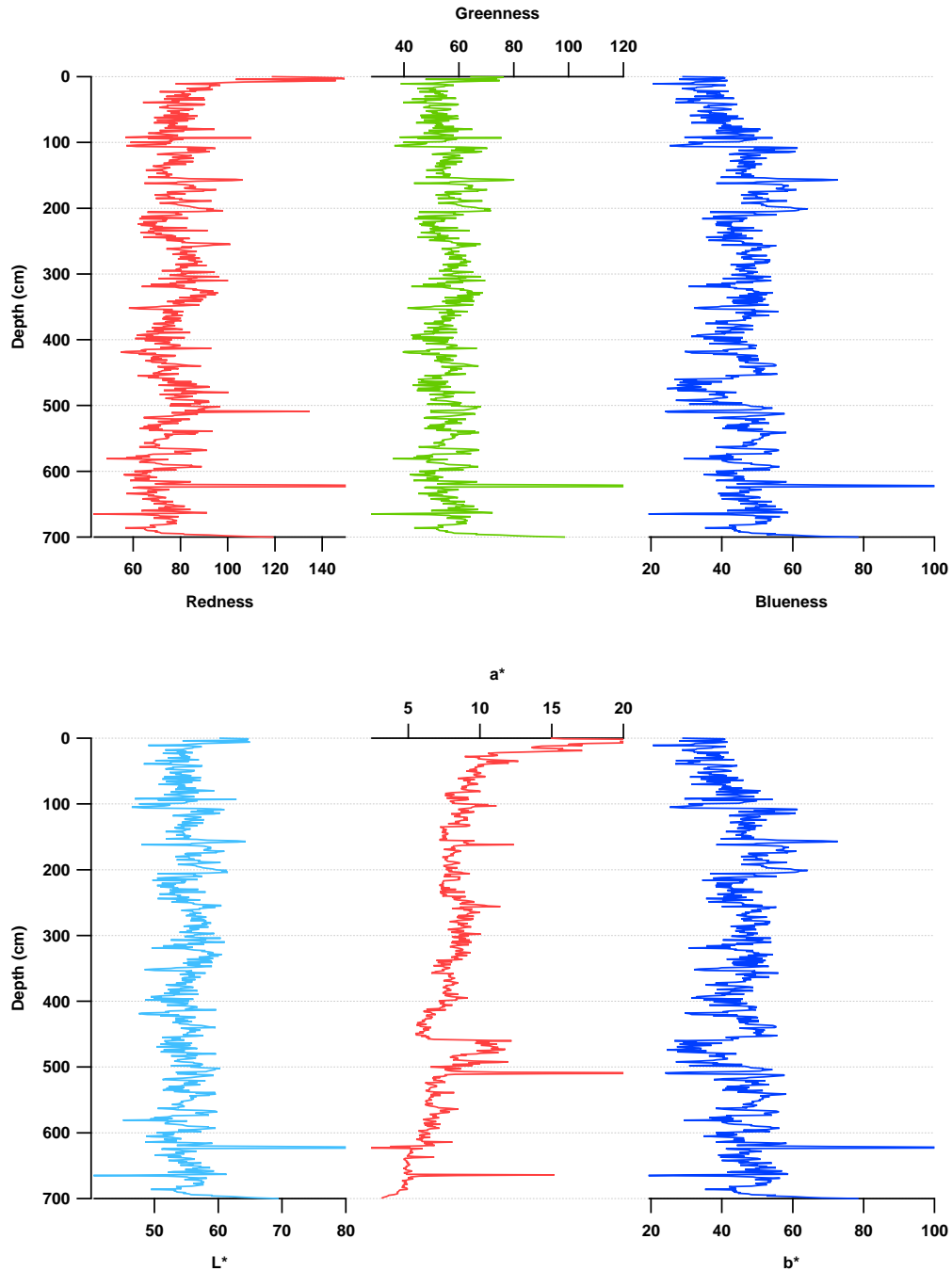
Figure 18.4: RGB colour spectra against peat core depth. The first graph shows redness, greenness and blueness parameters. The second graph show the transformed luminance parameters L*, a* and b*.
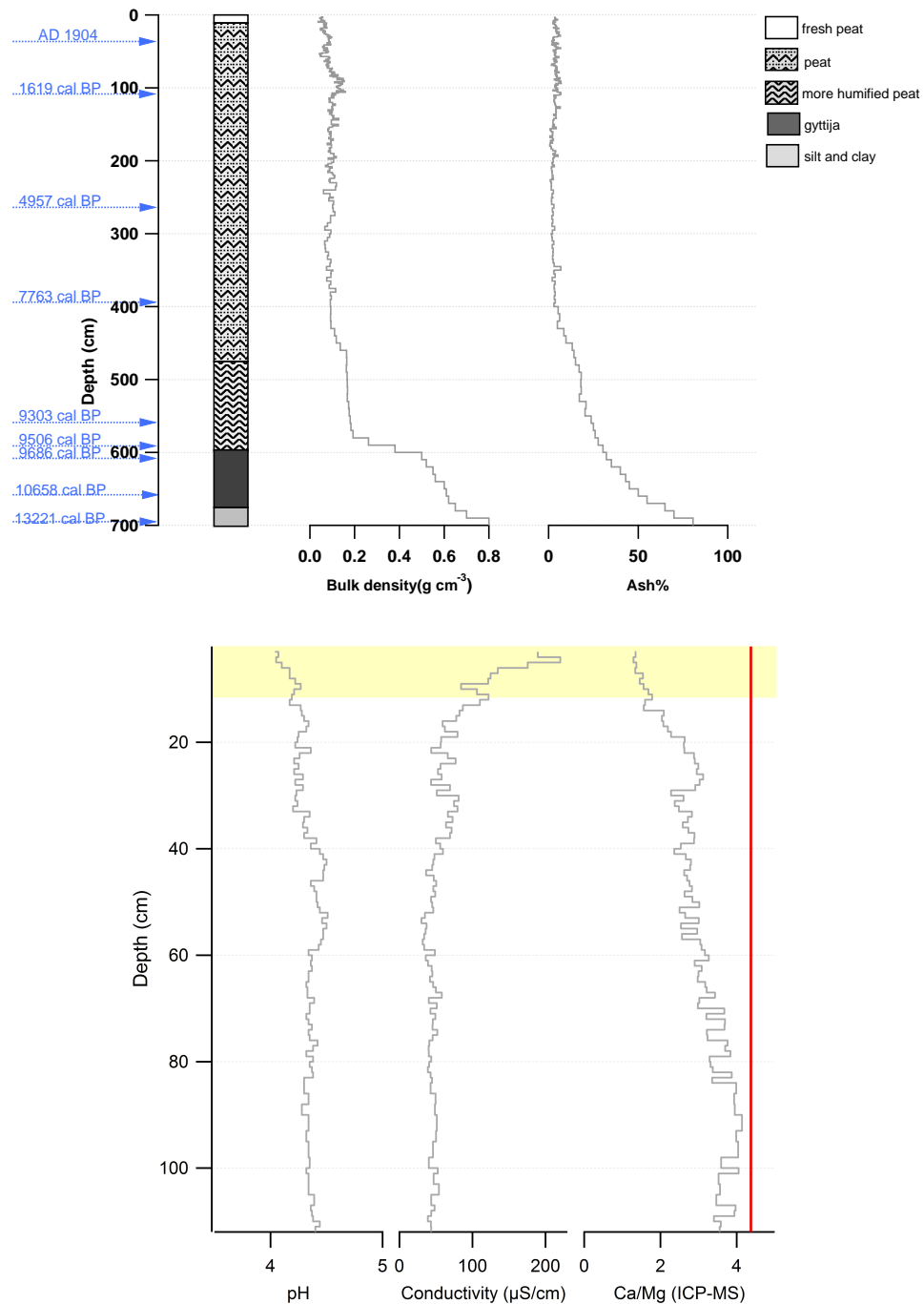
Figure 18.5: Graphs reported here show the summary of the physical characteristics of the bog. The first one plots the assessed in field peat bog stratigraphy, bulk density and ash profiles against depth and ^{14}C data points. The second one plots pH, conductivity and Ca/Mg values (discussed in section *Discussion - Ombrotrophic minerotrophic boundary layer*) profiles against depth; the red line represent the Ca/Mg ratio of rain samples collected from Danta di Cadore ("LIFE Nature Programme Danta: Project to safeguard the integrity of Danta di Cadore peat bogs"). The yellow bar emphasizes EC increment in the first cm of the bog, due to fresh plant activity.

Chapter 19

Chemio-stratigraphy

19.1   XRF

XRF core scanner analyses evaluated 13 chemical elements with a res-
olution of 2.5 mm along the entire 7-meters peat bog core. In figure 19.1
intensities derived from the XRF core logs are plotted versus depth. Inten-
sity range varies greatly between the elements observed, thus they appear
to reflect the same trend: the very high resolution records demonstrate that
the interval across time covered by peat accumulation is characterized by an
abrupt change, evident in every profile, under 500 cm of depth. This change
fits the already described transition from peat to sediments of different na-
ture. Trace lithogenic elements Rb and Sr follow the same characteristics
of Fe, Ti and Si: they start to increase under the boundary layer between
peat and gyttija, and even more under 600 cm of depth corresponding to
the transition to the mineral lacustrin layers. Ca started to increase before
all the other elements, at approximately 400 cm of depth reflecting that un-
der this boundary it may derive from several different sources. Fe has not
an increase with depth demonstrating no evidence for post-depositional mo-
bilization and the similarity between its concentration pattern with other
trace and major lithogenic elements suggest that its deposition is related to
erosional processes.

Lead trend is also shown in figure 19.1: its profile has some consistency
with the other elements and at the same time some peculiarities: under
600 cm of depth it shows the same increase that characterized all the other
elements, otherwise rising up to the surface it appears to reach high inten-
sity level probably related with anthropogenic emissions. Its immobility,
confirmed in several studies such as Shotyk et al. (1998) and Ferrat et al.
(2012), makes lead a perfect element to detect anthropogenic sources to the
bog. Comparing Pb profile with Ti profile, or with the other lithogenic ele-
ments, it is possible to explain that Pb in the upper part of the bog is not
related with natural erosional processes, because this trend is not present in
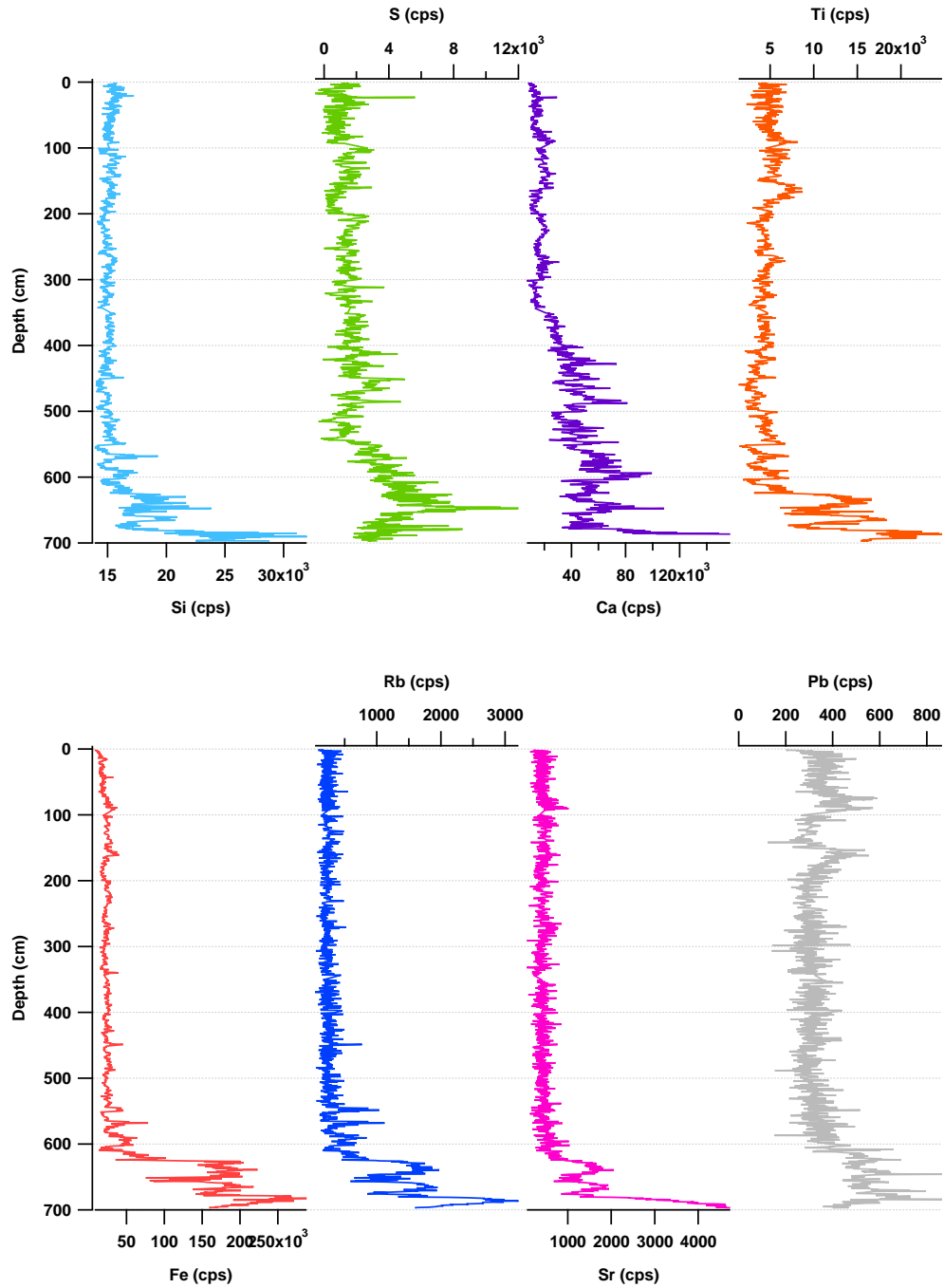
Figure 19.1: Si, S, Ca, Ti, Fe, Rb, Sr, Pb down-core intensities profiles as measured with XRF-core scanner and plotted versus depth.

the other elements profile.

XRF qualitative data have been calibrated with the ICP-MS (see section *Method validation and quality control*) permitting to distinguish and identify the precise metal sources, and the real enrichment the monitored elements in the bog. Calculation of Pb enrichment factor with ICP-MS data is reported and discussed in section *Discussion* as the relative individuation of different Pb sources by analyzing lead isotopes.

19.2 ICP-MS

19.2.1 General changes in major and trace elements profiles

Peat samples

Discrete samples were collected from the first meter of the core with a resolution of 1.0 cm and analyzed by ICP-MS technique for determining the concentrations of lithogenic elements, trace metals, and rare earth elements. In total the concentrations of 44 elements were determined. In figure 19.2 the summary statistics of the elements' concentration is presented and concentration profiles are reported in figure 19.3, 19.4, 19.5, 19.6 and 19.7. In each graph element concentrations (in ppm) are plotted versus depth (in cm). Measured concentrations differ by several order of magnitude ranging between ppb and ppm. As reported in figure 19.2 the higher concentrations were found for sodium (Na), magnesium (Mg), aluminum (Al), potassium (K), calcium (Ca), and iron (Fe) which are considered the major constituents of the Continental Crust (Wedepohl, 1995).

The first observation that can be done regards potassium (K), manganese (Mn) and zinc (Zn) profiles: they differ from all the other elements presenting the highest concentrations in the very top layers of the bog, 0 - 5 cm of depth. This zone is the uppermost part of the *acrotelm*, that consist predominantly of fibers of *Sphagnum* mosses largely still alive which use these elements as nutrients. Also alkaline earth metals as Ca and Mg are of primary importance for plant growth but their concentrations follow a different profile: Mg has a strong peak next to the top of the core and then slightly decrease reaching the bottom, Ca shows values that oscillate in the range of 1559 and 4394 ppm along the entire section with no distinct peaks. While Ca, Mg and K are of prime importance for plant growth, Na is also (like K) an alkaline metals but is a non-essential element. In fact it has not the highest concentrations in the top layers of the bog and it doesn't show a peculiar trend along the core ranging between 31 and 345 ppm.

Lithogenic elements such as Al, scandium (Sc), titanium (Ti), gallium (Ga), strontium (Sr) and yttrium (Y) show similar profiles: their concentrations increase with depth reaching a maximum value between 80 and 100 cm. The same trend is also followed by REE (rare earth elements): this

Figure 19.2: Descriptive statistic of ICP-MS measurements. For each element min value, max value, first and third quartile, median value and mean value are reported.

Li
Min.:0.0800
1stQu.:0.5700
Median:0.7700
Mean:0.8026
3rdQu.:0.9350
Max.:2.4300

Be
Min.:0.02000
1stQu.:0.05000
Median:0.08000
Mean:0.08182
3rdQu.:0.10000
Max.:0.23000

Na
Min.:31.06
1stQu.:104.98
Median:142.22
Mean:142.63
3rdQu.:169.14
Max.:345.86

Mg
Min.:308.6
1stQu.:519.9
Median:601.3
Mean:742.8
3rdQu.:836.0
Max.:2104.9

Al
Min.:705.2
1stQu.:2128.8
Median:2836.8
Mean:2999.3
3rdQu.:3569.2
Max.:6787.0

K
Min.:92.63
1stQu.:317.54
Median:437.37
Mean:507.59
3rdQu.:611.09
Max.:1577.51

Ca
Min.:1559
1stQu.:2648
Median:2931
Mean:2967
3rdQu.:3311
Max.:4394

Sc
Min.:0.1000
1stQu.:0.5000
Median:0.7800
Mean:0.8415
3rdQu.:1.0100
Max.:2.3400

Ti
Min.:30.83
1stQu.:110.06
Median:167.20
Mean:179.75
3rdQu.:209.84
Max.:578.74

V
Min.:1.440
1stQu.:3.650
Median:4.720
Mean:4.729
3rdQu.:6.030
Max.:8.430

Cr
Min.:0.860
1stQu.:2.805
Median:3.430
Mean:8.035
3rdQu.:4.090
Max.:174.550

Mn
Min.:1.780
1stQu.:3.375
Median:4.220
Mean:7.898
3rdQu.:5.880
Max.:72.300

Fe
Min.:476.7
1stQu.:1218.5
Median:1474.5
Mean:1454.3
3rdQu.:1612.3
Max.:2914.5

Co
Min.:0.370
1stQu.:0.900
Median:1.030
Mean:1.023
3rdQu.:1.125
Max.:2.070

Ni
Min.:0.890
1stQu.:1.725
Median:1.990
Mean:3.892
3rdQu.:2.320
Max.:74.460

Cu
Min.:2.330
1stQu.:4.250
Median:5.290
Mean:5.734
3rdQu.:6.970
Max.:13.870

Zn
Min.:1.210
1stQu.:2.005
Median:3.060
Mean:6.408
3rdQu.:7.480
Max.:33.910

Ga
Min.:0.850
1stQu.:2.090
Median:2.480
Mean:2.593
3rdQu.:3.065
Max.:5.340

As
Min.:0.200
1stQu.:0.830
Median:1.110
Mean:1.141
3rdQu.:1.360
Max.:2.320

Se
Min.:0.0200
1stQu.:0.1150
Median:0.1500
Mean:0.1584
3rdQu.:0.1900
Max.:0.3200

Rb
Min.:0.58
1stQu.:2.05
Median:2.59
Mean:2.90
3rdQu.:3.34
Max.:7.43

Sr
Min.:7.25
1stQu.:11.56
Median:14.02
Mean:13.98
3rdQu.:15.62
Max.:25.29

Y
Min.:0.230
1stQu.:0.615
Median:0.990
Mean:1.055
3rdQu.:1.310
Max.:2.660

Ag
Min.:0.0100
1stQu.:0.0600
Median:0.0800
Mean:0.1243
3rdQu.:0.1350
Max.:0.5400

Cd
Min.:0.0700
1stQu.:0.1000
Median:0.1100
Mean:0.1492
3rdQu.:0.1700
Max.:0.5100

Ba
Min.:13.92
1stQu.:33.03
Median:42.14
Mean:46.33
3rdQu.:57.20
Max.:105.32

Gd
Min.:0.0800
1stQu.:0.2250
Median:0.3700
Mean:0.3972
3rdQu.:0.4950
Max.:1.0400

Tb
Min.:0.01000
1stQu.:0.02000
Median:0.04000
Mean:0.04657
3rdQu.:0.06000
Max.:0.13000

Dy
Min.:0.0500
1stQu.:0.1550
Median:0.2600
Mean:0.2833
3rdQu.:0.3550
Max.:0.7800

Ho
Min.:0.01000
1stQu.:0.03000
Median:0.05000
Mean:0.04939
3rdQu.:0.06000
Max.:0.14000

Er
Min.:0.0300
1stQu.:0.0800
Median:0.1400
Mean:0.1522
3rdQu.:0.1900
Max.:0.4300

Tm
Min.:0.00000
1stQu.:0.01000
Median:0.02000
Mean:0.01788
3rdQu.:0.02000
Max.:0.05000

Yb
Min.:0.0200
1stQu.:0.0700
Median:0.1200
Mean:0.1325
3rdQu.:0.1650
Max.:0.3900

Lu
Min.:0.00000
1stQu.:0.01000
Median:0.02000
Mean:0.01758
3rdQu.:0.02000
Max.:0.05000

Tl
Min.:0.01000
1stQu.:0.04000
Median:0.05000
Mean:0.06556
3rdQu.:0.08000
Max.:0.35000

Pb
Min.:5.96
1stQu.:18.34
Median:22.92
Mean:25.29
3rdQu.:30.01
Max.:53.62

Th
Min.:0.0800
1stQu.:0.3200
Median:0.5400
Mean:0.6098
3rdQu.:0.7150
Max.:1.8300

U
Min.:0.0400
1stQu.:0.1450
Median:0.2500
Mean:0.2823
3rdQu.:0.3250
Max.:0.9300
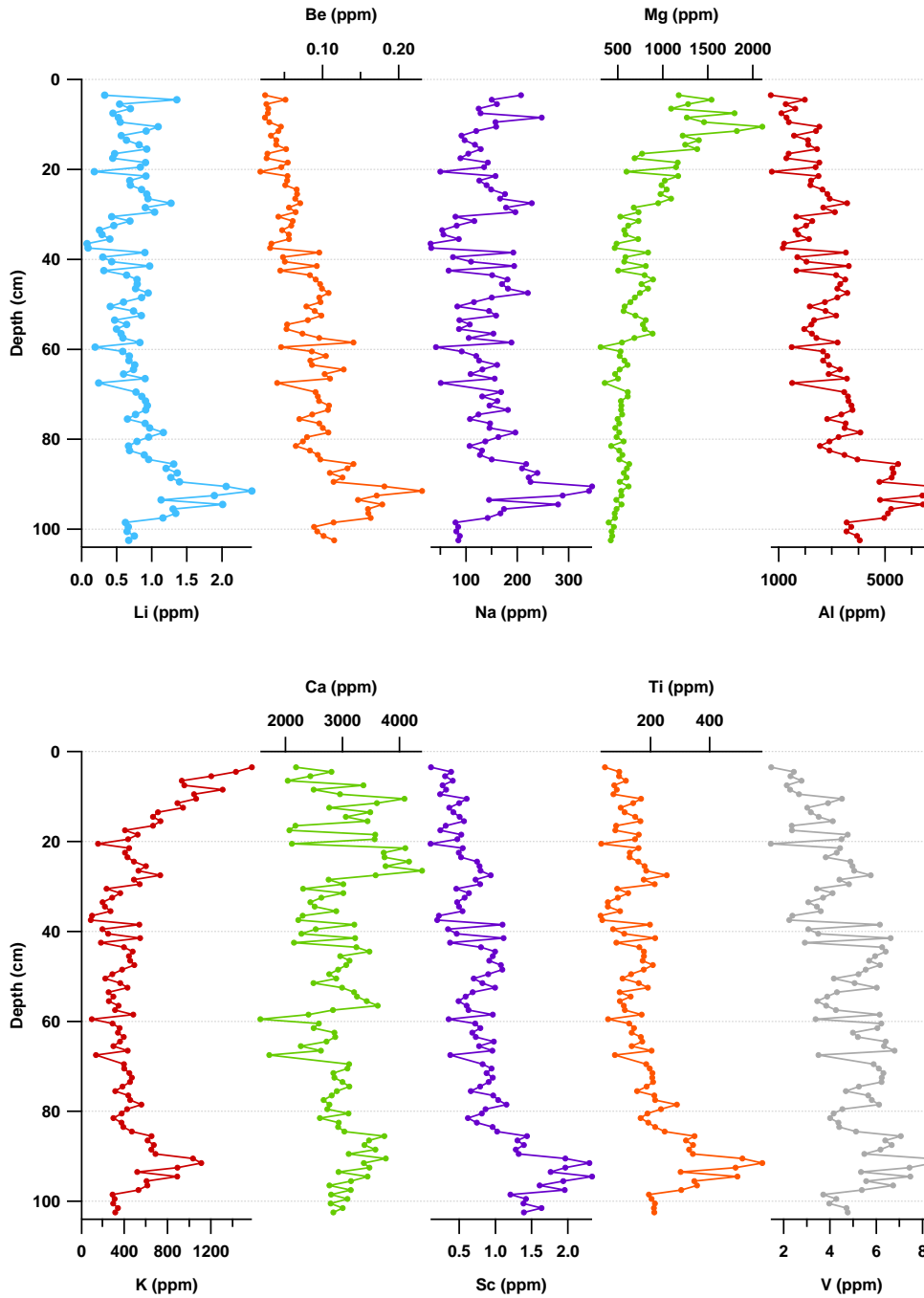
Figure 19.3: ICP-MS peat measurements: Li, Be, Na, Mg, Al, K, Ca, Sc, Ti, V concentration profiles plotted versus depth.
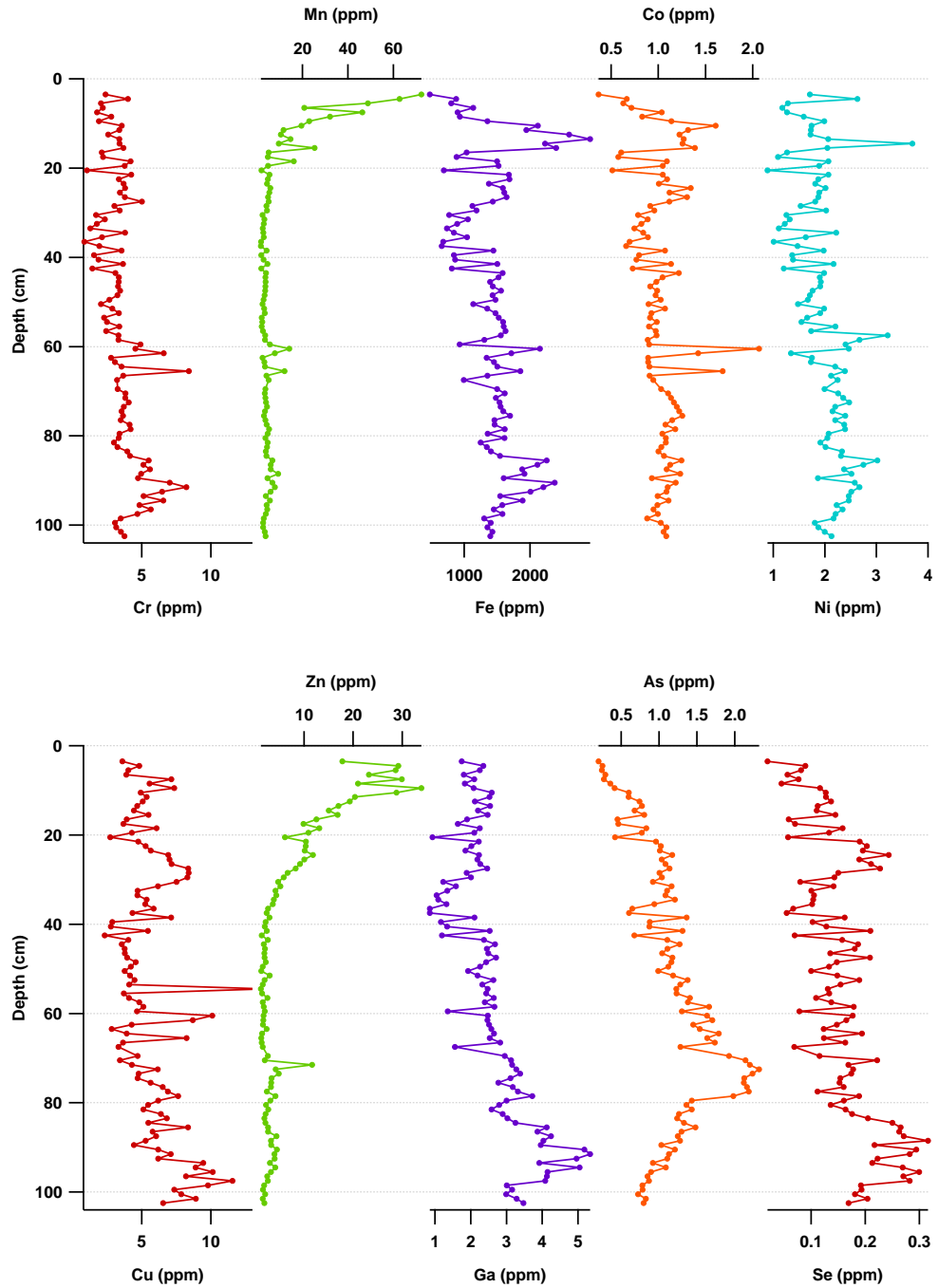
Figure 19.4: ICP-MS peat measurements: Cr, Mn, Fe, Co, Ni, Cu, Zn, Ga, As, Se concentration profiles plotted versus depth.
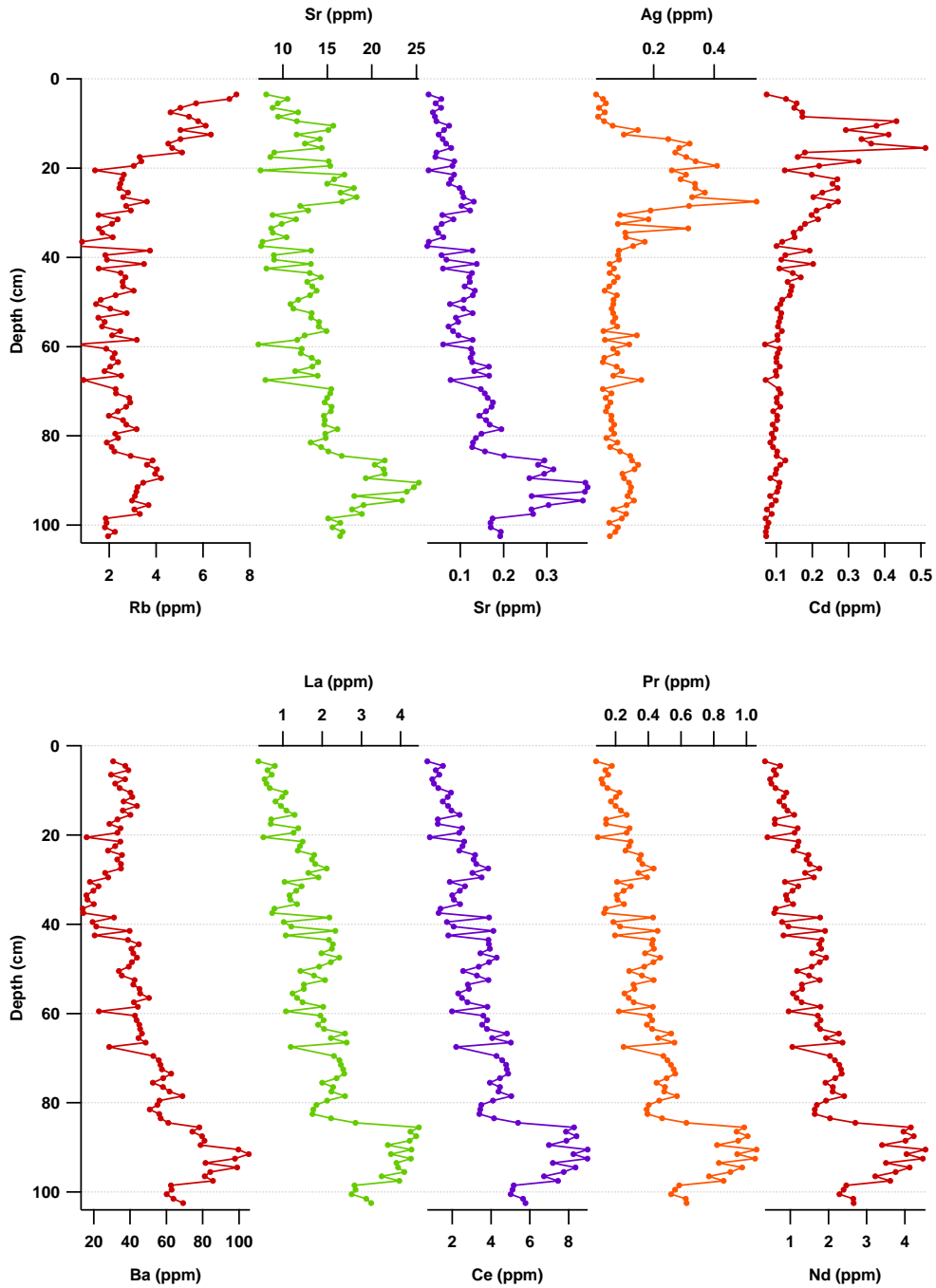
Figure 19.5: ICP-MS peat measurements: Rb, Sr, Y, Ag, Cd, Ba, La, Ce, Pr, Nd concentration profiles plotted versus depth.
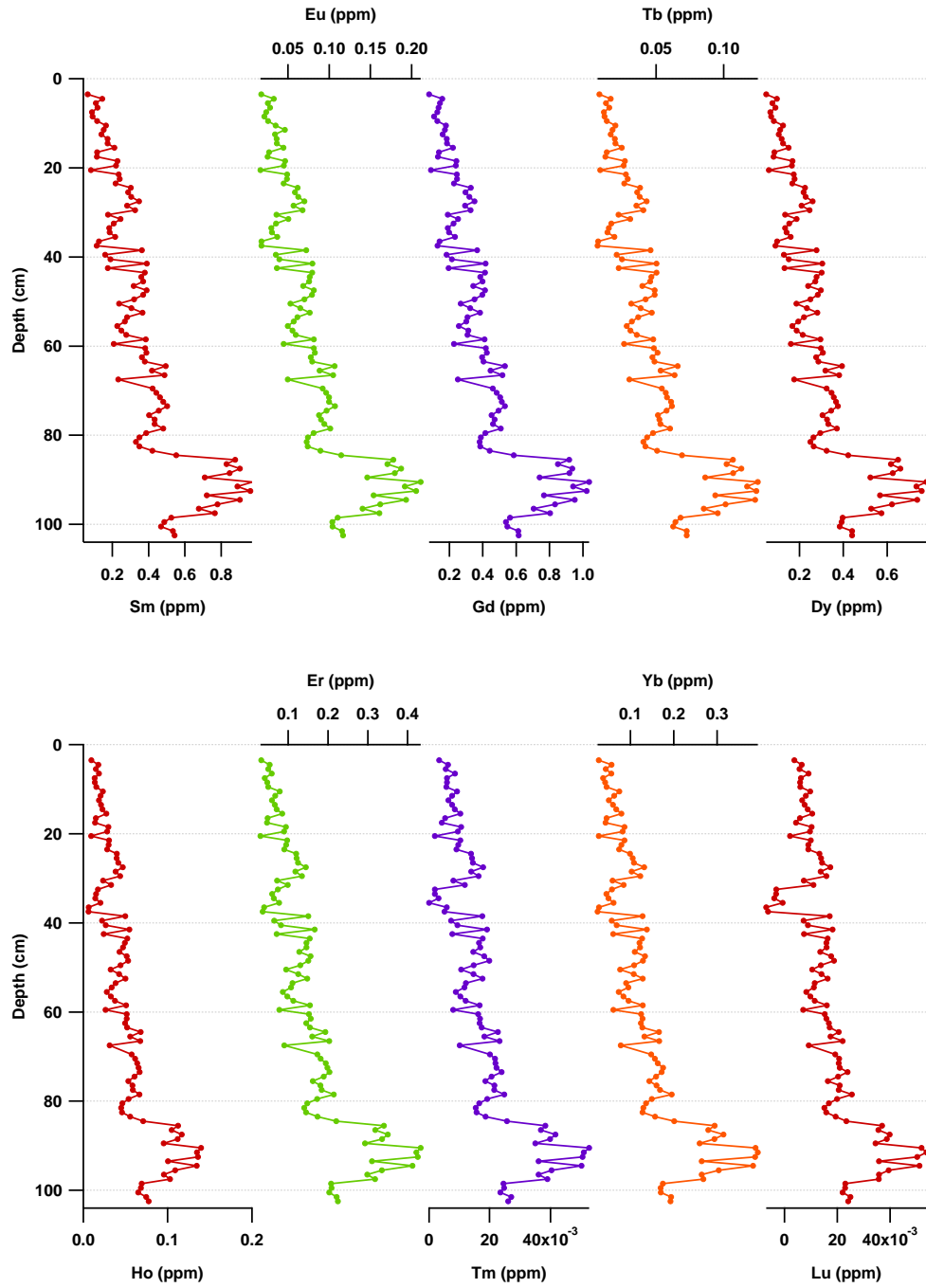
Figure 19.6: ICP-MS peat measurements: Sm, Eu, Gd, Tb, Dy, Ho, Er, Tm, Yb, Lu concentration profiles plotted versus depth.

Figure 19.7: ICP-MS peat measurements: Tl, Pb, Th, U concentration profiles plotted versus depth.
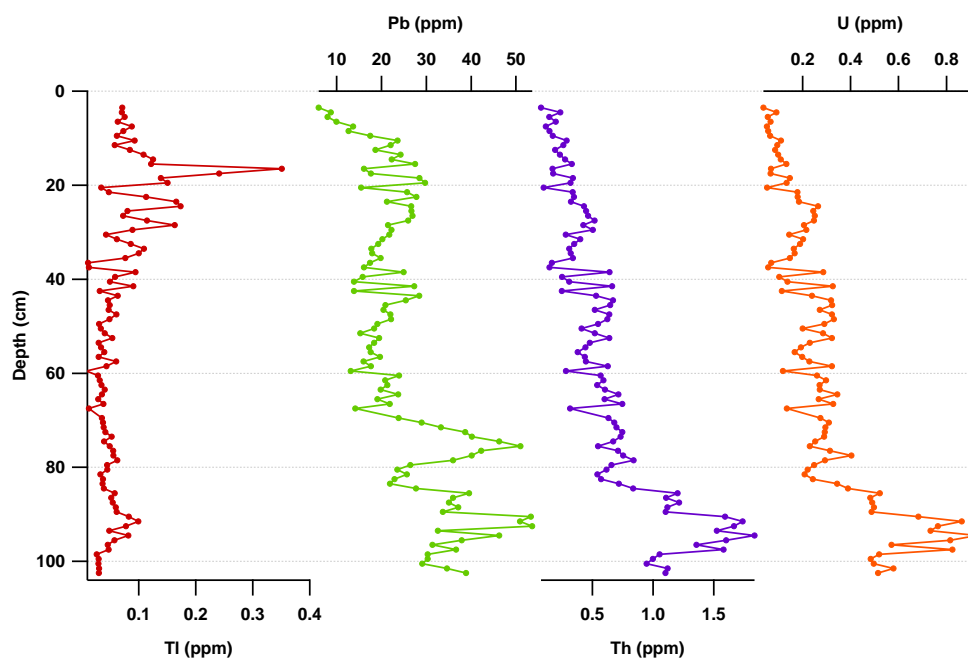
correlation with elements which are considered conservative (as Ti, Sc, and Sr) suggests that REE are also immobile in this archive and can be used as tracers of dust deposition.

Silver (Ag) and cadmium (Cd) profiles show a distinct and simultaneous increment between 15 and 40 cm of depth with concentration values of 0.6 and 0.5 ppm respectively. Under this depth they slightly decrease getting background values with very low concentrations. The same trend of enrichment is followed by thallium (Tl): after an increase between 15 and 40 cm of depth it shows a decreasing trend underlying that sediment has not contributed measurably to Tl inventories, such as for Ag and Cd. Thus mobilization of these elements is unlikely and they are considered effectively as immobile in the peat bog sequences, as already demonstrated by Shotyk and Krachler (2004). The similarity between these elements and in particular their increase in the modern section of the bog suggests that they can be involved in mining processes being released during the smelting of the argentiferous lead (Pb) ores during the Medieval and the pre-industrial and industrial period.

Another element that is considered absolutely immobile in peat is lead. Lead profile is reported in figure 19.7: it shows 2 strong peaks between 70 and 80 cm and then between 90 and 100 cm of depth. Moving to the top of the section its concentration ranges between 15 and 30 ppm, with minimum

values between 10 and 0 cm, around 5 ppm.

Also the presence of thorium (Th) and uranium (U) was investigated in the first meter of the bog. They show profiles comparable to crustal elements suggesting that their concentration in the bog is related to sediment weathering and erosional processes.

In order to divide natural enrichment from anthropogenic inputs phenomena in the *Discussion* section for the most interesting elements enrichment factor has been calculated. This allows to define how a single element is enriched compared to the natural crustal background value underlying the magnitude of trace elements depositions which are not related to crustal processes (e.g., anthropogenic emissions).

Pore water

We investigated pore water and peat sediments throughout the column as possible indicators of the ombrotrophic-minerotrophic boundary in the peat stratigraphy. Chemical pore water analysis were carried out at 1 cm of resolution on the first 85 cm of the core. In total 85 samples have been analyzed. The main aim of these measurements was to establish the Ca/Mg ratio, one of the most important parameters to define peatlands ombrotrophy. To identify the presence and extent of an ombrotrophic zone, the ratio of Ca/Mg in the pore water can be compared with the local ground water values: the assumption is that peat with a Ca/Mg ratio lower or comparable to rainwater is ombrotrophic; otherwise peat has an additional non atmospheric source of Ca and is therefore minerotrophic. Ca/Mg ratio in pore water was compared to that one calculated and determined by the "LIFE Nature Programme Danta: Project to safeguard the integrity of Danta di Cadore peat bogs" (http://www.torbieredanta.info/index.swf). These results are discussed together with all the other indicators of ombrotrophic or minerotrophic conditions in the *Discussion* section.

Thanks to the possibility given by the ICP-MS technique to detect simultaneously several elements, in addition to Ca and Mg ratio other 15 elements were measured: their concentrations are shown in figure 19.8 and 19.9.

Several elements, such as the case of K, Mg, Fe, Ca, Tl and Pb, show similar profiles in pore water and bulk sediments. This result is very significant because it allows to suppose that a vertical mobilization and migration of this elements is unlikely.
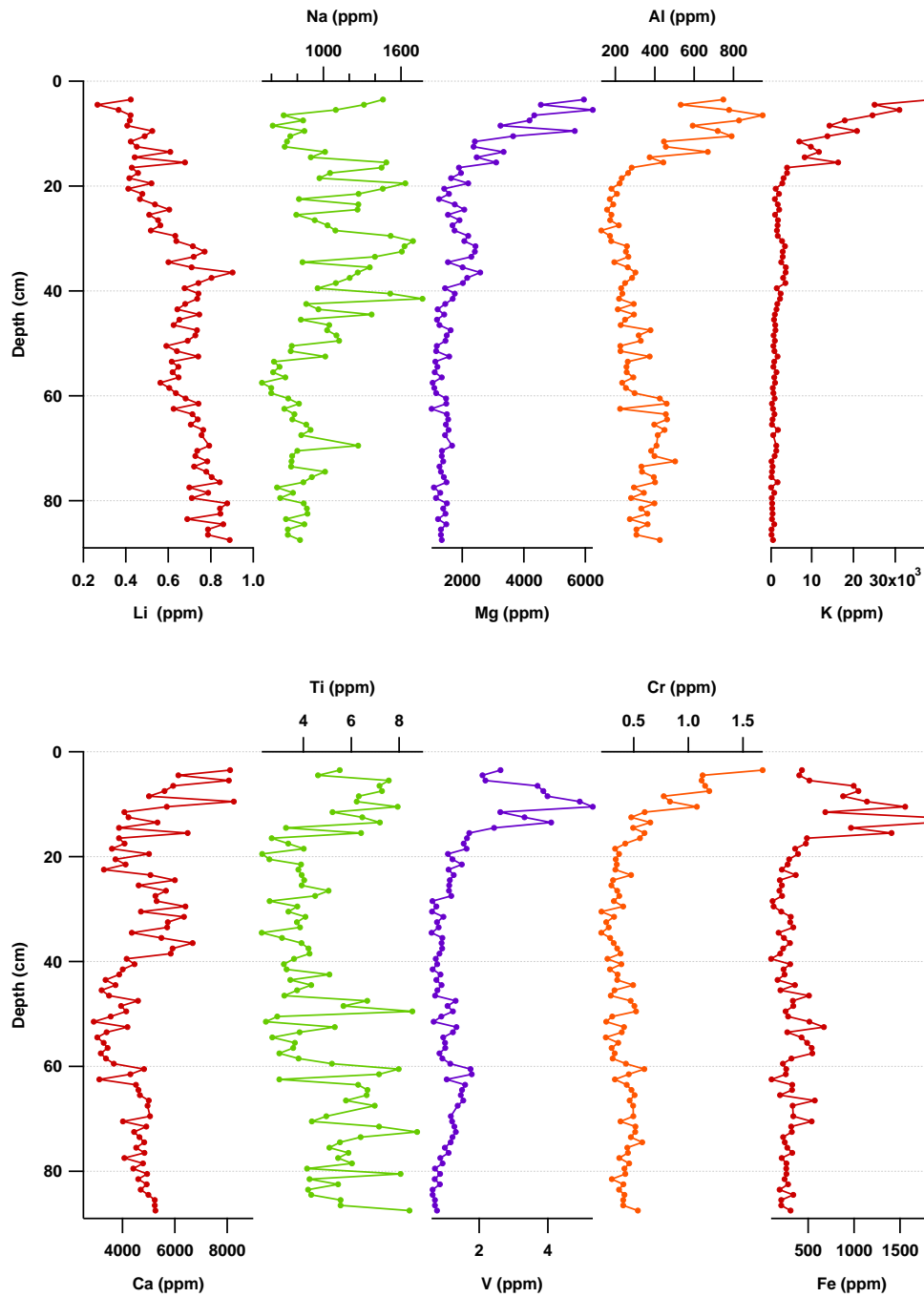
Figure 19.8: ICP-MS pore water measurements: Li, Na, Mg, Al, K, Ca, Ti, V, Cr and Fe concentration profiles plotted versus depth.

Figure 19.9: ICP-MS pore water measurements: Sr, Cd, Ba, Tl and Pb concentration profiles plotted versus depth.
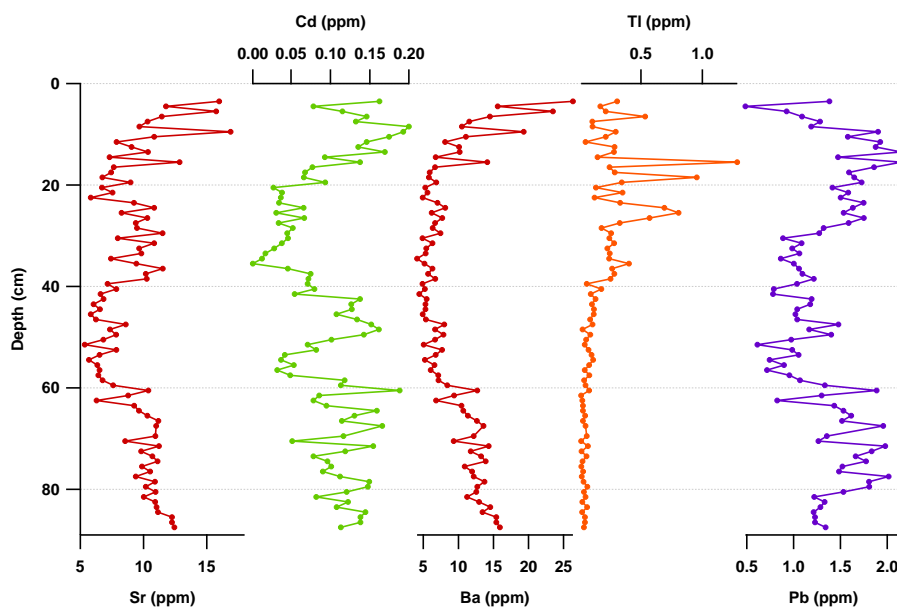
## 19.3   Pb isotopes

Lead is a pollution indicator in peat bog archives because it's strongly enriched by several anthropogenic activities (e.g., coal and leaded-gasoline combustions, mining, etc.) and it's also considered immobile in sediments (Shotyk et al., 1998; Ferrat et al., 2012). It is present in nature in four stable isotopes: the radiogenic ones ^{206}Pb, ^{207}Pb, ^{208}Pb and the non-radiogenic ^{204}Pb. ^{204}Pb is the only isotope that cannot derive from radiogenic decay, while the other three isotopes may also occur as radiogenic decay products of uranium and thorium. Specifically, ^{206}Pb is formed from ^{238}U, ^{207}Pb from ^{235}U, and ^{208}Pb from ^{232}Th.

Highly resolved (1 cm) lead isotope ratios (^{206}Pb/^{204}Pb, ^{206}Pb/^{207}Pb, and ^{207}Pb/^{204}Pb) were determined in acid digested peat samples by ICP-MS. Analyses have been done only in the first meter of the bog. In this section they reflect introductions of Pb from non-local soil weathering and anthropogenic sources, thus a precise characterization of the natural background level of the ratios is not possible. The summary statistics of isotopic measurements are presented in figure 19.10. In figure 19.11 ^{206}Pb/^{204}Pb, ^{206}Pb/^{207}Pb, and ^{207}Pb/^{204}Pb profiles are plotted against depth.

^{206}Pb/^{204}Pb pattern is characterized by a gradually increasing trend, with a strong fluctuation between 50 and 60 cm. It rises with a maximum value at 55 cm and then decreases to a minimum and rises again. This

variation is also present in the $^{207}Pb/^{204}Pb$ ratio profile, suggesting that is given by the increase of ^{204}Pb at these depths. At 55 cm $^{206}Pb/^{204}Pb$ profile reaches the maximum value of 18.36 and $^{207}Pb/^{204}Pb$ of 15.65. $^{206}Pb/^{207}Pb$ ratio shows a completely different pattern, constantly between 1.170 and 1.180 until 30 cm of depth, decreasing until approximately 15 cm and increasing again when reaching the top of the core.

$^{204}Pb/^{206}Pb$	$^{204}Pb/^{207}Pb$	$^{204}Pb/^{208}Pb$	$^{208}Pb/^{207}Pb$	$^{208}Pb/^{206}Pb$
Min. :0.05448	Min. :0.06388	Min. :0.02345	Min. :2.430	Min. :2.089
1st Qu.:0.05475	1st Qu.:0.06425	1st Qu.:0.02611	1st Qu.:2.453	1st Qu.:2.095
Median :0.05490	Median :0.06438	Median :0.02619	Median :2.460	Median :2.098
Mean :0.05505	Mean :0.06444	Mean :0.02619	Mean :2.459	Mean :2.100
3rd Qu.:0.05544	3rd Qu.:0.06459	3rd Qu.:0.02638	3rd Qu.:2.463	3rd Qu.:2.101
Max. :0.05575	Max. :0.06553	Max. :0.02660	Max. :2.726	Max. :2.328

$^{206}Pb/^{207}Pb$	$^{206}Pb/^{204}Pb$	$^{207}Pb/^{206}Pb$	$^{207}Pb/^{204}Pb$	$^{208}Pb/^{204}Pb$
Min. :1.153	Min. :17.94	Min. :0.8481	Min. :15.26	Min. :37.60
1st Qu.:1.170	1st Qu.:18.04	1st Qu.:0.8513	1st Qu.:15.48	1st Qu.:37.91
Median :1.173	Median :18.21	Median :0.8523	Median :15.53	Median :38.17
Mean :1.171	Mean :18.16	Mean :0.8543	Mean :15.52	Mean :38.16
3rd Qu.:1.175	3rd Qu.:18.27	3rd Qu.:0.8549	3rd Qu.:15.56	3rd Qu.:38.29
Max. :1.179	Max. :18.36	Max. :0.8677	Max. :15.65	Max. :42.65

Figure 19.10: Descriptive statistic of Pb stable isotopes measurements. For each ratio min value, max value, first and third quartile, median value and mean value are reported.

19.4 C/N and $\delta^{13}C$ profiles

Total carbon and nitrogen content in bulk peat samples and the isotopic ratios $^{13}C/^{12}C$ and $^{15}N/^{14}N$ were determined. The obtained data were corrected for moisture and ash content.

The isotopic values were expressed in $\delta‰$ vs. V-PDB (Vienna-Pee Dee Belemnite) for carbon, and AIR (Atmospheric nitrogen) for nitrogen, according to the following formula:

$$[(R_{sample} - R_{standard}) / R_{standard}] \times 1000$$

where R represents the ratio between the heavy and light isotopes. Trends of C/N ratio values and $\delta^{13}C$ plotted against depth are given in figure 19.13.

The summary statistics of carbon and nitrogen measurements are reported in figure 19.12 where total carbon and nitrogen are expressed as percentage. $\delta^{13}C$ values ranges between -28.29 and -23.81‰ indicate a dominant contribution of C_3 plants besides *Sphagnum*. Plants C_3, that differ from C_4 in the metabolic and photosynthetic pathway, are characterized by negative $\delta^{13}C$ values usually comprehended between -23 and -34‰ (Brader
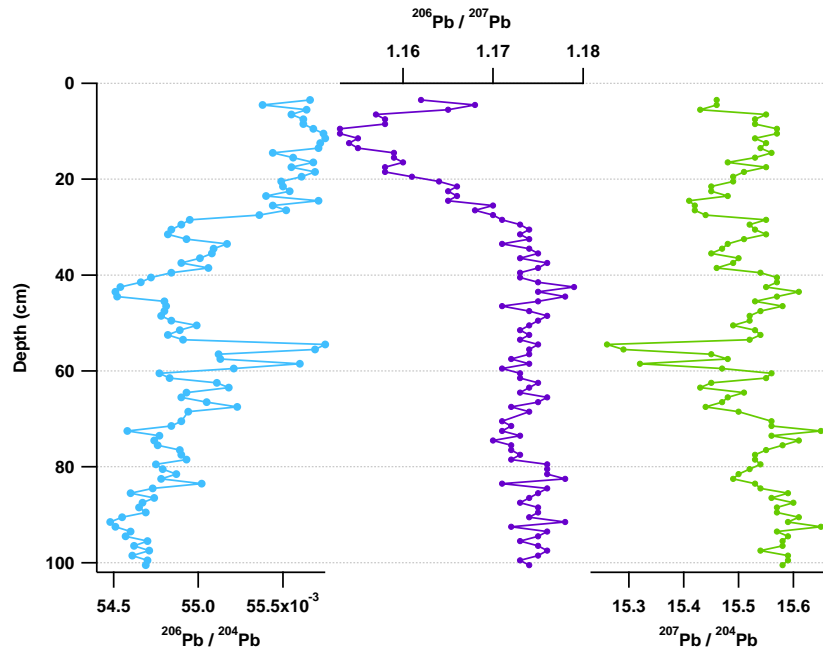
Figure 19.11: Pb isotopes profiles ^{206}Pb/^{204}Pb, ^{206}Pb/^{207}Pb, and ^{207}Pb/^{204}Pb plotted versus depth.

Nitrogen %	Carbon (TOC)%	δ^{15}N	δ^{13}C	C/N
Min. :0.460	Min. :40.28	Min. :-3.0200	Min. :-28.29	Min. :22.31
1st Qu.:1.090	1st Qu.:44.82	1st Qu.:-1.0800	1st Qu.:-26.42	1st Qu.:26.45
Median :1.630	Median :47.86	Median :-0.5800	Median :-25.69	Median :29.35
Mean :1.453	Mean :47.36	Mean :-0.4769	Mean :-25.75	Mean :37.62
3rd Qu.:1.840	3rd Qu.:49.47	3rd Qu.: 0.0300	3rd Qu.:-25.17	3rd Qu.:43.28
Max. :2.100	Max. :53.74	Max. : 2.3200	Max. :-23.81	Max. :91.74

Figure 19.12: Total carbon, total nitrogen, δ^{13}C and δ^{15}N summary statistics. For each indicator min value, max value, first and third quartile, median value and mean value are reported.

et al., 2010).

C/N ratio, ranging between 22.31 to 91.74 and with maximum values in the top layers of the bog, suggest an increase in humification with depth (figure 19.12). This finding is consistent with the gradual transformation of plant raw material into humus. This leads to a decreasing of the C/N ratio due to, for example, CO_2 production/release, C incorporation into microbial tissues, and chemical fixation of NH_3 and/or amines by lignin-like substances (Stevenson, 1994; Kuhry and Vitt, 1996).

The δ^{13}C and C/N mirror trend show an upper part of the core characterized by both the lowest δ^{13}C values and the highest C/N ones. During decay/humification processes a selective degradation of some macromolecules which results in an isotopic ratio shift, might occur. Some studies (Benner et al., 1987; Wedin et al., 1995) state that a differential loss of components during decomposition may lead to isotopic shifts. Our data seem to underline a conservative behaviour of δ^{13}C as demonstrated also by Zaccone et al. (2011). The non-significant correlation between C/N and δ^{13}C profile (r^2=0.04, p<0.0001) demonstrates that C signature is not compromised by the humification degree of peat which clearly increases along the profile.
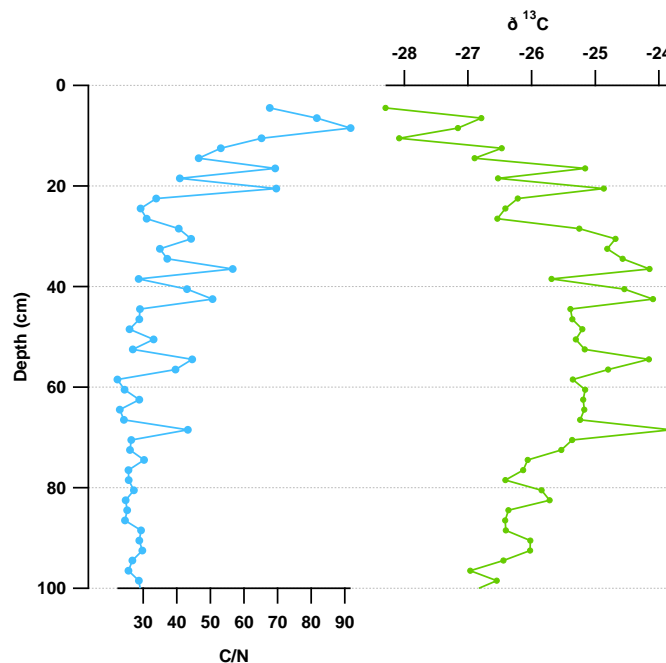
Figure 19.13: C/N and δ^{13}C profiles as measured in the first meter of Danta di Cadore peat bog core.

Chapter 20

Biostratigraphy

Well-aware of the importance of Southern Alps for paleo-botanical works, situated closed to glacial refuges of the most important plant species, we decided to focus the attention on vegetation assemblages that characterized the Late Glacial-Early Holocene transition.

Samples at 1-cm of resolution from the last section of the core (650-700 cm, 13,221-10,500 years cal BP) were prepared for pollen analysis. Every sample was subject to pollen identification and was counted at least for 400 pollen grains. Simultaneously also *Lycopodium* spores were counted: these spores were used like a kind of internal standard, allowing a precise calculation of the effective pollen concentration in the initial sample, derived from the certified number of spores per table. Every sample was also liable to micro-charcoal counting. Fragments of charcoal present on each slide were considered in order to obtain information about fire and land use history and human impacts. The results obtained from pollen and charcoal analysis are plotted versus age-depth chronology in figure 20.1.

The pollen diagram exhibits a succession of local pollen assemblages that characterized the time interval between approximately 13,300 years cal BP and 10,500 years cal BP. In this time frame three major interval are present:

- The Bölling-Alleröd interstadial, GI-1, 14,700-12,650 GRIP years cal BP;

- The Younger Dryas cooling event, GS-1, 12,650-11,500 GRIP years cal BP;

- The first part of the Early Holocene, between 11,500 and 10,500 years cal BP.
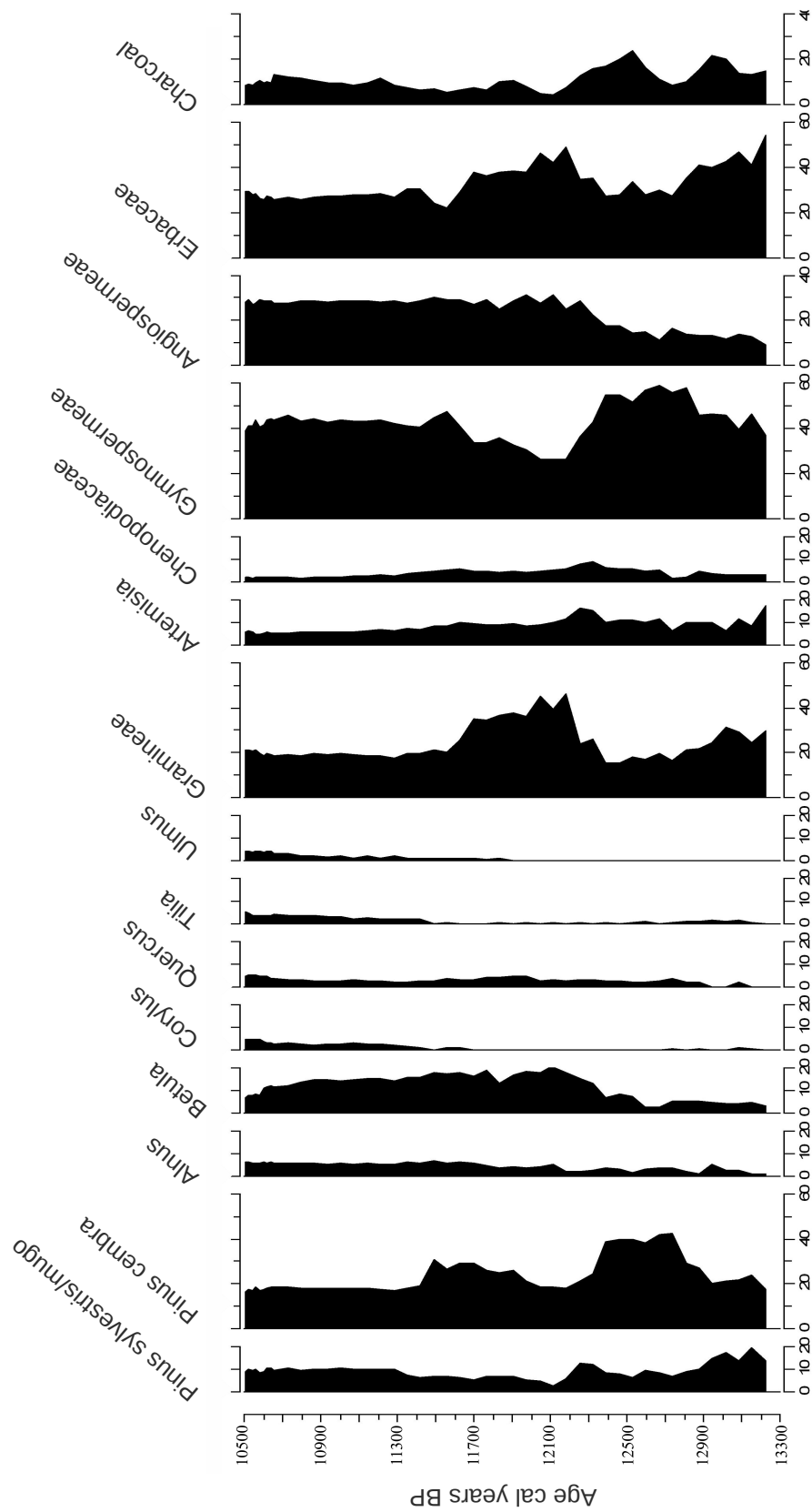
Figure 20.1: Selected percentage curves from the pollen record of the Danta di Cadore peat bog core, section between 650 and 700 cm of depth.

20.1   The Bölling-Alleröd interstadial

The final part of the core, in particular layers from 695 and 686 cm of depth (13,200 and 12,600 years cal BP), reflects the vegetation assemblages present in Danta di Cadore during the final part of the Bölling-Alleröd interstadial.

At that time vegetation (figure 20.2) appears to be characterized by forest of *Pinus sylvestris*, *Pinus cembra* and *Betula* with a high percentage of erbaceae among which *Artemisia* and *Chenopodiaceae* are present. Also a small percentage of *Alnus, Tilia, Quercus* and *Corylus* were found at these depths. These species confirm the warm and moist conditions that occurred at the end of the Late Glacial. Charcoal profile shows a peak in this section that can be associated with natural fire events for the high presence of biomass. *Pisidium* spp. remains and algae such as *Pediastrum* were found in the inorganic sediments at the bottom of the core.

20.2   The Younger Dryas cooling event

Layers in the final section between 686 and 670 cm comprehend the Younger Dryas cooling event (12,650-11,500 years cal BP). This severe climate deterioration is evidenced (figure 20.2) by grassland expansion with a contemporary decline of deciduous trees and *Gymnospermeae*. A peak in *Artemisia* and *Chenopodiaceae*, xerophytes adapted to survive in dry areas, is followed by a great peak in *Graminaceae* suggesting a period in which arid conditions are stronger. *Graminaceae* then slowly decreased and *Gymnospermeae* expanded again.

20.3   The Early Holocene

The uppermost part of the section reflects vegetation assemblages that developed during the first part of the Early Holocene (11,500 and 10,500 years cal BP). In this part of the pollen diagram (figure 20.2) a situation of increasing in deciduous trees and decreasing in herbs percentage correspond to the Late Glacial to Holocene transition. At that time mixed forest with *Pinus sylvestris*, *Pinus cembra*, *Betula*, *Quercus*, *Alnus* and *Tilia* is present. Also *Corylus* became an important vegetation component. This situation reflects the general climate improvement that characterized the beginning of the Holocene.
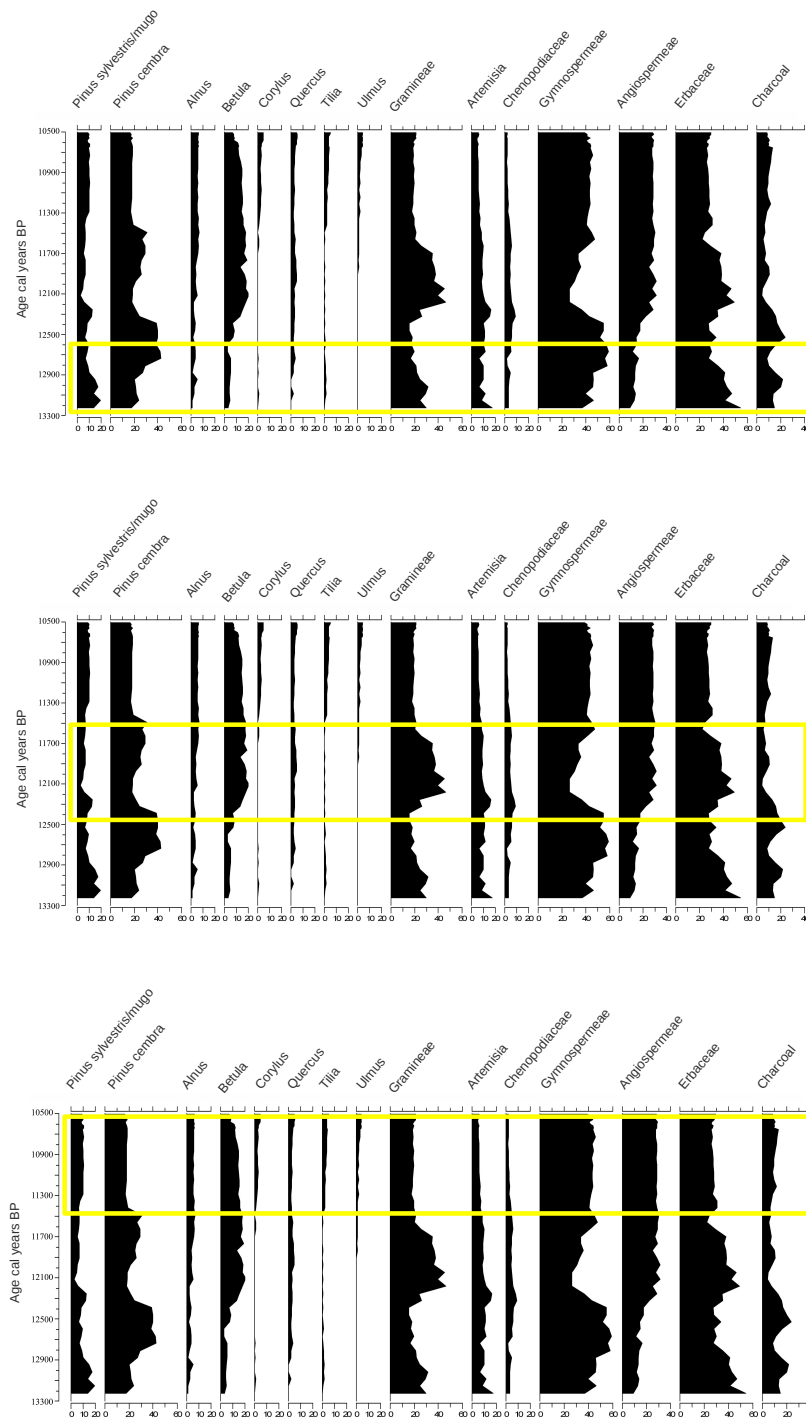
Figure 20.2: Selected percentage curves from the pollen record of the Danta di Cadore peat bog core, section between 650 and 700 cm of depth. The yellow rectangles indicate (from top to bottom) different time frame: the Bölling-Alleröd interstadial, the Younger Dryas and the Early Holocene.

Part V

Discussion

Chapter 21

The trophic signature of a bog 13,000 years old

21.1   Age-depth model and accumulation rate

Especially when multiple proxies need to be compared in the same natural archive, a reliable age-depth model is fundamental. Indeed, by providing calendar ages for undated depths, age-depth models allow to quantify the synchronicity of climate events.

While for the first 40 cm of Val di Ciampo peat bog core, ^{210}Pb chronology measured ages every 2 cm, the rest of the core shows limited quantities of radiocarbon determination. In particular, for 6 meters of peat covering more than 13,000 years, we have only eight radiocarbon measurements, provided by unevenly spaced samples.

In order to estimate the calendar ages of all the undated depths, a few considerations have been taken into account. A widely used age-depth model is based on the linear interpolation between the dated levels: this method presupposes and accepts abrupt changes in the accumulation rate , an unrealistic scenario in environments such as peat bogs. The results of this kind of interpolation are described by graph in figure 21.1, where calibrated ^{14}C dates are plotted versus depth. This graph, obtained with Calib software 6.0 (see section *Results*), shows that when dates are widely spaced out, changes in the rate of accumulation appear very sharped, suggesting the necessity of an alternative, more ecologically plausible model.

Another problem of modelling calibrated ^{14}C ages is represented by their uncertainties. Results shown in section *Results - Chronology* reveal that, while uncalibrated dates present symmetrical errors and normal distribution, the confidence intervals of calibrated radiocarbon ages are often multipeaked. Moreover, many calibrated ^{14}C ages present centennial scale uncertainties, making it very hard to individuate the single "best" calendar ages for each level.
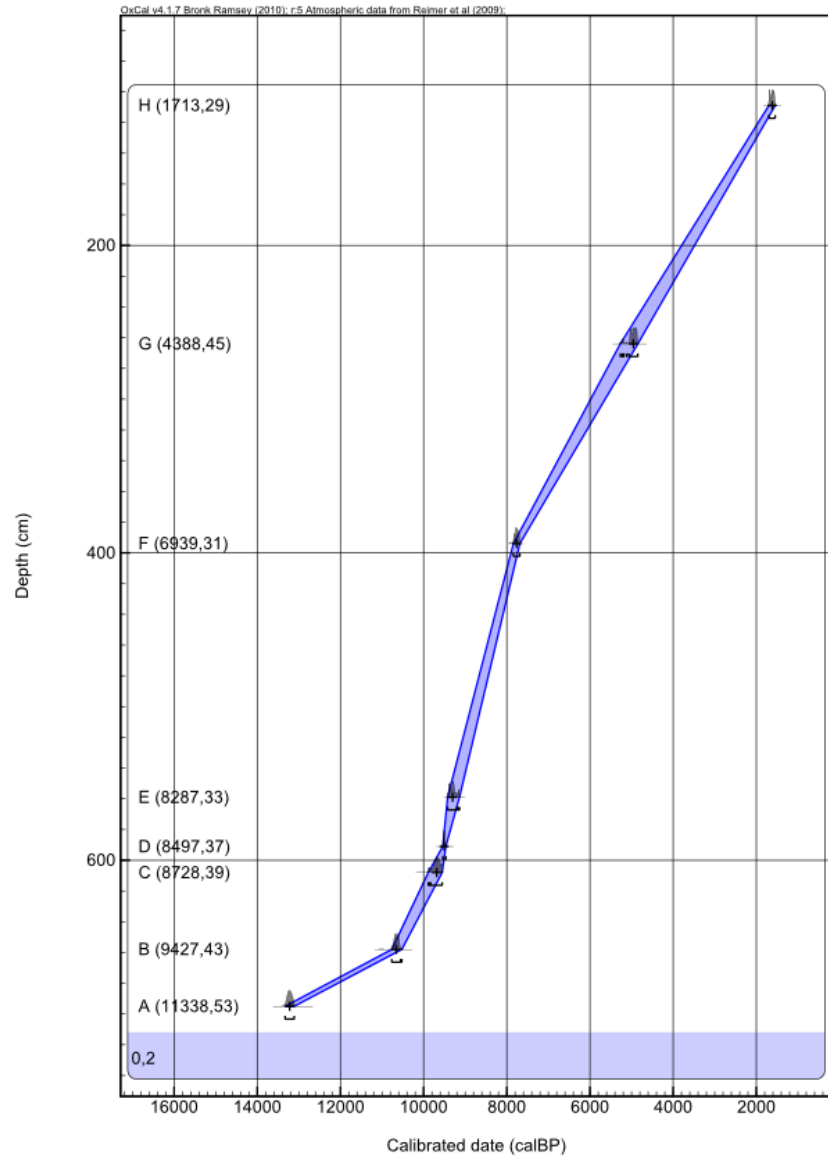
Figure 21.1: Linear interpolation between calibrated ^{14}C dates. Calibrated ages are plotted versus depth. The blue curve represents the linear interpolation with the 95% of interval confidence. Each age is reported on the curve with its asymmetrical distribution, and median values are indicated by means of a small black vertical line.

The "Clam" model was used to infer a high-resolution chronology, integrating data from both ^{14}C and ^{210}Pb measurements. The model was proposed by Blaauw (2010) and is one of the most widespread age-depth models for paleoclimate reconstruction based on lake and soil sequences. Confidence intervals for the undated levels are calculated using the Monte Carlo approach, through the following steps: (i) from the calibrated age distribution of every dated depth, a calendar age is sampled, (ii) an age-model is drawn through these points and finally (iii) for every depth (default 1 cm steps), the resulting calendar age is stored. The sampling process is repeated 1000 times and, at the end, "Clam" calculates for every depth the weighted mean of all sampled calendar ages, in order to find the single "best" age-depth model from all the iterated models (Blaauw, 2010).
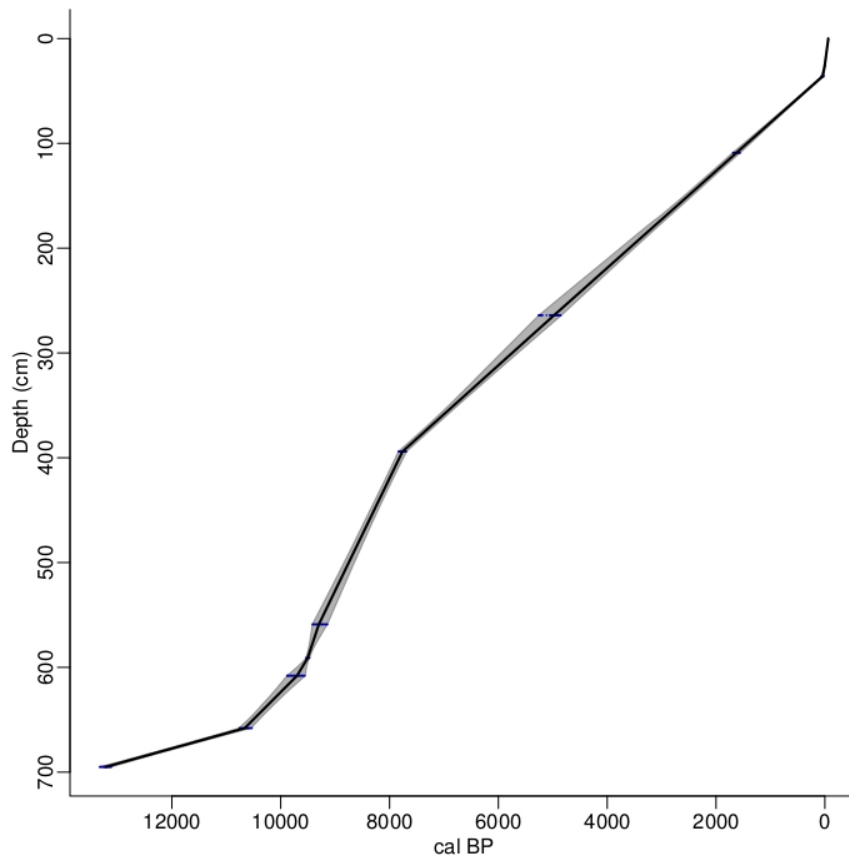
Figure 21.2: "Clam" age-depth model: blue blocks and grey envelopes show 95% confidence intervals.

The resulting age-depth model is shown in figure 21.2, where all ages between 1 cm and 695 cm of depth are plotted versus depth. Layers between 300 cm and the top of the core were characterized by paucity of macro-

remains to submit to ^{14}C measurements. This situation is reflected also by the shape of the curve in this interval, suggesting that new radiocarbon determinations are still needed. This consideration must be taken into account for all the observations about natural climate variations or anthropogenic impacts recorded by the archive at such depths.

The "Clam" age-depth model achieves a very high-resolution chronology that allows to calculate the sedimentation rate of the last 13,000 years (figure 21.3). The profile of sedimentation rate appears clearly characterized by two abrupt events between 500 and 700 cm of depth (10,600 - 9500 years cal BP).

A significant increase can be observed at around 10,600 years cal BP, when the rate of accumulation grows from 0.010 to 0.030 g cm^{-2} y^{-1}. This change (already described in section *Results - Physical stratigraphy*) corresponds to the transition from inorganic to organic sediments.

This peak is followed by a slight decrease, which anticipates a strong increase up to 0.040 g cm^{-2} y^{-1} at around 9,506 years cal BP. Above this depth, the rate of accumulation decreases again to values between 0.010 and 0.020 g cm^{-2} y^{-1}, and this change corresponds to a stratigraphic boundary layer: the transition between gyttija and peat. This latter rate of accumulation characterizes layers until 400 cm of depth, and then drops again to more stable values up to the top of the core. Physical analysis of the core individuates no stratigraphical differences at these depths where only peat is present. However, one can make the simple consideration that a decrease in the rate of accumulation means that nutrients supplied to the bog sink lower, suggesting changes in the trophic condition of the bog. This important turning point was considered as the first evidence of a probable transition from minerotrophic to ombrotrophic peats.

21.2 Peat bog trophic conditions

21.2.1 Ombro-minerotrophic boundary layer

In order to be used as archives of atmospheric depositions of trace metals, peat bogs must be ombrotrophic. In numerous studies, as reported by Chambers and Charman (2004), the trophic status of the bog was simply assumed to be constant with depth, basing the observations only on surface vegetation and on the pH values of surface waters. Ombrotrophic bogs tend to naturally overlie minerotrophic peats, where the water feeding the peat is enriched in elements as a result of the increasing influence of groundwater metal inputs. Thus, it is important to determine the thickness of the ombrotrophic layer in order to confirm that the changes in peat chemistry reflect only atmospheric deposition and not simply the increasing influence of groundwater inputs. There are several possible ways to determine this thickness: stratigraphy examination is usually integrated with information
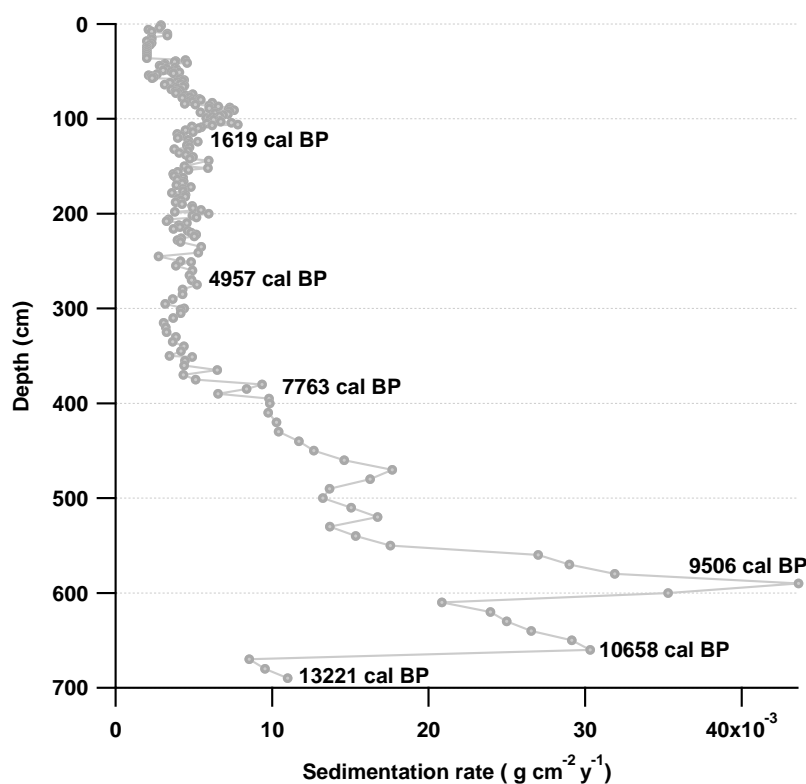
Figure 21.3: Val di Ciampo peat bog sedimentation rate. On the graph median values of some radiocarbon calibration are reported.

about bulk density, ash content, pore water Ca/Mg ratio, pH and EC, and some chemical elements profiles such as calcium (Ca), titanium (Ti) and stronzium (Sr) (Givelet et al., 2004; Chambers et al., 2012).

Pore water was extracted only from the first meter of the bog (see section *Results - Physical proprieties of the peat*). The natural condition of the archive does not permit to go below this depth, where pore water cannot be easily separated by manual squeezing from peat material.

Pore water Ca/Mg ratio was compared to the one calculated in rain samples from Danta di Cadore, as reported in "LIFE Nature Programme Danta: Project to safeguard the integrity of Danta di Cadore peat bogs" (http://www.torbieredanta.info). The relationship between the Ca/Mg ratios in pore waters and atmospheric precipitations is essential to evaluate whether the bog is fed only by atmospheric input or also by runoff, surface water or groundwater. As shown in section *Chemiostratigraphy - ICP-MS - Pore water*, Ca/Mg ratios in pore waters were lower than the corresponding ratios in atmospheric depositions, indicating ombrotrophic conditions in the

peat (Shotyk, 1996a). pH values indicate acid conditions with pH ranging from 4 and 4.5, associated with very low EC values, both indicative of an environment with low nutrient supply: indeed, the mineral matter supplied to the bog is not sufficient to neutralize the high acidity of pore water.

The first meter of the bog is also characterized by very low bulk density $(0.1 - 0.2$ g cm$^{-3})$ and ash content $(2 - 5\%)$, suggesting the presence of ombrotrophic peat as defined by the ASTM classification (American Society for Testing Material, 1990).

Additional information can be retrieved by looking at the Ca and Ti XRF profiles (figure 21.4). Ti, as Sr, is a lithogenically conservative element often used as a reference to evaluate natural variations in density and inorganic inputs. Its primary sources are atmospheric depositions by wind and rain-out of soil dusts released during weathering processes (Givelet et al., 2003). It provides an index of the amount of mineral matter in the peat and can be used as a sensitive proxy to distinguish ombrotrophic peats from minerotrophic ones, where mineral matter is derived from terrestrial and aquatic inputs as well as from the air. Although the solubility of Ti and Sr and their oxides can increase in acidic environments such as bogs, their high correlation with ash content (R^2=0.76 and 0.74, p $\leq$ 0.05, for Ti and Sr respectively) suggests that the post-depositional migration of these elements is minimal in the core.

Measurements of Ca are useful for determining whether elements in the bog derive from precipitation or groundwater input. We assume that ombrotrophic bogs receive Ca only from the atmosphere (windblown dust and precipitation). Thus, if we normalize Ca to Ti along the entire core, it is possible to remove the effect of natural changes in atmospheric input: as explained before, Ti is a lithogenic element that derives only from soil weathering, and it is an indicator natural variations in inorganic inputs through the peat.

This procedure therefore emphasizes modifications in trophic conditions and, through the first meter of Val di Ciampo bog, Ca, Ti, and Ca/Ti underline ombrotrophic conditions.

Under 100 cm of depth, pore water was not monitored and only the other proxies were considered. Under 400 cm of depth, bulk density, Ca and Ca/Ti start to increase, thereby jointly indicating a change in the trophic conditions of the peat. Bulk density values begin to distance themselves from the ombrotrophic signature, and Ca concentrations increase, indicating that, in these sections, the amount of Ca derives from both precipitations and groundwater. Ca/Ti profile and the age-depth model demonstrate higher accumulation rates at around 400 cm of depth, indicating differences in atmospheric inputs and in sediment composition and suggesting minerotrophic conditions. Among these depths, minerotrophic peat strata between 500 and 540 and below 630 cm show lower values of Ca/Ti ratio, probably related to particular climatic conditions which may correspond to dry episodes.

In light of the above information about the stratigraphy and rate of accumulation of the bog, and after integrating this information with all the relevant data about physical and chemical proprieties, the Val di Ciampo peat bog was considered to be ombrotrophic between 0 and 400 cm of depth, covering approximately the last 7,000 years of accumulation history.
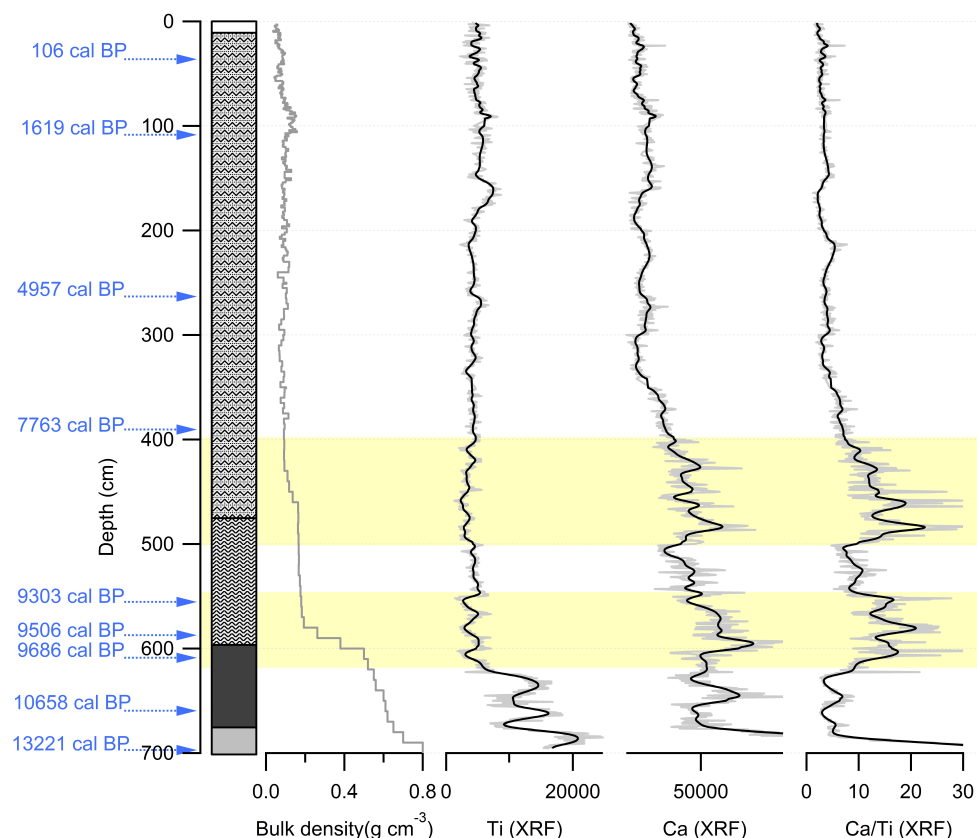
Figure 21.4: Lithological description, density profile (g cm^{-3}), ash concentration (%), and Sr, Ti, Ca, Ca/Ti (cps XRF). Lithological changes are related to differences in physical and chemical parameters (marked by yellow areas). Sr, Ti and Ca/Ti profiles are described by light-grey lines (real values) and black lines (10-point binomial smoothing values). Y-axis shows depth and age control points representing median values of the 2-sigma calibrated age ranges

21.2.2 Humification degree with depth

Although several studies have used bogs in order to reconstruct historical trends of atmospheric depositions, the question of whether ombrotrophic bogs provide a reliable record of past environmental changes remains rather controversial in scientific literature (Zaccone et al., 2011). Consequently, before using bogs as natural archives, it becomes essential to assess whether all the vegetational and climatic information is effectively preserved in peat

deposits during humification. To this end, C/N ratio and δ^{13}C values were determined and compared along the peat bog profile. The results are reported in section *Results - C/N and δ^{13}C profiles.*

The vegetation growing in peat bogs includes C_3 or C_4 plants characterized by different δ^{13}C values, which are the function of the photosynthetic pathway used to fix CO_2 (Smith and Epstein, 1971). C_3 plants (all trees, most shrubs and herbs, and many grasses) have δ^{13}C with an average value of ca. -27‰, much lower than those in atmospheric CO_2 (-7.7‰, average value). C_4 plants (i.e., dry climate grasses and some sedges and herbs), more efficient in fixing CO_2, exhibit a delta^{13}C average value of ca. -13‰, more similar to those of the atmosphere (Deines, 1980; O'Leary, 1988). The average ^{13}C (-25.75‰) and the range of variation (4.38‰) suggest both a possible dominant contribution of vascular C_3 plants besides *Sphagnum*, and a change in the dominant Sphagnum species (Brader et al., 2010).

As shown in the results (section *Results - C/N and δ^{13}C profiles*), δ^{13}C and C/N values underline an upper part of the core characterized by both the lowest δ^{13}C values and the highest C/N ones (figure 19.13). The slight decrease in δ^{13}C is due to the preservation of slowly decomposing ^{13}C depleted substances, such as lignin (Benner et al., 1987). As *Sphagnum* species present phenolic compounds very similar to lignin (Nimz and Tutschek, 1977; Rasmussen et al., 1995; Farmer and Morrison, 1964), a similar fractionation pattern can be expected in *Sphagnum* peats. Thus, the depth trend towards lower δ^{13}C values indicates an environment where the enrichment of recalcitrant material, intrinsically resistant to decomposition, dominates the isotopic profile.

A high correlation between δ^{13}C and C/N ratio may indicate a significant diagenesis which can alter the original record of δ^{13}C (Meyers, 1997; Sharma et al., 2005). Microbial degradation can act removing ^{12}C preferentially to ^{13}C, resulting in a depleted δ^{13}C. An enrichment of δ^{13}C can occur as a result of aerobic decomposition. R^2 value for C/N versus δ^{13}C is 0.024, suggesting that δ^{13}C record is not significantly altered by diagenetic processes. On this basis, the shifts from negative to more positive values of δ^{13}C can be interpreted in relation to stress factor of water and aridity, and more negative values can be interpreted as a possible result of a wetter period (Alewell et al., 2011). With future investigations (i.e., on pollen) it will be possible to better relate changes in δ^{13}C with temperature or humidity changes.

Overall, the most important information derived from these results is that the humification degree, even if growing with depth, does not influence δ^{13}C variations and, thus, vegetation preserves climatic information. This is of primary importance, as it supports the use of ombrotrophic peat bogs as archives of past and present climatic information.

Chapter 22

Deep insights into climate dynamics

22.1 Late Glacial - Early Holocene transition

The Late Glacial interval between the Last Glacial Maximum termination and the beginning of the Holocene is characterized by several events. Chronological constraints of the deglaciation processes in the Southern Alps are fewer than those available for the Northern slope of the Alps (Ravazzi et al., 2007) and this is also the case for the Piave glacier, whose deglaciation is well-documented only for the first part of the Late Glacial (Carton et al., 2009).

The mode and timing of deglaciation in the mid-Piave basin are well defined by Pellegrini et al. (2004), but this process is not yet outlined in the upper section of the Piave basin. The only information available is extrapolated according to the general framework of expansion/retreat reported by Carton et al. (2009), as already explained in section *Introduction - Study area*.

In this context of very limited data, the oldest radiocarbon age proves a very valuable result. Prior to any possible evaluation of the measured age, it is possible to determine that the presence of *Pisidium* shells implies that this sector of the Piave basin was already ice-free, and that deglaciation processes have favored the establishment of an oligotrophic shallow lake in a depression underlined with a mineral clay layer. The calibrated radiocarbon age calculated from these shells corresponds to 13,220 years cal BP, the median value in the two sigma range between 13,110 - 13,330 years cal BP (figure 22.1). This age provides strong evidence that this part of the Piave basin was already ice-free during the Bölling-Alleröd interstadial. It is worth noting that this radiocarbon age represents a minimum age for the deglaciation in Danta di Cadore area, because older sediments do exist in the bog.
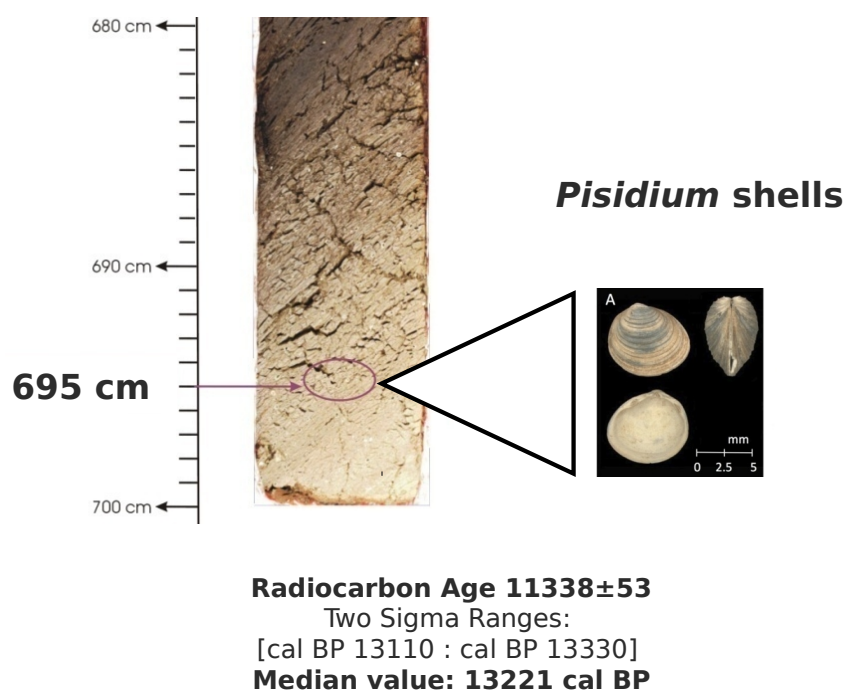
Figure 22.1: In this figure the last 20 cm of Val di Ciampo peat bog core are represented: in particular depth from which *Pisidium* shells remains have been sampled is highlighted and the radiocarbon determination and calibration are reported.

The end moraine system of the Piave glacier was individuated by previous studies at Vittorio Veneto. Its last glacial advance was dated at around 18,000 years cal BP (Carton et al., 2009). Thus, by adding the new data collected from *Pisidum* shells, it is possible to assess that the Piave deglaciation was very rapid as already suggested by previous studies regarding the main alpine valleys (Ravazzi, 2005). In particular, this study provides for the first time important information about the timing of the Piave glacier's retreat: as reported and summarized in figure 22.2, the Piave glacier appears to have retreated from Vittorio Veneto over about 5,000 years, losing more than 90 Km of extension and 1,200 meters of thickness.

The alpine deglaciation and retreat of the LGM Piave Glacier were followed by the development of a completely different environment from the initial oligoptrohic lake. All the climatic variations that characterized the transition from the Late Glacial to the Holocene were recorded by the Val di Ciampo archive. Given the lack of information about the climatic-stratigraphical subdivision of the Bölling-Alleröd interstadial in the Southern section of the Alps (Ravazzi, 2005), a particular research effort was dedicated to this time span. A high-resolution pollen analysis was carried out to de-
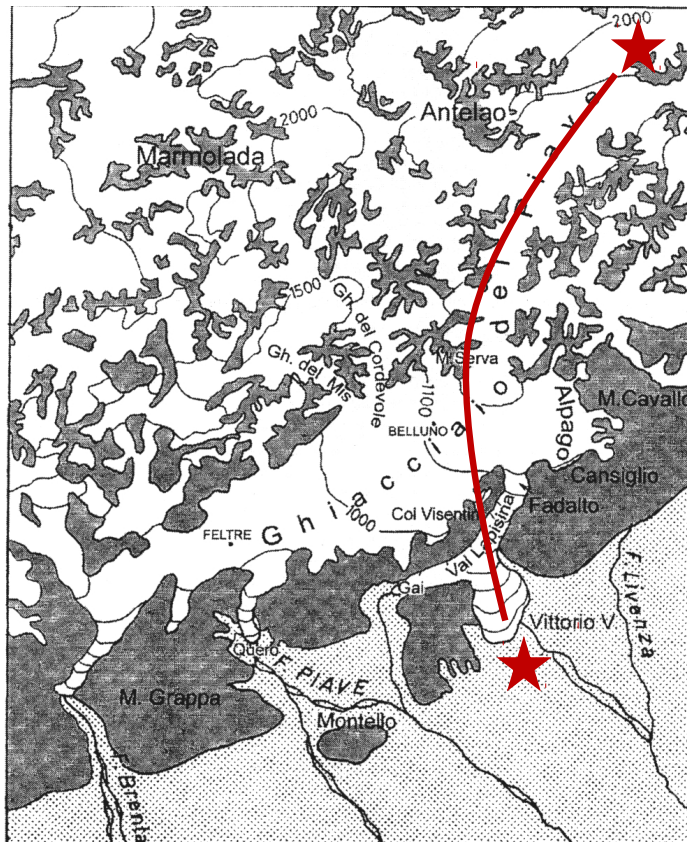
Figure 22.2: Reconstruction of the Piave glacier extension during the Last Glacial Maximum (Castiglioni, 1941) in which the end moraine system of Vittorio Veneto and Danta di Cadore are highlighted by two red stars.

tect vegetation responses driven by climate changes. As already described in section *Results - Biostratigraphy*, pollen analysis of the last section of the core reveals that a vegetation typical of steppic environments was present in Danta di Cadore after the deglaciation of the Piave glacier. It was dominated by herbaceae *Gramineae, Artemisia, Chenopodiaceae*, with a modest pollen percentage of *Gymnospermeae*. The contemporary and growing presence of *Pinus* stomata suggests that the transport of pollen grains from the pre-alpine valley was not the only factor responsible for the presence of this species. Indeed, conifer fossil stomata are a potential paleoenvironmental proxy for deriving information on the plants which grew in a given area, and serve as a substitute for observations of fossil plants. The cold and oligotrophic conditions of the lake are suggested by *Pisidium* and confirmed by the presence of algae such as *Pediastrum*. Successively, the pollen graph shows a gradual reforestation of the area by *Gymnospermeae* with a slowly

decrease of *Gramineae* and *Chenopodiaceae* percenteges, a light-demanding herbs. The presence of *Alnus*, *Tilia*, *Quercus* and *Corylus* suggests that these trees were starting to rise from pre-alpine lands.

About 15,000 years ago, while Northern Europe's ice sheets were retreating, several short-term returns to colder conditions took place. The most evident of these cold event was identified in different climatic reconstructions from all Europe, and is called Younger Dryas. Pollen diagrams across Europe record the effects of this event that caused forest decline, increase of erosion and the expansion of tundra. The Younger Dryas represents one of the best examples of an abrupt climate event that has had consequences on land and oceans (Alley et al., 1993). This cold event occurred between 12,650 and 11,500 GRIP years BP (GS-1) and appears to be one of the most important turning points recorded by the peat core.

In the stratigraphical sequence of peat from Danta di Cadore, Younger Dryas is represented by only 17 cm indicating a low sedimentation rate during this time. This low sedimentation rate, showed also in figure 21.3, is common to other paleoclimate records from Northern Italy such as those from Pian di Gembro (Pini, 2002), Cerete Basso (Orombelli e Ravazzi, 1995), and Passo del Tonale (Gehir, 1997). It is usually correlated to low rates of precipitation and of detrital supply to the lake-peat basin.

This particular low sedimentation rate usually prevents high resolution chemical analyzes. In our case, the XRF core scanner approach allows to reconstruct inputs of atmospheric elements deposition at a resolution of 2.5 mm. The lithogenic elements Si, Rb, and Sr show the same behavior as Ti and Ca/Ti, suggesting that below 630 cm of depth, they are all related to the same climatic condition: the high-resolution XRF data, related to ^{14}C data points, make it possible to match, at these depths, the elevated soil dust fluxes of lithogenic elements and the period of the Younger Dryas cooling.

Pollen analysis underline that vegetation from Danta di Cadore was also influenced by the climatic deterioration during the Younger Dryas. In our core, this climatic deterioration is characterized by a decrease in *Pinus* percentages and by an increase of *Betula* and herbs. As already testified by other pollen diagrams from the southern part of the Alpine chain (Wick, 1996) , the Younger Dryas interval can be subdivided in three different parts, because the different climatic conditions affected different taxa. Initially *Betula* increased and *Pinus* decreased, with a parallel increase of *Artemisia* and *Chenopodiaceae*. Later, *Artemisia* shows a maximum value alongside the increase of other steppic herbs, suggesting that the most unfavorable period of the Younger Dryas was characterized by hard dryness. Finally, a decrease of *Artemisia* was combined with an increase of *Ulmus*, *Quercus*, *Alnus* and *Pinus*, suggesting a climatic improvement in the final part of the Younger Dryas. The response of *Artemisia*, together with thermophilus species, indicates that the climate of that time was colder but also dryer. In the middle part of the Younger Dryas, the growth of *Quercus*, *Tilia* and *Alnus* was

also affected, meaning a decrease in humidity combined with colder temperatures. The dry conditions, identified by data about lithology, stratigraphy and XRF profiles (figure 21.4), are confirmed by pollen analysis results.

The Preboreal period corresponds to the Younger Dryas/Holocene transition, characterized by an abrupt increase in air temperature testified in the Southern Alps as well as in the central Swiss Alps with July air temperature reconstructions from chironomids assemblages (Heiri et al. , 2007; Larocque and Finsinger, 2008; Ilyashuk et al., 2009). Moreover, Tinner et al. (2005) suggest an increase in July air temperature of 4.8°C in the central Alps, evidenced by a rapid shift in the treeline 800 m upwards. In this period, an oscillation called "Preboreal Oscillation", dated at ca. 11,300 years cal BP, and which lasted 200 years, was widespread in the North Atlantic region (Fritz, 2003), as recorded in the Swiss Alps (Lotter et al., 1992) as well as in GRIP and NGRIP records: during this cooling event, the temperature decreased between 0.6 and 2.8°C in the Alps (Samartin, 2012). In pollen reconstruction, this oscillation usually corresponds to a tree-less condition with a decrease of tree pollen (Gobet et al., 2005). The general situation of temperature increase is recorded by the pollen assemblages in Danta di Cadore: in fact the beginning of the Holocene is marked by a decrease in *Pinus*, *Betula*, *Artemisia* and *Chenopodiaceae*, and by an increase of thermophilus species such as *Quercus* and *Tilia*. The starting expansion of *Corylus*, a warmth-requiring tree, is also visible. At this point, the forests in Danta di Cadore were probably dominated by deciduous trees and by a modest percentage of *Pinus*. Preboreal Oscillation was not identified by pollen analysis, probably because of its relatively low temporal resolution.

A general continuity in the rise of air temperature has characterized both the Boreal (9,000 - 7,500 years cal BP) and the Atlantic chronozones (7,500 - 5,000 years cal BP). This favorable condition allowed the accumulation of organic materials through the core. In correspondence with the beginning of the Boreal chronozone, an abrupt decrease in the rate of accumulation is particularly evident and a transition from gyttija to peat sediments is a key event of the lake-basin paludification. This process continues through the Atlantic section with a lower rate of accumulation linked to the presence of ombrotrophic peats.

22.2   The last 2000 years - Anthropic impact

One of the major aims of this study was to define whether elements distribution in the Val di Ciampo peat profile can be useful to determine the history of anthropogenic activities on a regional and global scale. Trace and major elements accumulated through the first meter of the bog, reflecting atmospheric conditions of the last 1600 years, were directly related to the available information about the history of human impact in the Cadore area.

In order to investigate the general correlation between the variables observed in the uppermost part of the bog, we firstly applied an univariate statistical approach using the *Pearson* and *Spearman* correlation indexes. This second index can be used even if data do not have a normal distribution. Results of both indices show significant values of "r", rejecting the zero hypothesis (of no correlation) for Pb with Al, Ti, Zn, Ag, Cd and Tl.

Then, considering the amount of data and the dimensions of the matix of trace elements concentrations (100x44), a multivariate statistical approach was also applied: Principal Component Analysis (PCA) was selected in order to underline patterns in data and to highlight their similarities and differences. Results of PCA are reported in figure 22.3: the percentage of variance attributable to the first two independent loading factors is 76,1%, explaining most of the variance that underlies the data.

The two-dimensional plot describes the rules of the variables by grouping the samples in different clusters. PC1 appears to divide samples in two major groups: in the negative part of its axis, samples from the top of the core to 60 cm of depth are clustered; the positive part gathers the rest of the samples. Considering the age-depth model, 60 cm of depth correspond approximately to AD 1300, falling in the Medieval period. Starting from this consideration, we can suppose that this primary subdivision along the PC1 follows a discrimination between samples in which trace elements concentrations are substantially enriched by anthropogenic inputs, from those which are closer to the local ground composition. PC2 helps to better discriminate samples characterized by anthropic influences: in particular, layers between the top of the core and 30 cm of depth are grouped in the positive values of the axis, while samples from 30 to 60 cm of depth are clustered in the negative values of the axis. This subdivision appears to imply different sources of anthropogenic emission: the first 30 cm of depth covers the last century, a period that includes the second and third industrial revolution, with several economical and industrial innovations. Layers from 30 to 60 cm of depth cover the time period from the 14th to the 20th century, when trace elements depositions had different emission sources. One of the most important economic activities in the Cadore area since the Middle Ages derived from ores, with several mines located along the valley. The increasing inputs of elements from mining activity in the peat seems well explained by the PC2 axis. It is still not entirely clear why samples between 85 and 95 cm of depth appear to be divided by positive values on PC2. More information about these samples are expected with new chronological data: in these sections of the core, other samples were recently subjected to radiocarbon dating, in order to make more solid climate and historical inferences.

Looking at the loading plot (figure 22.3), overlapped here to the score plot, the increase in mining activity is explained also by the rules of the variables. In particular, when compared to samples in the negatives loadings, samples in the positive ones are correlated with Zn, Cd, Tl, Mn and
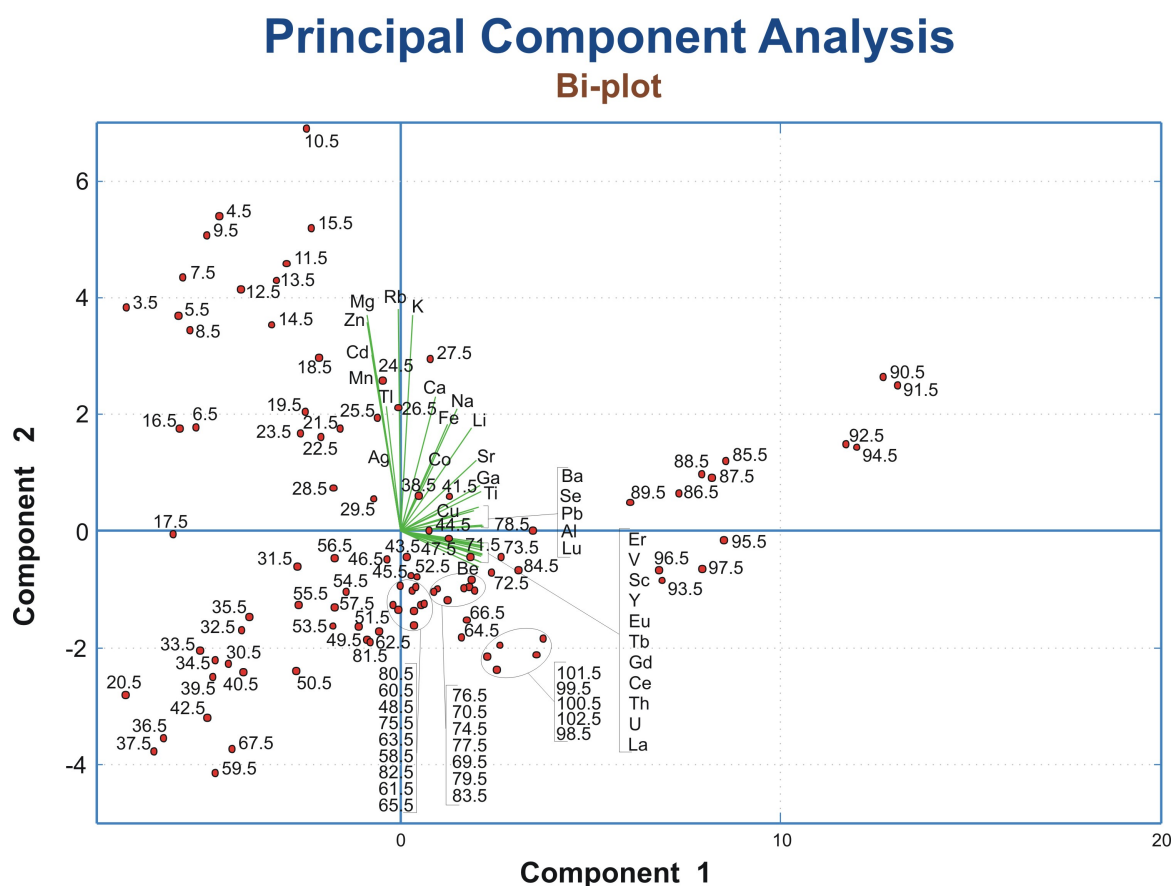
Figure 22.3: Bi-plot resulted from the PCA. PC1 is plotted versus PC2 explaining the 76.12% of the total variability.

Ag, which are all elements present in the loades. (Pugh et al., 2002). Mining sites in the Cadore area were initially used to extract Pb: indeed silver was extracted and processed from argentiferous-lead ores (Klein, 2004). Pb seems to be divided from the other group of variables linked to mining activity, but this could be explained by the fact that Pb, in that time period, was also emitted by other important sources such as leaded-gasoline combustion (Ferrat et al., 2012) . Its correlation to Zn, Cd, Tl and Ag was previously underlined with *Pearson* and *Spearman* correlation indexes. Also in this case, additional information about the meaning of the position of Pb in the Bi-plot, is expected with future new chronological data.

In order to identify the relative importance of natural versus anthropogenic components of trace elements concentrations, we calculated the *Enrichment Factor* (EF). Each element was normalized with a conservative lithogenical element (Sc in this case), on the assumption that the conser-
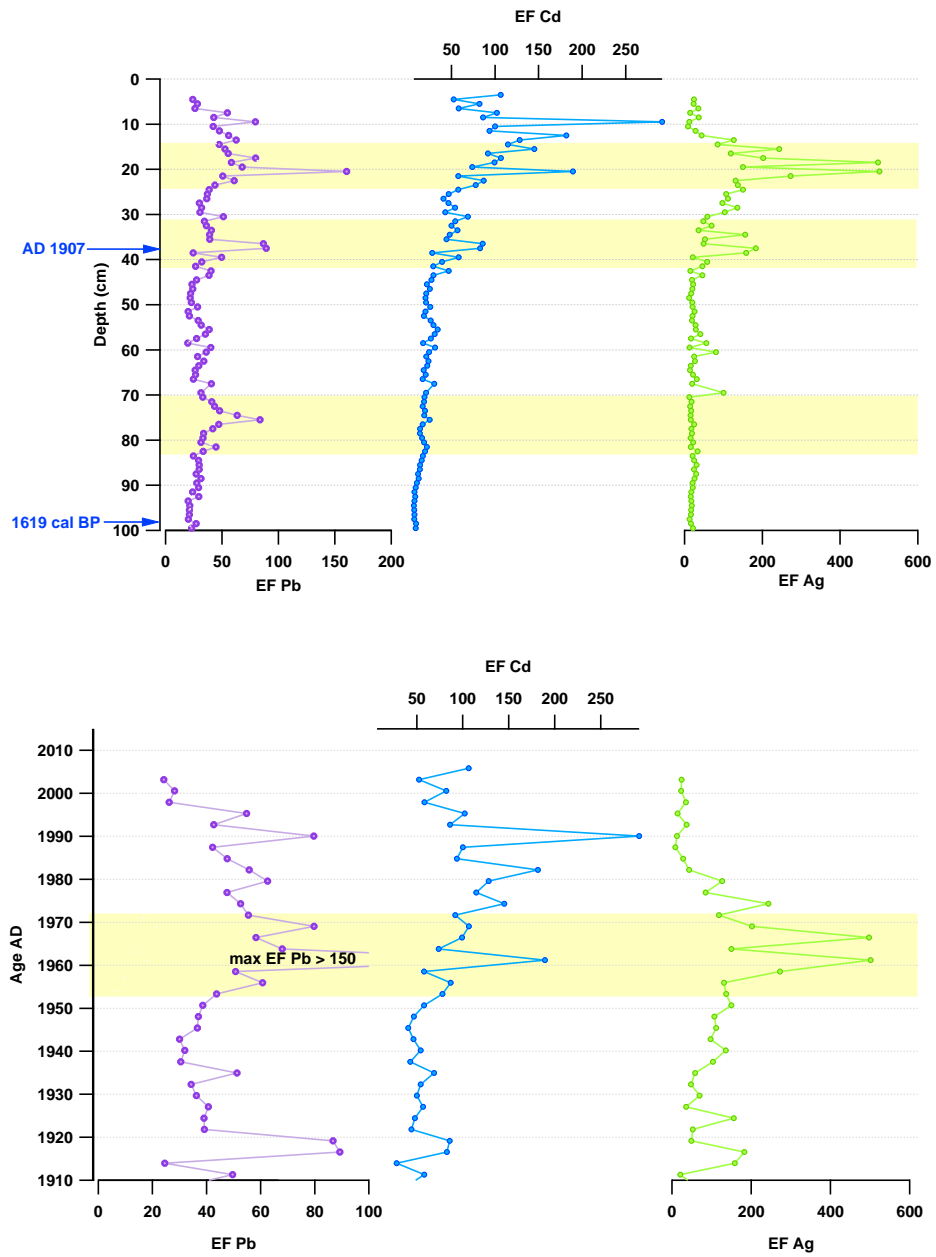
Figure 22.4: Enrichment factors profiles of Pb, Cd and Ag. In the first graph they are plotted versus depth and 2 ages data points. Second graph focuses on the uppermost part of the core and EF are plotted versus age (1910 AD - to present). Yellow bars indicate intervals of high levels of EF.

vative element has an uniform flux through time, and that it enters the atmospheric aerosols from natural rather than anthropogenic sources. EF is an empirical index that allows to identify and quantify human interferences on the global biogochemical cycle. EF has been calculated as:

$$(\mathrm{TE/Sc})_{sample}/(\mathrm{TE/Sc})_{background}$$

where TE represents the trace element considered each time, and Sc is the lithogenic element used to calculated the number of times a sample is enriched compared to the natural, pre-anthropogenic background value. By definition, if EF>10, the element is considered as originated from anthropogenic sources. The Enrichment Factor (EF) was determined for Pb, Ag and Cd. Values for the background level of the elements were calculated following the ones indicated by Wedepohl (1995) for the UCC (Upper Continental Crust) (see section *Field work and Methods - Data analysis*).

A faint increase of the EF_{Pb} can be observed between 81 and 82 cm (EF>50). From this depth, it gradually starts to rise, with a major peak around 74-75 cm (EF>80), $\sim AD1050$. This period coincides with the expansion of mining activity in Europe, following the discovery of new deposits and the reactivation of old mining sites. German mining activity was particularly developed and, thanks to one of the most important centres for silver mining (Rammelsberg), the territory soon became a major silver producer (Brännvall et al., 1999). At the same time, in the province of Belluno, between the Ansiei and the Piave rivers near Auronzo, the Argentiera mine was active under German workforces, as known by the first concessions compiled according to German rules (Cecchi, 1988; De Vecchi, 1990). This mine site was initially used to extract Pb.

Between 40 cm of depth and the top of the core, other significant increases of EF_{Pb} are visible. In this section, an enrichment in Cd and Ag is also recorded. A strong increase can be observed between 40 and 35 cm: EF_{Pb} reaches 100 times the background level, while other elements also undergo high EF increments. This particular event can be explained by a new method used for the mining activity at the Argentiera mine site: around the end of the 19th century, the activity was taken over by the society "Montanistica di Sagor" (Lubljana), which began with the *open-pit mining* technique, extracting minerals by removing them from an open borrow (De Vecchi, 1990).

Increases in trace metals concentrations were strong also in the 1960s, a period in which almost the half of total emission of trace metals in Europe derived from metallurgical production (Pacyna et al., 2007). In the same chronological time span, this global signal is accompanied by a regional one: strong rises in trace elements concentrations can be linked with the opening of a new mining site, Salafossa, on the orographical left of Piave river, near Santo Stefano di Cadore. This mine was active from AD 1959 to AD 1986.

At the time, more precisely in AD 1971 the Argentiera mine was closed. Reaching the surface, a gradually decreasing concentration trend characterizes all the elements. This trend reflects the inactivity of the mining sites and also the global reduction of air pollutants in the atmosphere, following the increasing attention to atmospheric conditions in Europe from the 1990s onwards.
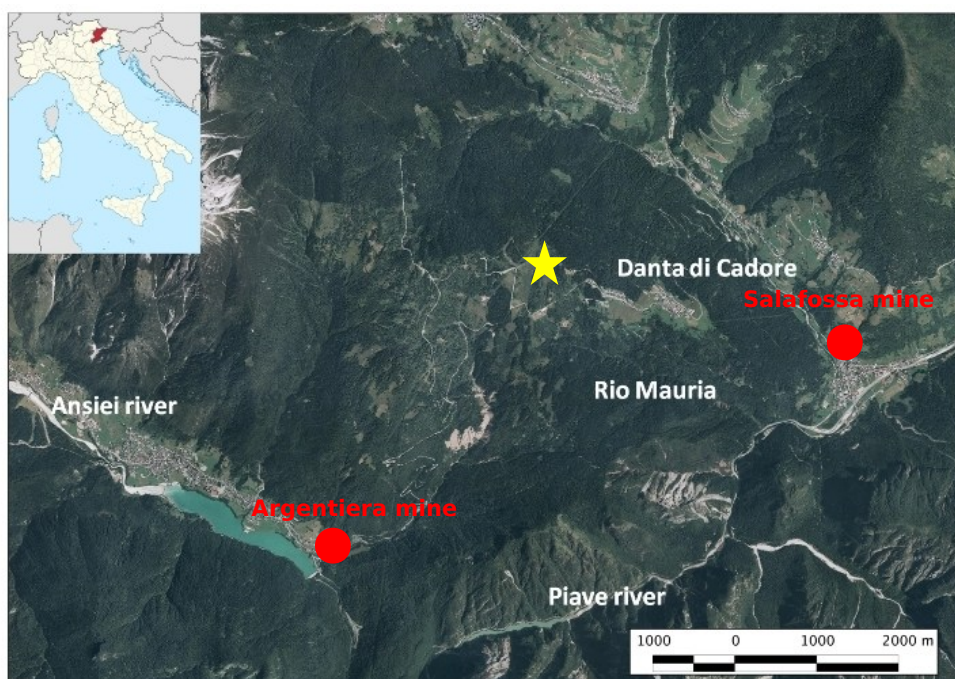
Figure 22.5: Geographical location of Argentiera and Salafossa sites. As shown by the figure Danta di Cadore bog (yellow star) is located between the two mining sites (in red).

Lead was also investigated for its four stable isotopes: the radiogenic ^{206}Pb, ^{207}Pb, ^{208}Pb and the non-radiogenic one ^{204}Pb. To distinguish among anthropogenic Pb sources, each radiogenic isotopes was normalized to ^{204}Pb. In figure 22.6, ^{206}Pb/^{204}Pb is plotted versus ^{206}Pb/^{207}Pb and the samples appear to be divided in two major groups: the first is composed by layers from 100 to 28 cm of depth, while the other includes samples from 28 to the top of the core. The subdivision is clearly expressed by the radiogenic fingerprint of the samples: the deepest layers are characterized by more radiogenic inputs than those on the surface. This result suggests that the layers at the bottom of this section are influenced from inputs that derive from soil weathering, and, on the contrary, layers at the top of the core registered inputs from anthropogenic sources. The same figure (22.6) describes another intrinsic characteristic of the samples: plotting ^{206}Pb/^{204}Pb versus
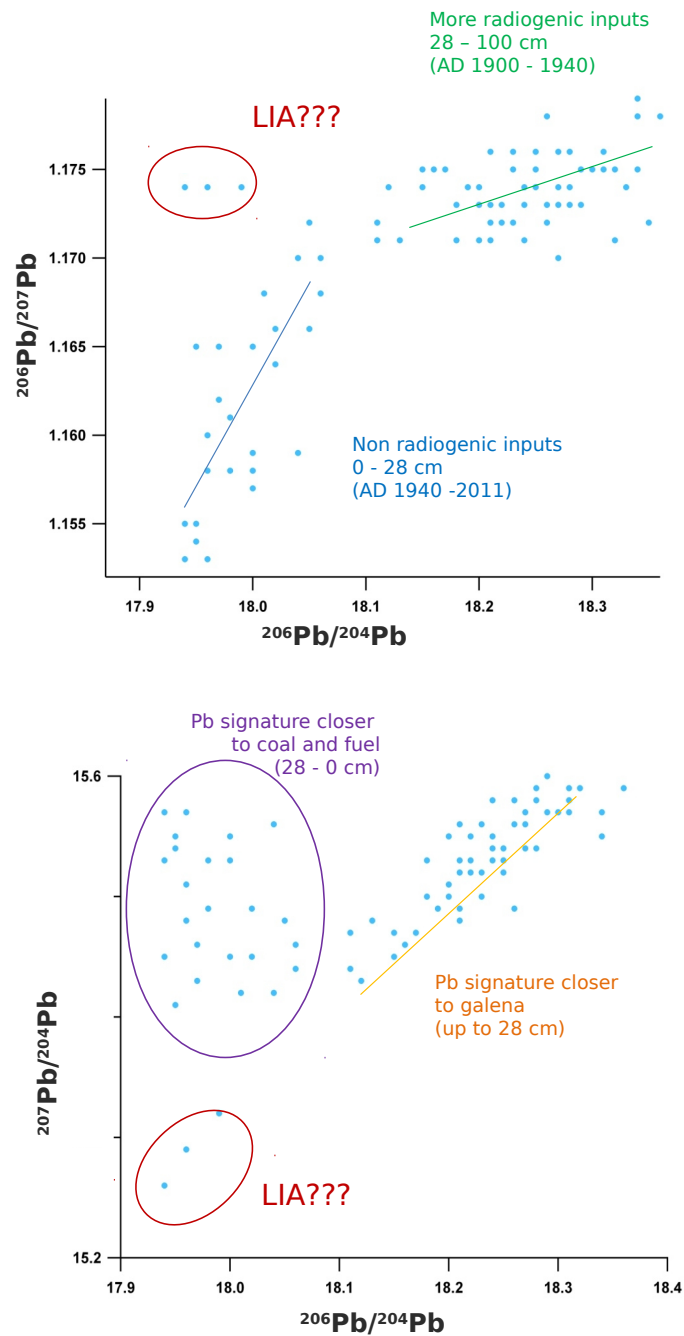
Figure 22.6: In the first graph $^{206}Pb/^{204}Pb$ is plotted versus $^{206}Pb/^{207}$: non radiogenic and more radiogenic inputs are well divided. In the second graph $^{206}Pb/^{204}Pb$ is plotted versus $^{207}Pb/^{204}Pb$: Pb with signature closer to coal and fuel is here divided by Pb with signature closer to galena.

^{207}Pb/^{204}Pb, samples appear separated on the basis of Pb signature closer to galena or to coal (Swaine, 1990). All this new information, combined with information regarding trace elements PCA and enrichment factors profiles, finally assessed the effective impact of mining activity in Danta di Cadore area, as recorded by the Val di Ciampo peat bog archive.

A small group of 3 samples has a completely different Pb source: its feature is highlighted in both graphs in figure 22.6. By looking at the results reported in section *Results - Pb isotopes* and comparing with the trend of ^{206}Pb/^{204}Pb and ^{207}Pb/^{204}Pb ratio profiles, it is possible to suggest that in this section of the bog, corresponding to the Little Ice Age, peculiar inputs have characterized atmospheric precipitations, probably related to the particular climate conditions. Unfortunately, neither trace and major elements and nor REE measured show any particular sign which can be correlated to this climatic event. In this respect, more investigations are needed.
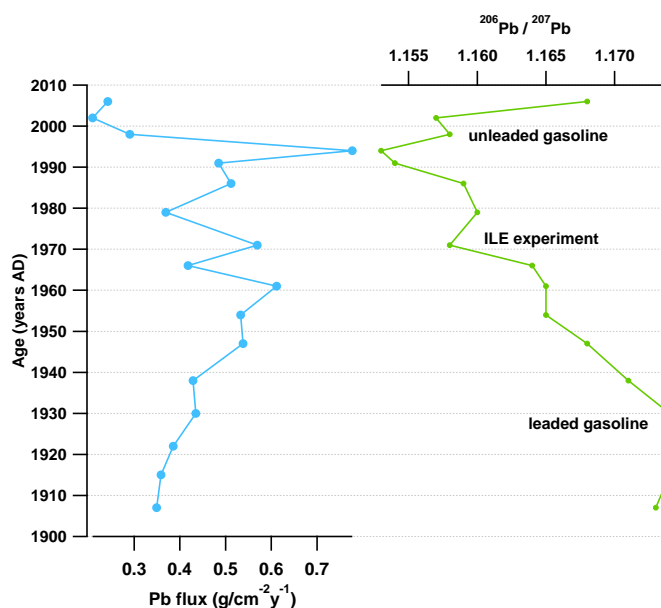
Figure 22.7: Pb flux e isotopes

Finally, on the basis of Pb concentrations and peat bulk density values, Pb fluxes were also calculated in the first 40 cm of the core. Results are presented in figure 22.7 and are related to the ^{206}Pb/^{207}Pb profile.

A decrease of ^{206}Pb/^{207}Pb can be observed in conjunction with the introduction of leaded gasoline (1940s) in Europe and successively in Italy, a trend seen in other natural archives of climate changes. This decrease is correlated with a parallel increase of Pb flux from 0.4 up to 0.7 g cm^{-2}y^{-1}.

At about AD 1970, there is a small event in which the ^{206}Pb/^{207}Pb

profile decreases and then suddenly increases again: it coincides with the famous ILE experiment (Isotopic Lead Experiment) (Facchetti and Geiss, 1982). This experiment was performed in Turin between 1975 and 1980: scientists tried to determine the rate of Pb from motor vehicle emissions in human blood. Pb in petrol was completely substituted by Pb with a different isotopic composition (the australian Broken Hill), in particular with a ^{206}Pb/^{207}Pb of about 1.04. This probably emphasized the ongoing decreasing pattern.

The lowest ^{206}Pb/^{207}Pb ratio value, 1.153, coincides with the highest value of Pb flux in the 1990s, 0.75 g cm^{-2} y^{-1}. After this peak, ^{206}Pb/^{207}Pb ratio rises again with the simultaneously decrease of Pb flux: this can be correlated with the period in which leaded fuels were totally banned, in Europe by the D.E. 98/70/CE. Even if in Europe the measure air pollution by emissions from motor vehicles started from the 1970s with the D.E. 70/220/CEE, we must wait until 1994 for cars to be designed to work only with unleaded gasoline. As for Italy, it banned unleaded gasoline only in 2002, after receiving the European D.E. 98/70/CE.

Part VI

Conclusions

The main aim of this thesis was to reconstruct Holocene climate and environmental variability from a peat bog archive located in Danta di Cadore, Eastern Italian Alps. Behind this general goal, a few research questions were raised as reported in the section *Introduction - Research Objectives*. These points have been investigated and discussed throughout the thesis.

- ***Does Danta di Cadore peat bog represent an ideal natural archive to reconstruct past climate changes in the Dolomites?***

  The first important and essential feature which allows to use peat in Holocene climate studies, is its ombrotrophic signature. In fact, only ombrotrophic peat bogs record atmospheric conditions, without any influence from the surrounding ground and surface waters. The identification of the ideal environmental archive, in which the records of atmospheric depositions are preserved, has to be associated to an adequate age-depth model. Only this strategy allows us to put data in a precise chronological framework.

  For the Val di Ciampo bog, the analysis of botanical, physical and chemical parameters permitted the discrimination of different trophic conditions through the core. The parallel determination of bulk density, ash content, core stratigraphy and trace elements concentrations, enabled us to distinguish clay, gyttija, minerotrophic peat and ombrotrophic peat sections. The combination of radiocarbon, ^{210}Pb and ^{137}Cs dating methods and the application of the "Clam" method, provided a valuable chronology. The Val di Ciampo peat bog core covers the last 13,000 years giving a great potential to provide new insights into Late Glacial and Holocene climate dynamics. In particular, the multi-proxy approach confirmed that the uppermost 400 cm of the bog are ombrotrophic, and that all the elements supplied in the last 7,000 years of peat accumulation derive exclusively from atmospheric inputs.

  In the first meter of the bog δ^{13}C and C/N ratio were also determined. The absence of a correlation between δ^{13}C and C/N confirms that humification processes don't compromise C signature, suggesting that there aren't significant post-depositional modifications that can alter elements concentration through the peat profile. Post-depositional migrations are also unlikely due to the following evidence: (i) there is a high correlation between trace elements (e.g., Pb) concentrations in the bulk peat and pore water along the core; (ii) the clustering of some elements obtained both by PCA and Pearson/Spearman indexes suggests that the trace elements composition is not biased by pH or microbial activity. Thus, post-depositional migration of these elements is unlikely in the peat.

All these considerations indicate that Val di Ciampo archive represents an ideal archive to reconstruct the climate variability that characterized the Dolomites during the Holocene. This also represents the longest ombrotrophic archive ever recovered in the Southern part of the Alps.

- **When does the Piave Glacier disappear during the Early Holocene and which is the timing that characterizes the retreating of the glacier?**

As underlined in the previous sections, the course of the deglaciation in the Southern Alps is not well defined and its chronological constraints are not so clear, especially if we compare this section of the Alps with the Northern slope. This is also the case for the Piave glacier and its deglaciation processes in the Vallone Bellunese.

Chronological constraints of the course of deglaciation in the Southern Alps are fewer than those available for the northern slope of the Alps. For the Piave basin, the mode and timing of deglaciation are well-defined only for the mid-part, while no data are available for the upper section. In such a context of very limited data the oldest radiocarbon age (13,110-13,330 years cal BP) represents a very valuable result, providing clear evidence that, during the Bölling-Alleröd interstadial, the upper part of the Piave Glacier was ice free. The last glacial advance of the Piave glacier occurred at around 18,000 cal BP, and the end-moraine system is located at Vittorio Veneto: thus it is possible to realize that in 5,000 years Piave glacier retreated of 90 km and 1,200 meters of gain. The widely accepted idea that the glaciers in the Dolomites (as in the entire Alpine chain) retreated very fast at the end of the Late Glacial, is here confirmed for the first time. It is very interesting to notice that this radiocarbon age represents a minimum age for the deglaciation in Danta di Cadore area because older sediments do exist in the bog.

- **What is the history subsequent to the Piave glacier retreat? And in particular can we divide the amplitude of Holocene climate natural variability from changes related to anthropogenic impacts?**

The most important and widely accepted scientific consensus about current climate changes is that the observed trends, during the last century, cannot be explained solely by natural climate processes, and reflect also human influences. An important question in climate changes

research is whether it is possible to distinguish the human fingerprint on climate, from natural variability.

The primary description of the litho-stratigraphy of Val di Ciampo peat bog core gives a clear view on the development in which the bog evolved: at the end of the Late Glacial, the Piave glacier retreat gives way to an oligotrophic shallow lake, in a depression underlined with a clay layer that holds the water. During the Holocene organic matter filled the lake, sinking to the bottom of the water, and didn't rot because of the highly anoxic conditions. Waters became acidic and plants grew in the lake. Moss started to develop and the buried organic material was transformed into peat. The *Sphagnum* moss mat continued to grow on the top of it, forming the ombrotrophic raised *Sphagnum* bog. This development scheme was also confirmed within the parallel determination of chemical and physical proxies of oligotrophic or eutrophic conditions.

The 7-meters long core covers 13,000 years. During that time, it recorded climate changes related both to natural and anthropogenic factors. Natural variations were identified through biological and chemical analyzes. Trends in lithogenic elements such as Ti and Sr through the core show phases of natural climate variations in soil dust fluxes related to colder or drier climates (e.i., Younger Dryas cooling). Also pollen analysis suggests a relationship between vegetation assemblages that characterized the final part of the Bölling-Alleröd interstadial, the Younger Dryas cooling and the first part of the Early Holocene.

Human impacts on climate were evaluated through the determination of trace and major elements concentrations, lead isotopic signature and Enrichment Factors (EF) calculation. In particular Enrichment Factors permitted us to distinguish where trace elements concentrations exceeded the natural background, and the lead isotopic signature inferred other information about atmospheric inputs related to anthropogenic activity. It was possible to show the impact of mining activity, as well as from other sources e.i., coal and fuel combustion. The combination of traditional ICP-MS technique with XRF core scanner represented a novel analytical approach. After a proper calibration, it was possible to convert XRF signals into concentration units, allowing an high-resolution quantification of trace elements deposition along the entire core.

- *Is our natural archive a record of climate changes on a regional scale and global scale? Can we compare data from this archive with data from other natural archives located in the Southern and Northern Alps?*

Records of natural and anthropogenic climate variations are influenced by parameters such as latitude, distance from the sea, elevation and air mass pathways. Thus, anomalies recorded in climate archives can be affected by geographical parameters and, in some cases, climate trends don't reflect any signal of global climate deviation but only regional patterns of climate evolution. Our record shows climatic variability which certainly follows the global climate signature (e.g., transition from the Late Glacial to the Early Holocene, leaded-gasoline combustion), but also climatic and environmental changes related to more regional or local dynamics, (e.g., ILE experiment, mining activity).

Pollen results can be compared to other palynological studies carried out in the Alps. During the Bölling-Alleröd interstadial, a climatic improvement at around 14,500 years cal BP caused a rapid development of forests that initiated in the lowlands and continued to the higher altitudes (Ravazzi et al., 2007). The vegetation, dominated by grassland with shrubs, changed into forests of *Pinus* and *Betula*. This early reforestation of the Southern Alps is proven also on the Northern side of the Alps (Tobolski, 1985) and also in Austria (Drescher-Schneider, 2008). At the same time the spread of *Picea* in the Po plain is described by Ravazzi et al., (2006) and also in the Cansiglio plain with studies carried out by Avigliano et al., (2000).

During Bölling-Alleröd interstadial the timberline is assumed to have risen to 1,600 - 1,700 m a.s.l. (Pini, 2002; Heiss et al., 2005): the spread to higher altitudes of pioneer species like *Pinus cembra, Pinus mugo* demonstrated by Pini (2002), are confirmed also from Danta di Cadore pollen results. Warmer temperatures at the end of the Late Glacial are followed by colder conditions during the Younger Dryas. The Younger Dryas climatic deterioration had dramatic effects on deciduous trees, and led to a recolonization and expansion of grasslands. In Val di Ciampo bog the "tripartite" structure of the Younger Dryas is visible, as described previously in Brianza by Wick (1996) (see section *Discussion - Deep insights into climate dynamics*).

Temperature and moisture increasing at the beginning of the Holocene favoured the immigration and spread of new species. The development of different forest communities was influenced by topography, exposure, altitude and other factors typical of the area under study. *Pinus, Pinus cembra* and *Betula* dominated forests of the Alpine belt during the

Early Holocene (Ravazzi et al., 2007). The thermophilous species such as *Alnus* immigrated rapidly and reached altitudes of 1,400 m a.s.l., as also demonstrated by Val di Ciampo archive. *Corylus* became an important member of the vegetation as previously suggested at these altitudes by Pini (2002).

Chemical data recorded in the Val di Ciampo archive can be compared with other studies focused on anthropogenic impacts in the Alps during the last centuries.

Val di Ciampo results could be linked with data from ombrotrophic peat bog archives in the Northern part of the Alps. In fact, chemical proxies of climate changes have been deeply studied in several Swiss ombrotrophic bogs (Shotyk et al., 1998, 2001, 2002b). Val di Ciampo shows strong similarities with these archives: in particular the profiles of Pb concentration, fluxes and EF follow the same strong increase between the 1960s and the 1980s, due to the introduction of Pb additives for gasoline in Europe. After 1980s, Swiss bogs show a decrease related to the first environmental policies in Europe, which started to limit pollutants emission at that time. On the contrary Pb in Val di Ciampo bog continues to increase until 1990s, probably reflecting the delay that characterized Italy in adopting European rules about the introduction of unleaded gasoline. This hypothesis is also confirmed by lead isotopic profiles ($^{206}Pb/^{207}Pb$).

No other records of environmental changes from ombrotrophic bogs are available from the Southern part of the Alps. However, interesting comparisons can be done between Val di Ciampo and the ice core collected form Monte Rosa (Gabrieli, 2008, PhD thesis, unpublished).

- *Did this archive record the human activity that characterized the recent history at a regional scale? Can we use this data to improve the historical and archaeological knowledge that we already have about Cadore region and more generally about Belluno province?*

The Eastern Alps are characterized by Pb-Ag mineralization of volcano-sedimentary origin, which have been of some economic importance in the past for metal production (McCann, 2008). In the province of Belluno, and particularly in the Cadore region, there were two important deposits, Argentiera and Salafossa, which was considered one of the most important Pb/Ag ores in Northern Italy (Mancuso, 1990). The impact of Cadore mining on the local environment during the last centuries is not as well defined as in other part of the Alpine chain, but the high quality chronology of this record permitted us to relate the

general increase of atmospheric aerosols with specific human impact from mining activity on a regional scale. Trace elements and heavy metals concentrations (such as Pb and Ag) provide important information about how mining activity developed from the 11th century in Belluno Province, and these data represent a significant added value to the limited knowledge about mining history in that area.

Part VII

Future perspectives

With every new discovery in science, new scientific questions arise. This is also the case during this study. This research provides a very strong basis for future investigations and has motivated a follow-up project, lead by CNR-IDPA, which aims to investigate Holocene climate variability in the North-Eastern Italian Alps.

The large suite of physical, chemical and biological data indicate that a very high-quality paleoclimatic and paleoenvironmental information can be inferred from the Val di Ciampo peat bog. This work represents only a first step. Up to now, effort was mostly directed at understanding if this natural archive is valuable for reconstructing past climatic variability. The results show that the Val di Ciampo peat-bog core is the longest continuous ombrotrophic peat bog record from the Dolomites. Moreover, to our knowledge, it represents the only fully preserved paleoclimatic archive which covers the entire Holocene and the last late Glacial in the Southern Alps.

Chemical and biological analysis of the Val di Ciampo peat bog samples will continue increasing the resolution and the extension of the present record. In particular, high-resolution pollen measurements will be carried out covering the section from 0 to 650 cm in order to reconstruct vegetation changes on both a local and regional scale. The comparison of pollen profiles with those of charcoal and other chemical proxies, will enhance the knowledge of how human activities have impacted vegetation assemblages. The human history in the Cadore valley from the first human settlements to our days will be studied and described in detail.

The combination of the analytical methods XRF-CS and ICP-MS applied to peat bogs, is a novelty: it represent a great resource for climate reconstruction at very high time resolution. In order to confirm the remarkable potential of this analytical strategy, other tests will be done on different peat bog archives. First of all on the Coltrondo peat bog core (Comelico - North-Eastern Italian Alps), archive that is under study with a PhD program at the University Ca' Foscari of Venice.

Additional data from paleo-temperature proxies will be also obtained. Following the molecular approach known as "compound-specific isotope analysis", it will be possible to measure isotopes of specific compounds such as lipids. These data, correlated with temperatures recorded by meteorological stations during the last century, will allow the possibility to create a unique complete temperature-series for the Cadore area.

Climate and environmental variability on decadal to century timescales is too spatially heterogeneous to be adequately characterized by the small number of existing highly resolved, well-dated paleo-climate records. Additional archives will be compared to that of Val di Ciampo in order to achieve an adequate length of the climate record and sufficient temporal resolution to be incorporated into regional-scale climate reconstruction and model simulations. Two thousand years is a critical time frame that includes both the industrial era and a significant length of time prior to the advent of anthro-

pogenic influences on climate. A multidisciplinary approach integrating the geosphere, atmosphere, cryosphere and biosphere is the only way to examine environmental cause and effect mechanisms. The comparison between these results and those obtained from other Alpine archives, including the northern slope and the Western Alps will provide new elements to better interpret the puzzle of the global system. Chemical records obtained from different archives will be compared and the results used as input data of regional-scale environmental and climate models.

Finally, future investigations will be aimed at collecting samples below the bottom of the core, in order to extend and refine the stratigraphy and chronology of the site. It will also improve the chronological constraints on Alpine deglaciation in the Piave valley. The results offer new insights into the chronological constraints that characterized the Late Glacial period, and will have a great potential and strong impact in the scientific community, given the well-known lack of information that characterized this section of the Alps.

Bibliography

Aaby, B. (1976). Cyclic climatic variations in climate over the past 5,500 yr reflected in raised bogs. *Nature*, 263:281–284.

Aarnes, I., Bjune, A., Birks, H., Balascio, N., Bakke, J., and Blaauw, M. (2012). Vegetation responses to rapid climatic changes during the last deglaciation 13,500-8,000 years ago on southwest andoya, arctic norway. *Vegetation History and Archaeobotany*, 21(1):17–35. cited By (since 1996)3.

Alley, R., Meese, D., Shuman, C., Gow, A., Taylor, K., Grootes, P., White, J., Ram, M., Waddington, E., Mayewski, P., and Zielinski, G. (1993). Abrupt increase in greenland snow accumulation at the end of the younger dryas event. *Nature*, 362(6420):527–529. cited By (since 1996)631.

Appleby, P. G. (2001). *Chronostratigraphic techniques in recent sediments. In Tracking Environmenta Change Using Lake Sediments Volume 1: Basin Analysis, Coring, and Chronological Techniques.*, pages 171–203.

Appleby, P. G., Nolan, P. J., Gifford, D. W., Godfrey, M. J., Oldfield, F., Anderson, N. J., and Battarbee, R. W. (1986). ^{210}pb dating by low background gamma counting. *Hydrobiologia*, 143:21–27.

Appleby, P. G. and Oldfield, F. (1978). The calculation of lead-210 dates assuming a constant rate of supply of unsupported ^{210}pb to the sediment. *Catena*, 5:1–8.

Appleby, P. G., Shotyk, W., and Fankhauser, A. (1997). Lead-210 age dating of three peat cores in the jura mountains, switzerland. *Water, Air, and Soil Pollution*, 100:223–231.

Arnold, J. R. Libby, W. F. (1949). Age determinations by radiocarbon content: Checks with samples of known age. *Science*, 110 (2869):678–680.

Atkinson, T., Briffa, K., and Coope, G. (1987). Seasonal temperatures in britain during the past 22,000 years, reconstructed using beetle remains. *Nature*, 325(6105):587–592.

Auer, I., Böhm, R., Jurković, A., Orlik, A., Potzmann, R., Schöner, W., Ungersböck, M., Brunetti, M., Nanni, T., Maugeri, M., Briffa, K., Jones, P., Efthymiadis, D., Mestre, O., Moisselin, J.-M., Begert, M., Brazdil, R., Bochnicek, O., Cegnar, T., Gaji-Capka, M., Zaninović, K., Majstorović, Z., Szalai, S., Szentimrey, T., and Mercalli, L. (2005). A new instrumental precipitation dataset for the greater alpine region for the period 1800-2002. *International Journal of Climatology*, 25(2):139–166. cited By (since 1996)77.

Avigliano, R., Anastasio, G. D., Improta, S., Peresani, M., and Ravazzi, C. (2000). A new late glacial to early holocene palaeobotanical and archaeological record in the eastern pre-alps: The palughetto basin (cansiglio plateau, italy). *Journal of Quaternary Science*, 15:789.

Backeus, I. (1985). Aboveground production and growth dynamics of vascular bog plants in central sweden. *Acta Phytogrographica Suecica*, 74:1–98.

Balascio, N. L., Zhang, Z., Bradley, R. S., Perren, B., Dahl, S. O., and Bakke, J. (2011). A multi-proxy approach to assessing isolation basin stratigraphy from the lofoten islands, norway. *Quaternary Research*, 75:288–300.

Barber, K. (1981). *Peat stratigraphy and climate change: a palaeoecological test of the theory of cyclic peat bog regeneration (Cumbria England)*.

Belokopytov, I. E. and Beresnevich, V. V. (1955). Giktorf's peat borers. *Trof. Prom.*, 8:9–110.

Berset, J. D., Kuehne, P., and Shotyk, W. (2001). Concentrations and distribution of some polychlorinated biphenyls (pcbs) and polycyclic aromatic hydrocarbons (pahs) in an ombrotrophic peat bog profile of switzerland. *Science of the Total Environment*, 267:67–85.

Birks, H. and Birks, H. (2004). *Quaternary Palaeoecology*. Blackburn Press.

Bjorck, S., Walker, M., Cwynar, L., Johnsen, S., Knudsen, K.-L., Lowe, J., and Wohlfarth, B. (1998). An event stratigraphy for the last termination in the north atlantic region based on the greenland ice-core record: a proposal by the intimate group. *Journal of Quaternary Science*, 13(4):283–292.

Blaauw, M. (2010). Methods and code for 'classical' age modelling of radiocarbon sequences. *Quater*, 5:512–518.

Blaauw, M., Bakker, R., Andrés Christen, J., Hall, V., and van der Plicht, J. (2007). A bayesian framework for age modeling of radiocarbon-dated peat deposits: Case studies from the netherlands. *Radiocarbon*, 49(2):357–367. cited By (since 1996)23.

Blaauw, M. and Christen, J. (2005). Radiocarbon peat chronologies and environmental change. *Journal of the Royal Statistical Society. Series C: Applied Statistics*, 54(4):805–816. cited By (since 1996)86.

Blytt, A. (1876). *Essay on the Immigration of the Norwegian Flora During Alternating Rainy and Dry Periods, by Axel Blytt*. A. Cammermeyer.

Boelter, D. H. (1969). Physical properties of peats as related to degree of decomposition. *Soil Science Soc America-proc*, 33(4):606–609. cited By (since 1996)87.

Bond, G., Showers, W., Cheseby, M., Lotti, R., Almasi, P., DeMenocal, P., Priore, P., Cullen, H., Hajdas, I., and Bonani, G. (1997). A pervasive millennial-scale cycle in north atlantic holocene and glacial climates. *Science*, 278(5341):1257–1266.

Bowen, D. (1978). *Quaternary geology: a stratigraphic framework for multidisciplinary work*. Pergamon Press.

Brader, A. V., van Winden, J. F., Bohncke, S. J., Beets, C. J., Reichart, G.-J., and de Leeuw, J. W. (2010). Fractionation of hydrogen, oxygen and carbon isotopes in n-alkanes and cellulose of three sphagnum species. *Organic Geochemistry*, 41(12):1277 – 1284.

Bradley, R. (1999). *Paleoclimatology: Reconstructing Climates of the Quaternary*. Elsevier Science.

Brännvall, M.-L., Bindler, R., Renberg, I., Emteryd, O., Bartnicki, J., and Billström, K. (1999). The medieval metal industry was the cradle of modern large-scale atmospheric lead pollution in northern europe. *Environmental Science and Technology*, 33(24):4391–4395. cited By (since 1996)105.

Briffa, K. and Matthews, J. (2002). Advance-10k: A european contribution towards a hemispheric dendroclimatology for the holocene. *Holocene*, 12(6):639–642. cited By (since 1996)9.

Brook, G., Burney, D., and Cowart, J. (1990). Desert paleoenvironmental data from cave speleothems with examples from the chihuahuan, somalichalbi, and kalahari deserts. *Palaeogeography, Palaeoclimatology, Palaeoecology*, 76(3-4):311–329.

Bruckner, E. (1909). *Die venezianischen Gletscher. In: Penck A. & Buckner - Die Alpen im Eiszeitalter*.

Burney, D., Brook, G., and Cowart, J. (1994). A holocene pollen record for the kalahari desert of botswana from a u-series dated speleothem. *Holocene*, 4(3):225–232.

Cairns, W. R. L. (2008). the use of icp-ms (inductively coupled plasma-mass spectrometry) in the field of chemistry and cultural heritage. In *Chemistry and conservation Science*.

Campbell, I., Campbell, C., Apps, M., Rutter, N., and Bush, A. (1998). Late holocene 1500 yr climatic periodicities and their implications. *Geology*, 26(5):471–473.

Camuffo, D. (1993). Analysis of the sea surges at venice from a.d. 782 to 1990. *Theoretical and Applied Climatology*, 47(1):1–14.

Carton, A., Bondesan, A., Fontana, A., Meneghel, M., Miola, A., Mozzi, P., Primon, S., and Surian, N. (2009). Geomorphological evolution and sediment transfer in the piave river system (northeastern italy) since the last glacial maximum. *Evolution gÃČÂĺomorphologique et transfert sÃČÂĺdimentaire dans le bassin du piave (italie nord-orientale) depuis le dernier maximum glaciaire*, pages 155–174.

Castiglioni, B. (1940). *L'Italia nell'Etá Quaternaria. In Danielli G. - Atlante Fisico Economico d'Italia*.

Castiglioni, B. (1967). *Carta delle morene stadiali della regione Dolomitica. In Leonardi P. - Le Dolomiti, geologia dei monti tra Isarco e Piave*.

Chambers, F., Barber, K., Maddy, D., and Brew, J. (1997). A 5500-year proxy-climate and vegetation record from blanket mire at talla moss, borders, scotland. *Holocene*, 7(4):391–399.

Chambers, F. and Charman, D. (2004). Holocene environmental change: Contributions from the peatland archive. *Holocene*, 14:1–6.

Chambers, F. M., Booth, R. K., De Vleeschouwer, F., Lamentowicz, M., Le Roux, G., Mauquoy, D., Nichols, J. E., and van Geel, B. (2012). Development and refinement of proxy-climate indicators from peats. *Quaternary International*, 268:21–33.

Chapman, M. and Shackleton, N. (2000). Evidence of 550-year and 1000-year cyclicities in north atlantic circulation patterns during the holocene. *Holocene*, 10(3):287–291.

Chappellaz, J., Barnola, J., Raynaud, D., Korotkevich, Y., and Lorius, C. (1990). Ice-core record of atmospheric methane over the past 160,000 years. *Nature*, 345(6271):127–131.

Charman, D., Caseldine, C., Gearey, B., Hatton, J., and Proctor, C. (2001). Paleohydrological records from peat profiles and speleothems in sutherland, nortwest scotland. *Quaternary Research*, 55(2):223–234.

Chu, P. C., Li, H.-C., Fan, C., and Chen, Y. (2012). Speleothem evidence for temporal-spatial variation in the east asian summer monsoon since the medieval warm period. *JQS. Journal of Quaternary Science*, 27(9):901–910.

Church, J., White, N., and Arblaster, J. (2005). Significant decadal-scale impact of volcanic eruptions on sea level and ocean heat content. *Nature*, 438(7064):74–77. cited By (since 1996)81.

CLIMAPMembers (1976). The surface of the ice-age earth: By climap project members. *Science*, 191:1131–1137.

CLIMAPMembers (1984). The last interglacial ocean. *Quaternary Research*, 21(2):123 – 224.

Clymo, R. S. (1983). *Mires: Swamp, Bog, Fen and Moor, Ecosystems of the World, 4A*, chapter Peat, pages 159–224. Elsevier Scientific Publishing Co. New York.

Clymo, R. S. (1984). Limits of the peat growth. *Proceedings of the Royal Society, London, Series B*, 303:604–654.

Clymo, R. S. and Hayward, P. M. (1982). *The ecology of Spaghum.* Chapman and Hall, London.

Croll, J. (1875). *Climate and Time in Their Geological Relations: A Theory of Secular Changes of the Earth's Climate.* D. Appleton.

Crutzen, P. J. and Stoermer, E. (2000). The anthropocene. *Global Change Newsletter*, 41:17–18.

Cunningham, L., Austin, W., Knudsen, K., EirÃŋksson, J., Scourse, J., Wanamaker, A., Butler, P., Cage, A., Richter, T., Husum, K., Hald, M., Andersson, C., Zorita, E., Linderholm, H., Gunnarson, B., Sicre, M.-A., Sejrup, H., Jiang, H., and Wilson, R. (2013). Reconstructions of surface ocean conditions from the northeast atlantic and nordic seas during the last millennium. *Holocene*, 23(7):921–935. cited By (since 1996)0.

Damman, A. W. H. (1995). Major mire vegetation units in relation to the concepts of ombrotrophy and minerotrophy: a worldwide perspective. *Gunneria*, 70:23–34.

Dansgaard, W., Johnsen, S., Clausen, H., Dahl-Jensen, D., Gundestrup, N., Hammer, C., Hvidberg, C., Steffensen, J., Sveinbjörnsdottir, A., Jouzel, J., and Bond, G. (1993). Evidence for general instability of past climate from a 250-kyr ice-core record. *Nature*, 364(6434):218–220.

de Jong, R., Björck, S., Björkman, L., and Clemmensen, L. (2006). Storminess variation during the last 6500 years as reconstructed from an ombrotrophic peat bog in halland, southwest sweden. *Journal of Quaternary Science*, 21(8):905–919.

De Putter, T., Loutre, M.-F., and Wansard, G. (1998). Decadal periodicities of nile river historical discharge (a.d. 622-1470) and climatic implications. *Geophysical Research Letters*, 25(16):3193–3196.

De Vleeschouwer, F., Pazdur, A., Luthers, C., Streel, M., Mauquoy, D., Wastiaux, C., Le Roux, G., Moschen, R., Blaauw, M., Pawlyta, J., Sikorski, J., and Piotrowska, N. (2012a). A millennial record of environmental change in peat deposits from the misten bog (east belgium). *Quaternary International*, 268:44–57.

De Vleeschouwer, F., Pazdur, A., Luthers, C., Streel, M., Mauquoy, D., Wastiaux, C., Le Roux, G., Moschen, R., Blaauw, M., Pawlyta, J., Sikorski, J., and Piotrowska, N. (2012b). A millennial record of environmental change in peat deposits from the misten bog (east belgium). *Quaternary International*, 268:44–57.

Douglass, A. E. (1920). Evidence of climatic effects in the annual rings of trees. *Ecology*, 1(1):24–32.

Dreyer, A., Blodau, C., Turunen, J., and Radke, M. (2005a). The spatial distribution of pah depositions to peatlands of eastern canada. *Atmospheric Environment*, 39:3725–3733.

Dreyer, A., Radke, M., Turunen, J., and Blodau, C. (2005b). Long-term change of polycyclic aromatic hydrocarbon deposition to peatlands of eastern canada. *Environmental Science and Technology*, 39:3918–3924.

Dunbar, R., Wellington, G., Colgan, M., and Glynn, P. (1994). Eastern pacific sea surface temperature since 1600 a.d.: the ^{18}o record of climate variability in galapagos corals. *Paleoceanography*, 9(2):291–315.

Edwards, R., Beck, J., Burr, G., Donahue, D., Chappell, J., Bloom, A., Druffel, E., and Taylor, F. (1993). A large drop in atmospheric14c/12c and reduced melting in the younger dryas, documented with230th ages of corals. *Science*, 260(5110):962–968.

Engeset, R., Elvehoy, H., Andreassen, M., Haakensen, N., Kjollmoen, B., Roald, A., and Roland, E. (2000). Modelling of historic variations and future scenarios of themass balance of svartisen ice cap, northern norway. *Annals of Glaciology*, 31:97–103.

Epstein, R., Lattimer, J., and Schramm, D. (1976). The origin of deuterium. *Nature*, 263(5574):198–202.

Etheridge, D., Steele, L., Langenfelds, R., Francey, R., Barnola, J.-M., and Morgan, V. (1996). Natural and anthropogenic changes in atmospheric co2 over the last 1000 years from air in antarctic ice and firn. *Journal of Geophysical Research D: Atmospheres*, 101(D2):4115–4128.

Evans, M., Fairbanks, R., and Rubenstone, J. (1999). The thermal oceanographic signal of el niño reconstructed from a kiritimati island coral. *Journal of Geophysical Research C: Oceans*, 104(C6):13409–13421.

Faegri, K. and Iversen, J. (1964). *Textbook of pollen analysis [by] Knut Faegri [and] Johs. Iversen. With a chapter on Pre-Quaternary pollen analysis.* Hafner Pub. Co.

Fairchild, I. J., Baker, A., Borsato, A., Frisia, S., Hinton, R. W., McDermott, F., and Tooth, A. F. (2001). Annual to sub-annual resolution of multiple trace-element trends in speleothems. *Journal of the Geological Society*, 158:831–841.

Fallon, S., White, J., and McCulloch, M. (2002). Porites corals as recorders of mining and environmental impacts: Misima island, papua new guinea. *Geochimica et Cosmochimica Acta*, 66(1):45–62.

Ferrat, M., Weiss, D. J., Spiro, B., and Large, D. (2012). The inorganic geochemistry of a peat deposit on the eastern qinghai-tibetan plateau and insights into changing atmospheric circulation in central asia during the holocene. *Geochimica et Cosmochimica Acta*, 91:7–31.

Finsinger, W., Tinner, W., Van Der Knaap, W. O., and Ammann, B. (2006). The expansion of hazel (corylus avellana l.) in the southern alps: A key for understanding its early holocene history in europe? *Quaternary Science Reviews*, 25:612–631.

Fischer, M. J., Treble, P. C., and Anonymous (2009). A model, and the fidelity of climate reconstructions from speleothems. *Geophysical Research Abstracts*, 11:EGU2009–6287.

Fischer, M. J., Treble, P. C., and Anonymous (2010). Holocene climate reconstructions and modelling from australian speleothems. *Abstracts - Geological Society of Australia*, 98:125–126.

Foley, J., Kutzbach, J., Coe, M., and Levis, S. (1994). Feedbacks between climate and boreal forests during the holocene epoch. *Nature*, 371(6492):52–54.

Frisia, S., W. J. (2012). *Stalactites and stalagmites.* cited By (since 1996)0.

Fritz, S. (1996). Paleolimnological records of climatic change in north america. *Limnology and Oceanography*, 41(5):882–889.

Frolking, S., Roulet, N. T., Moore, T., Richard, P. J. H., Lavoie, M., and Muller, S. (2001). Modelling northern peatland decomposition and peat accumulation. *Ecosystems*, 4:479–498.

Gallagher, D., McGee, E. J., and Mitchell, P. I. (2001). A recent history of14c, 137cs, 210pb, and241am accumulation at two irish peat bog sites: An east versus west coast comparison. *Radiocarbon*, 43:517–525.

Gasse, F. (2000). Hydrological changes in the african tropics since the last glacial maximum. *Quaternary Science Reviews*, 19(1-5):189–211.

Giralt, S., Rico-Herrero, M. T., Vega, J. C., and Valero-Garcãs, B. L. (2011). Quantitative climate reconstruction linking meteorological, limnological and xrf core scanner datasets: The lake sanabria case study, nw spain. *Journal of Paleolimnology*, 46:487–502.

Givelet, N., Le Roux, G., Cheburkin, A., Chen, B., Frank, J., Goodsite, M. E., Kempter, H., Krachler, M., Noernberg, T., Rausch, N., Rheinberger, S., Roos-Barraclough, F., Sapkota, A., Scholz, C., and Shotyk, W. (2004). Suggested protocol for collecting, handling and preparing peat cores and peat samples for physical, chemical, mineralogical and isotopic analyses. *Journal of Environmental Monitoring*, 6:481–492.

Givelet, N., Roos-Barraclough, F., and Shotyk, W. (2003). Predominant anthropogenic sources and rates of atmospheric mercury accumulation in southern ontario recorded by peat cores from three bogs: Comparison with natural "background" values (past 8000 years). *Journal of Environmental Monitoring*, 5:935–949.

Given, P. H. and Dickinson, C. H. (1975). *Soil Biochemistry*, chapter Biochemistry and microbiology of peat. E.A. Paul and A.D. Mclaren.

Gore, A. J. P. (1983). *Ecosystem of the World. Mires: Swamp, bog, fen and moor*. Elsevier.

Grove, J. (1988). *The Little Ice Age*. Methuen, New York.

Haeberli, W. (1995). Glacier fluctuations and climate change detection. *Geografia Fisica e Dinamica Quaternaria*, 18(2):191–199. cited By (since 1996)26.

Haug, G. H., Hughen, K. A., Sigman, D. M., Peterson, L. C., and Rohl, U. (2001). Southward migration of the intertropical convergence zone through the holocene. *Science*, 293:1304–1308.

Hays, J., Imbrie, J., and Shackleton, N. (1976). Variations in the earth's orbit: Pacemaker of the ice ages. *Science*, 194(4270):1121–1132.

Heiss, A. G., Kofler, W., and Oeggl, K. (2005). The ulten valley in south tirol, italy: Vegetation and settlement history of the area, and macrofossil record from the iron age cult site of st. walburg. *Palyno-Bullettin of the Institute of Botany, University of Innsbruck*, 1-2:63–73.

Hembrow, S., Taffs, K., Atahan, P., Parr, J., Zawadzki, A., and Heijnis, H. (2013). Diatom community response to climate variability over the past 37,000years in the sub-tropics of the southern hemisphere. *Science of the Total Environment*, 468-469:774–784. cited By (since 1996)0.

Hodell, D., Curtis, J., and Brenner, M. (1995). Possible role of climate in the collapse of classic maya civilization. *Nature*, 375(6530):391–394.

Imbrie, J. (1984). *The orbital theory of Pleistocene climate: support from a revised chronology of the marine d18O record.*

Ingram, M., Underhill, D., and Wigley, T. (1978). Historical climatology. *Nature*, 276(5686):329–334.

Jansen, J. H. F., Van der Gaast, S. J., Koster, B., and Vaars, A. J. (1998). Cortex, a shipboard xrf-scanner for element analyses in split sediment cores. *Marine Geology*, 151:143–153.

Kemp, A. E. S., editor (1996). *Palaeoclimatology and palaeoceanography from laminated sediments*. Geological Society.

Krachler, M., Emons, H., Barbante, C., Cozzi, G., Cescon, P., and Shotyk, W. (2002). Inter-method comparison for the determination of antimony and arsenic in peat samples. *Analytica Chimica Acta*, 458:387–396.

Kuhry, P. and Vitt, D. (1996). Fossil carbon/nitrogen ratios as a measure of peat decomposition. *Ecology*, 77(1):271–275.

Lamy, F., Hebbeln, D., Rohl, U., and Wefer, G. (2001). Holocene rainfall variability in southern chile: a marine record of latitudinal shifts of the southern westerlies. *Earth and Planetary Science Letters*, 185:369–382.

Langdon, C., Takahashi, T., Sweeney, C., Chipman, D., Goddard, J., Marubini, F., Aceves, H., Barnett, H., and Atkinson, M. (2000). Effect of calcium carbonate saturation state on the calcification rate of an experimental coral reef. *Global Biogeochemical Cycles*, 14(2):639–654.

Langdon, P. G., Brown, A. G., Caseldine, C. J., Blockley, S. P. E., and Stuijts, I. (2012). Regional climate change from peat stratigraphy for the mid- to late holocene in central ireland. *Quaternary International*, 268:145–155.

Large, D. J., Spiro, B., Ferrat, M., Shopland, M., Kylander, M., Gallagher, K., Li, X., Shen, C., Possnert, G., Zhang, G., Darling, W. G., and Weiss, D. (2009). The influence of climate, hydrology and permafrost on holocene peat accumulation at 3500 m on the eastern qinghai-tibetan plateau. *Quaternary Science Reviews*, 28:3303–3314.

Lauritzen, S. (1993). Natural environmental change in karst: The quaternary record. *CATENA SUPPL.*, 25:21–40.

Lauritzen, S.-E. (1991). Uranium series dating of speleothems: a glacial chronology for nordland, norway, for the last 600 ka. *Striae*, 34:127–133.

Lauritzen, S.-E. and Gascoyne, M. (1980). The first radiometric dating of norwegian stalgamites - evidence of pre-weichselian karst caves. *Norsk Geografisk Tidsskrift*, 34(2):77–82.

Lauritzen, S.-E., Lavlie, R., Moe, D., and Ãstbye, E. (1990). Paleoclimate deduced from a multidisciplinary study of a half-million-year-old stalagmite from rana, northern norway. *Quaternary Research*, 34(3):306–316.

Lauterbach, S., Brauer, A., Andersen, N., Danielopol, D., Dulski, P., Hüls, M., Milecka, K., Namiotko, T., Obremska, M., and Von Grafenstein, U. (2011). Environmental responses to lateglacial climatic fluctuations recorded in the sediments of pre-alpine lake mondsee (northeastern alps). *Journal of Quaternary Science*, 26(3):253–267.

Le Roux, G., Fagel, N., De Vleeschouwer, F., Krachler, M., Debaille, V., Stille, P., Mattielli, N., van der Knaap, W. O., van Leeuwen, J. F., and Shotyk, W. (2012). Volcano- and climate-driven changes in atmospheric dust sources and fluxes since the late glacial in central europe. *Geology*, 40:335–338.

Linsley, B., Dunbar, R., Wellington, G., and Mucciarone, D. (1994). A coral-based reconstruction of intertropical convergence zone variability over central america since 1707. *Journal of Geophysical Research*, 99(C5):9977–9994.

Mancuso, F. (1990). *Archeologia industriale nel Veneto.*

Manley, G. (1974). Central england temperatures: Monthly means 1659 to 1973. *Quarterly Journal of the Royal Meteorological Society*, 100:389–405.

Mann, M., Bradley, R., and Hughes, M. (1999). Northern hemisphere temperatures during the past millennium: Inferences, uncertainties, and limitations. *Geophysical Research Letters*, 26(6):759–762.

Marcelli, A., Hampai, D., Giannone, F., Sala, M., Maggi, V., Marino, F., Pignotti, S., and Cibin, G. (2012). Xrf-xanes characterization of deep ice core insoluble dust. *Journal of Analytical Atomic Spectrometry*, 27:33–37.

Martinez-Cortizas, A., Pontevedra-Pombal, X., Garcia-Rodeja, E., Novoa-Munoz, J. C., and Shotyk, W. (1999). Mercury in a spanish peat bog: Archive of climate change and atmospheric metal deposition. *Science*, 284:939–942.

Martinson, D., Pisias, N., Hays, J., Imbrie, J., Moore Jr., T., and Shackleton, N. (1987). Age dating and the orbital theory of the ice ages: Development of a high-resolution 0 to 300,000-year chronostratigraphy. *Quaternary Research*, 27(1):1–29.

Matyasovszky, I. and Ljungqvist, F. (2013). Abrupt temperature changes during the last 1,500 years. *Theoretical and Applied Climatology*, 112(1-2):215–225. cited By (since 1996)0.

Mayewski, P., Meeker, L., Twickler, M., Whitlow, S., Yang, Q., Berry Lyons, W., and Prentice, M. (1997). Major features and forcing of high-latitude northern hemisphere atmospheric circulation using a 110 000-year-long glaciochemical series. *Journal of Geophysical Research*, 102(C12):26345–26366.

McCann, T. (2008). *The Geology of Central Europe: Mesozioc and cenozoic*. The Geology of Central Europe. Geological Society of London.

McCormac, F. G., Hogg, A. G., Blackwell, P. G., Buck, C. E., Higham, T. F. G., and Reimer, P. J. (2004). Shcal04 southern hemisphere calibration, 0-11.0 cal kyr bp. *Radiocarbon*, 46:1087–1092.

Messager, E., Belmecheri, S., Von Grafenstein, U., Nomade, S., Ollivier, V., Voinchet, P., Puaud, S., Courtin-Nomade, A., Guillou, H., Mgeladze, A., Dumoulin, J.-P., Mazuy, A., and Lordkipanidze, D. (2013). Late quaternary record of the vegetation and catchment-related changes from lake paravani (javakheti, south caucasus). *Quaternary Science Reviews*, 77:125–140. cited By (since 1996)0.

Milanković, M. (1969). *Canon of insolation and the ice-age problem: (Kanon der Erdbestrahlung und seine Anwendung auf das Eiszeitenproblem) Belgrade, 1941*. Posebna izdanja. Israel Program for Scientific Translations; [available from U.S. Dept. of Commerce, Clearinghouse for Federal Scientific and Technical Information, Springfield, Va.].

Mitchell, P. I., Schell, W. R., McGarry, A., Ryan Sanchez-Cabeza, T. P. J. A., and Vidal-Quadras, A. (1992). Studies of the vertical distribution of 134cs, 137cs, 238pu, 239,240pu, 241pu, 241am and 210pb in ombrogenous mires at mid-la. *Journal of Radioanalytical and Nuclear Chemistry*, 156:361–387.

Moore, P., Webb, J., and Collinson, M. (1991). *Pollen Analysis*. Wiley.

Moreno, A. and Amelung, B. (2009). Climate change and tourist comfort on europe's beaches in summer: A reassessment. *Coastal Management*, 37(6):550–568.

Nicholson, S., Nash, D., Chase, B., Grab, S., Shanahan, T., Verschuren, D., Asrat, A., LÃľzine, A.-M., and Umer, M. (2013). Temperature variability over africa during the last 2000 years. *Holocene*, 23(8):1085–1094. cited By (since 1996)0.

O'Brien, S., Mayewski, P., Meeker, L., Meese, D., Twickler, M., and Whitlow, S. (1995). Complexity of holocene climate as reconstructed from a greenland ice core. *Science*, 270(5244):1962–1964.

Orombelli, G., Ravazzi, C., and Cita, M. B. (2005). Osservazioni sul significato dei termini lmg (umg), tardoglaciale e postglaciale in ambito globale, italiano e alpino. *Il Quaternario - Italian Journal of Quaternary Sciences*, 18(2):147–155.

Osvald, K. (1923). *Die Vegetation des Hochmoores Komosse*. Svenska vxtsociologiska sllskapet 1, 1-436.

Pacyna, E., Pacyna, J., Fudala, J., Strzelecka-Jastrzab, E., Hlawiczka, S., Panasiuk, D., Nitter, S., Pregger, T., Pfeiffer, H., and Friedrich, R. (2007). Current and future emissions of selected heavy metals to the atmosphere from anthropogenic sources in europe. *Atmospheric Environment*, 41(38):8557–8566. cited By (since 1996)40.

Pellegrini, G. B., Albanese, D., Bertoldi, R., and Surian, N. (2005). La deglaciazione alpina nel vallone bellunese, alpi meridionali orientali. *Geogr. Fis. Dinam . Quat.*, Suppl. VII:271–280.

Pellegrini, G. B., Surian, N., and Urbinati, C. (2004). Dating and explanation of late glacial - holocene landslides: A case study from the southern alps, italy. *Zeitschrift fur Geomorphologie*, 48:245–258.

Pheiffer Madsen, P. (1981). Peat bog records of atmospheric mercury deposition. *Nature*, 293:127–130.

Pini, R. (2002). A high-resolution late-glacial - holocene pollen diagram from pian di gembro (central alps, northern italy). *Vegetation History and Archaeobotany*, 11:251–262.

Piotrowska, N., Blaauw, M., Mauquoy, D., and Chambers, F. (2011). Constructing deposition chronologies for peat deposit using radiocarbon dating. *Mires and Peat*, 7.

Preunkert, S., Wagenbach, D., Legrand, M., and Vincent, C. (2000). Col du dome (mt blanc massif, french alps) suitability for ice-core studies in

relation with past atmospheric chemistry over europe. *Tellus, Series B: Chemical and Physical Meteorology*, 52(3):993–1012.

Pugh, R., Dick, D., and Fredeen, A. (2002). Heavy metal (pb, zn, cd, fe, and cu) contents of plant foliage near the anvil range lead/zinc mine, faro, yukon territory. *Ecotoxicology and Environmental Safety*, 52(3):273–279.

Railsback, L., Brook, G., Chen, J., Kalin, R., and Fleisher, C. (1994). Environmental controls on the petrology of a late holocene speleothem from botswana with annual layers of aragonite and calcite. *Journal of Sedimentary Research A: Sedimentary Petrology and Processes*, 64 A(1):147–155.

Ravazzi, C. (2005). Il tardoglaciale: suddivisione stratigrafi ca, evoluzione sedimentaria e vegetazionale nelle alpi e in pianura padana. *Studi Trent. Sci. Nat., Acta Geol*, 82:17–29.

Reimer, P. J., Baillie, M. G. L., Bard, E., Bayliss, A., Beck, J. W., Blackwell, P., Bronk Ramsey, C., Buck, C. E., Burr, G., Edwards, R. L., Friedrich, M., Grootes, P. M., Guilerson, T., Hajdas, I., Heaton, T. J., Hogg, A. G., Hugen, K. A., Kaiser, K. F., Kromer, B., McCormac, F. G., Manning, S. W., Reimer, R. W., Richards, D. A., Southon, J. R., Talamo, S., Turney, C. S. M., van der Plicht, J., and Weyhenmeyer, C. E. (2009). Intcal09 and marine09 radiocarbon age calibration curves, 0âĂŞ50,000 years cal bp. *Radioca*, 51:1111–1150.

Reimer, P. J., Reimer, R. W., and Blaauw, M. (2013). {RADIOCARBON} {DATING} | calibration of the 14c record. *Encyclopedia of Quaternary Science*.

Richards, D. A., Beck, J. W., Donahue, D. J., Smart, P. L., Edwards, R. L., and Anonymous (2000). Radiocarbon in speleothems from the bahamas; implications for climate and solar/geomagnetic field variation during the last glacial period. *Cave and Karst Science*, 27(3):134–134.

Robock, A. (2000). Volcanic eruptions and climate. *Reviews of Geophysics*, 38(2):191–219. cited By (since 1996)573.

Röpke, A., Stobbe, A., Oeggl, K., Kalis, A. J., and Tinner, W. (2011). Late-holocene land-use history and environmental changes at the high altitudes of st antönien (switzerland, northern alps): Combined evidence from pollen, soil and tree-ring analyses. *Holocene*, 21:485–498.

Ruddiman, W. (2003). The anthropogenic greenhouse era began thousands of years ago. *Climatic Change*, 61(3):261–293.

Ruddiman, W. (2007). The early anthropogenic hypothesis: Challenges and responses. *Reviews of Geophysics*, 45(4).

Ruddiman, W. (2008). *Earth's Climate: Past and Future*. W. H. Freeman.

Ruddiman, W. and McIntyre, A. (1981). Oceanic mechanisms for amplification of the 23,000-year ice-volume cycle. *Science*, 212(4495):617–627.

Rudzka, D., McDermott, F., and Suric, M. (2012). A late holocene climate record in stalagmites from modric cave (croatia). *JQS. Journal of Quaternary Science*, 27(6):585–596.

Sahagian, D. and Melack, J. (1998). Global wetland distribution and functional characterization: trace gases and the hydrologic cycle.

Sapkota, A., Cheburkin, A. K., Bonani, G., and Shotyk, W. (2007). Six millennia of atmospheric dust deposition in southern south america (isla navarino, chile). *Holocene*, 17:561–572.

Seki, O., Meyers, P. A., Kawamura, K., Zheng, Y., and Zhou, W. (2009). Hydrogen isotopic ratios of plant wax n-alkanes in a peat bog deposited in northeast china during the last 16 kyr. *Organic Geochemistry*, 40(6):671 – 677.

Sernander, R. (1908). On the evidences of postglacial changes of climate furnished by the peat-mosses of northern europe. *Geologiska Föreningen i Stockholm Förhandlingar*, 30:465–473.

Shi, F., Yang, B., and Von Gunten, L. (2012). Preliminary multiproxy surface air temperature field reconstruction for china over the past millennium. *Science China Earth Sciences*, 55(12):2058–2067. cited By (since 1996)2.

Shotyk, W. (1988). Review of the inorganic geochemistry of peats and peatland waters. *Earth-Science Reviews*, 25:95–176.

Shotyk, W. (1996). Peat bog archives of atmospheric metal deposition: Geochemical evaluation of peat profiles, natural variations in metal concentrations, and metal enrichment factors. *Environmental Reviews*, 4:149–183.

Shotyk, W. and Steinmann, P. (1994). Pore-water indicators of rainwater-dominated versus groundwater-dominated peat bog profiles (jura mountains, switzerland). *Chemical Geology*, 116:137–146.

Shotyk, W., Weiss, D., Appleby, P. G., Cheburkin, A. K., Frei, R., Gloor, M., Kramers, J. D., Reese, S., and Van Der Knaap, W. O. (1998). History of atmospheric lead deposition since 12,370 14c yr bp from a peat bog, jura mountains, switzerland. *Science*, 281:1635–1640.

Shotyk, W., Weiss, D., Heisterkamp, M., Cheburkin, A., Appleby, P., and Adams, F. (2002a). New peat bog record of atmospheric lead pollution in switzerland: Pb concentrations, enrichment factors, isotopic composition,

and organolead species. *Environmental Science and Technology*, 36:3893–3900.

Shotyk, W., Weiss, D., Heisterkamp, M., Cheburkin, A. K., Appleby, P. G., and Adams, F. C. (2002b). New peat bog record of atmospheric lead pollution in switzerland: Pb concentrations, enrichment factors, isotopic composition, and organolead species. *Environmental Science and Technology*, 36:3893–3900.

Shotyk, W., Weiss, D., Kramers, J. D., Frei, R., Cheburkin, A. K., Gloor, M., and Reese, S. (2001). Geochemistry of the peat bog at etang de la gru'are, jura mountains, switzerland, and its record of atmospheric pb and lithogenic trace metals (sc, ti, y, zr, and ree) since 12,370 14c yr bp. *Geochimica et Cosmochimica Acta*, 65:2337–2360.

Sigl, M., Jenk, T., Kellerhals, T., Szidat, S., GÃd'ggeler, H., Wacker, L., Synal, H.-A., Boutron, C., Barbante, C., Gabrieli, J., and Schwikowski, M. (2009). Instruments and methods towards radiocarbon dating of ice cores. *Journal of Glaciology*, 55(194):985–996. cited By (since 1996)10.

Singh, H. B. and Kanakidou, M. (1993). An investigation of the atmospheric sources and sinks of methyl bromide. *Geophysical Research Letters*, 20:133–136.

Solomon, S., on Climate Change, I. P., and on Climate Change. Working Group I., I. P. (2007). *Climate Change 2007 - The Physical Science Basis: Working Group I Contribution to the Fourth Assessment Report of the IPCC*. Assessment report (Intergovernmental Panel on Climate Change): Working Group. Cambridge University Press.

Spotl, C. and Mangini, A. (2007). Speleothems and paleoglaciers. *Earth and Planetary Science Letters*, 254(3-4):323–331.

Stanley, D. W. (1970). *Water for Larsa; an Old Babylonian archive dealing with irrigation*. Yale University Press.

Steinmann, P. and Shotyk, W. (1997). Chemical composition, ph and redox state of sulfur and iron in complete vertical porewater profiles from two sphagnum peat bogs, jura mountains, switzerland. *Geochimica et Cosmochimica Acta*, 61:1143–1163.

Stockmarr, J. (1971). Tablets with spores used in absolute pollen analysis. *Pollen at Spores*, 13:615–621.

Stuiver, M. and Reimer, P. J. (1993). Extended 14c data base and revised calib 3.0 14c age calibration program. *Radiocarbon*, 35:215–230.

Surian, N. (1996). The terraces of the piave river in the vallone bellunese, eastern alps, italy. *Geografica Fisica e Dinamica Quaternaria*, 19:119–127.

Swaine, D. (1990). *Trace elements in coal*. Butterworths (Canada) Limited.

Tanzil, J., Brown, B., Tudhope, A., and Dunne, R. (2009). Decline in skeletal growth of the coral porites lutea from the andaman sea, south thailand between 1984 and 2005. *Coral Reefs*, 28(2):519–528.

Tareq, S. M., Tanaka, N., and Ohta, K. (2004). Biomarker signature in tropical wetland: Lignin phenol vegetation index (lpvi) and its implications for reconstructing the paleoenvironment. *Science of the Total Environment*, 324:91–103.

Taylor, R. (2000). *Inductively Coupled Plasma - Mass Spectrometry: practices and techniques*. Academic Press, San Diego, CA, USA.

Thompson, L., Yao, T., Davis, M., Henderson, K., Mosley-Thompson, E., Lin, P.-N., Beer, J., Synal, H.-A., Cole-Dai, J., and Bolzan, J. (1997). Tropical climate instability: The last glacial cycle from a qinghai- tibetan ice core. *Science*, 276(5320):1821–1825.

Tian, J., Xie, X., Ma, W., Jin, H., and Wang, P. (2011). X-ray fluorescence core scanning records of chemical weathering and monsoon evolution over the past 5 myr in the southern south china sea. *Paleoceanography*, 26.

Tillman, P. K., Holzkämper, S., Kuhry, P., Sannel, A. B. K., Loader, N. J., and Robertson, I. (2010). Stable carbon and oxygen isotopes in sphagnum fuscum peat from subarctic canada: Implications for palaeoclimate studies. *Chemical Geology*, 270(1âĂŞ4):216 – 226.

Tinner, W., Hubschmid, P., Wehrli, M., Ammann, B., and Conedera, M. (1999). Long-term forest fire ecology and dynamics in southern switzerland. *Journal of Ecology*, 87:273–289.

Tjallingii, R., Roehl, U., Koelling, M., and Bickert, T. (2007). Influence of the water content on x-ray fluorescence core-scanning measurements in soft marine sediments. *Geochemistry Geophysics Geosystems*, 8.

Tudhope, A., Chilcott, C., McCulloch, M., Cook, E., Chappell, J., Ellam, R., Lea, D., Lough, J., and Shimmield, G. (2001). Variability in the el niño-southern oscillation through a glacial-interglacial cycle. *Science*, 291(5508):1511–1517.

Valsecchi, V., Tinner, W., Finsinger, W., and Ammann, B. (2006). Human impact during the bronze age on the vegetation at lago lucone (northern italy). *Vegetation History and Archaeobotany*, 15:99–113.

Van Geel, B. (1978). A palaeoecological study of holocene peat bog sections in germany and the netherlands, based on the analysis of pollen, spores and macro- and microscopic remains of fungi, algae, cormophytes and animals. *Review of Palaeobotany and Palynology*, 25:1–120.

Van Geel, B., Bohncke, S., and Dee, H. (1980). A palaeoecological study of an upper late glacial and holocene sequence from "de borchert", the netherlands. *Review of Palaeobotany and Palynology*, 31(C):367–392,397–448.

Vasskog, K., Nesje, A., Storen, E., Waldmann, N., Chapron, E., and Ariztegui, D. (2011). A holocene record of snow-avalanche and flood activity reconstructed from a lacustrine sedimentary sequence in oldevatnet, western norway. *Holocene*, 21(4):597–614.

Vescovi, E., Ravazzi, C., Arpenti, E., Finsinger, W., Pini, R., Valsecchi, V., Wick, L., Ammann, B., and Tinner, W. (2007). Interactions between climate and vegetation during the lateglacial period as recorded by lake and mire sediment archives in northern italy and southern switzerland. *Quaternary Science Reviews*, 26:1650–1669.

Vivaldo, G. (2012). Climate variability and amplification revealed from indicators in the gulf of taranto. *Nuovo Cimento della Societa Italiana di Fisica C*, 35(5):115–127. cited By (since 1996)0.

von Post, L. (1916). Skogträdpollen i sydsvenska torvmosselagerfÃűljder (forest tree pollen in south swedish peat bog deposits). *Geologiska FÃűreningens i Stockholm FÃűrhandlingar*, 38:433–465.

Von Post, L. and Granlund, E. (1926). Peat resources in southern sweden i. *Sveriges Geologiska Undersökning*, 335:1–128.

von Post, L. and Sernander, R. (1910). *Pflanzen-physiognomische Studien aus Torfmooren in Nrke*. XI International Geological Congress: Excursion Guide No. 14 (A7); Stockholm; 48 pp.

Walker, M. J. C., B′arck, S., Lowe, J. J., Cwynar, L. C., Johnsen, S., Knudsen, K. L., and Wohlfarth, B. (1999). Isotopic 'events' in the grip ice core: A stratotype for the late pleistocene. *Quaternary Science Reviews*, 18:1143–1150.

Wardenaar, E. C. P. (1987). A new hand tool for cutting soil monoliths. *Canadian Journal of Soil Science*, 67:405–407.

Wassenburg, J. A., Immenhauser, A., Richter, D. K., Jochum, K. P., Fietzke, J., Deininger, M., Goos, M., Scholz, D., and Sabaoui, A. (2012). Climate and cave control on pleistocene/holocene calcite-to-aragonite transitions

in speleothems from morocco; elemental and isotopic evidence. *Geochimica et Cosmochimica Acta*, 92:23–47.

Wedepohl, H. K. (1995). The composition fo the continental crust. *Geochi*, 59:1217–1232.

Weiss, D., Shotyk, W., Kramers, J. D., and Gloor, M. (1999). Sphagnum mosses as archives of recent and past atmospheric lead deposition in switzerland. *Atmospheric Environment*, 33:3751–3763.

Weiss, D., Shotyk, W., Rieley, J., Page, S., Gloor, M., Reese, S., and Martinez-Cortizas, A. (2002). The geochemistry of major and selected trace elements in a forested peat bog, kalimantan, se asia, and its implications for past atmospheric dust deposition. *Geochimica et Cosmochimica Acta*, 66:2307–2323.

Westerhold, T. and Roehl, U. (2009). High resolution cyclostratigraphy of the early eocene - new insights into the origin of the cenozoic cooling trend. *Climate of the Past*, 5:309–327.

Whittaker, T. E., Hendy, C. H., Hellstrom, J., and Anonymous (2008). Did heinrich events impact climate in the southwest pacific? evidence from new zealand speleothems. *Eos, Transactions, American Geophysical Union*, 89(53, Suppl.):Abstract PP41A–1433.

Wick, L. (1996). Late-glacial to early-holocene paleoenvironments in brianza, n italy. *Il Quaternario*, 9:653–660.

Wilhelms-Dick, D., Westerhold, T., Röhl, U., Wilhelms, F., Vogt, C., Hanebuth, T., Römmermann, H., Kriews, M., and Kasten, S. (2012). A comparison of mm scale resolution techniques for element analysis in sediment cores. *Journal of Analytical Atomic Spectrometry*, 27(9):1574–1584.

Wood, E. (1983). *Reef corals of the world: biology and field guide*. T.F.H. Publications.

Woodhead, J. and Pickering, R. (2012). Beyond 500 ka; progress and prospects in the u/pb chronology of speleothems, and their application to studies in palaeoclimate, human evolution, biodiversity and tectonics. *Chemical Geology*, 322-323:290–299.

Yafa, C., Farmer, J. G., Graham, M. C., Bacon, J. R., Barbante, C., Cairns, W. R. L., Bindler, R., Renberg, I., Cheburkin, A., Emons, H., Handley, M. J., Norton, S. A., Krachler, M., Shotyk, W., Li, X. D., Martinez-Cortizas, A., Pulford, I. D., MacIver, V., Schweyer, J., Steinnes, E., Sjobakk, T. E., Weiss, D., Dolgopolova, A., and Kylander, M. (2004). Development of an ombrotrophic peat bog (low ash) reference material for

the determination of elemental concentrations. *Journal of Environmental Monitoring*, 6:493–501.

Zaccone, C., Casiello, G., Longobardi, F., Bragazza, L., Sacco, A., and Miano, T. M. (2011). Evaluating the 'conservative' behavior of stable isotopic ratios (d13c, d15n, and d18o) in humic acids and their reliability as paleoenvironmental proxies along a peat sequence. *Chemical Geology*, 285:124–132.

Zaccone, C., Cocozza, C., Cheburkin, A. K., Shotyk, W., and Miano, T. M. (2007). Highly organic soils as "witnesses" of anthropogenic pb, cu, zn, and 137cs inputs during centuries. *Water, Air, and Soil Pollution*, 186:263–271.

Zaccone, C., D'Orazio, V., Shotyk, W., and Miano, T. (2009a). Chemical and spectroscopic investigation of porewater and aqueous extracts of corresponding peat samples throughout a bog core (jura mountains, switzerland). *Journal of Soils and Sediments*, 9(5):443–456.

Zaccone, C., Gallipoli, A., Cocozza, C., Trevisan, M., and Miano, T. M. (2009b). Distribution patterns of selected pahs in bulk peat and corresponding humic acids from a swiss ombrotrophic bog profile. *Plant and Soil*, 315:35–45.

Zaccone, C., Miano, T. M., and Shotyk, W. (2012). Interpreting the ash trend within ombrotrophic bog profiles: Atmospheric dust depositions vs. mineralization processes. the etang de la gruäre case study. *Plant and Soil*, 353:1–9.